

**Surface EMG Examination of  
Amyotrophic Lateral Sclerosis**

BY

FAEZEH JAHANMIRI NEZHAD

B.S., Amirkabir University of Technology, Tehran, Iran, 2003

M.S., University of Waterloo, Waterloo, ON, Canada, 2005

THESIS

Submitted as partial fulfillment of the requirements  
for the degree of Doctor of Philosophy in Bioengineering  
in the Graduate College of the  
University of Illinois at Chicago, 2014

Chicago, Illinois

Defense Committee:

James L. Patton, Chair

William Zev Rymer, Advisor

Ping Zhou, Co-Advisor, Physical Medicine and Rehabilitation, University of  
Texas at Houston

Paul Barkhaus, Department of Neurology, Medical College of Wisconsin

Thomas Royston

Hananeh Esmailbeigi

This thesis is dedicated to the solicitous *ALS* subjects participated in our experiments,  
and whoever is suffering from this disease.

## **ACKNOWLEDGEMENT**

I would like to express my sincere appreciation for supportive mentorship and advisership of Dr. Ping Zhou, Dr. Paul E. Barkhaus, and supervisors of Dr. William Zev Rymer. They all patiently walked me through the ups and downs of this journey, helping me not only with the technical and editorial aspects of this dissertation, but moreover helped me to comprehend the steps of a scientific approach. I am also much honored to have Doctors James Patton, Thomas Royston, and Hananeh Esmailbeigi in my thesis committee, and greatly appreciate their effort. I also greatly thank Susan Lee, the student program coordinator, at bioengineering department, UIC, and Sue Penwarden, the executive assistant, at sensory motor performance program (SMPP), Rehabilitation Institute of Chicago. Being a member of Single Motor Unit lab was a great honor for me. Dr. Nina Suresh has been a lab mentor and a life adviser. I also had the pleasure of company of Renee Thesis, Jinsook Roh, Xiaoyan Li, Xiaogang Hu, Jie Lu, Derek Miller, Andrew Lai, Sabrina Lee, Margaret Duff, Matthieu Chardon, Janina Madoff, Henry Shin, Brian Jeon, Sudarshan Srivatsan, Emily Lazzaro, Kathleen Pacholski, Mary Wu, Andres Cardona, Bahar Sharafi, and Farnaz Abdollahi during this journey, at SMPP. I lost my father in an accident, in Nov 2012. He always was a big support for me to continue my education. This unfortunate event made me deeply appreciate the warmth of the family I was raised in. I will always feel his kindness in my heart and will never forget that genuine smile on his face. I also cannot leave this page without mentioning my sister, Saeedeh, other dear family members and loyal sincere friends at Mahfel of Chicago. The last but not the least, I would like to appreciate my beloved husband, Ali, for his support and patience and my daughters, Sana and Suefia, for making home a place full of joy and happiness (and beyond!).

## CONTRIBUTION OF AUTHORS

All the chapters presented in this dissertation are primarily written by this author. Implemented techniques, the figures and tables are also provided by this author. Dr. Ping Zhou, my mentor, has closely assisted me with defining the research questions, conducting the corresponding experiments, analyzing the data, and publishing the outcome. He has contributed to the writing of Chapters 2 to 9. I assisted Dr. Ping Zhou with experimental data collection, used in Chapters 2 to 6, which was performed at Dr. Paul Barkhaus' ALS clinic. Dr. Barkhaus has significantly commented on the neuro-pathophysiology sections of this research. He has significantly helped me in editing Chapters 2-4, and 9.

Dr. Rymer, my primary adviser, has supervised me throughout this research and has always provided valuable comments. Chapter 1 was carefully commented and edited by Dr. Rymer. It includes an introductory to ALS disease and muscle structure, followed by specific aims of this research study.

I collected the data presented in Chapters 7 and 8 at Single Motor Unit Lab, conducted by Dr. Rymer, while Dr. Zhou was the Principal Investigator. Drs. Hu and Suresh supervised me with this data collection. Dr. Hu also contributed to the writing of Chapter 7. Dr. Ales Holobar contributed in Chapter 8 study, by providing EMG decomposition results.

# TABLE OF CONTENTS

<u>CHAPTER</u>	<u>PAGE</u>
1 OVERVIEW .....	1
1.1 AMYOTROPHIC LATERAL SCLEROSIS .....	1
1.2 ELECTROMYOGRAPHY .....	2
1.3 MUSCLE FIBER ACTION POTENTIALS AND MOTOR UNIT POTENTIALS .....	2
1.4 FORCE GENERATION .....	3
1.5 HIGH DENSITY SURFACE EMG .....	4
1.6 OVERALL OBJECTIVE.....	5
1.7 WORK PLAN.....	5
1.7.1 Aim1: To detect and analyze abnormal spontaneous EMG activity .....	6
1.7.2 Aim2: To investigate the waveform of Fasciculation Potentials, in an effort to describe differences from a typical MU potential.....	7
1.7.3 Aim3: To Assess muscle function and its deficits by studying the relationship between surface EMG and joint torque.....	7
1.7.4 Aim4: To examine the motor unit firing rate behavior in ALS compared with aged matched controls...7	7
2 A CLINICALLY APPLICABLE APPROACH FOR DETECTING SPONTANEOUS ACTION POTENTIAL SPIKES IN AMYOTROPHIC LATERAL SCLEROSIS WITH A LINEAR ELECTRODE ARRAY .....	9
2.1 INTRODUCTION .....	10
2.2 2.2. METHODS.....	12
2.2.1 Testing Signals.....	12
2.2.2 Spontaneous Spike Detection.....	13
2.3 RESULTS .....	16
2.4 DISCUSSION .....	21
2.5 ACKNOWLEDGEMENTS .....	24
3 SENSITIVITY OF FASCICULATION POTENTIAL DETECTION IS DRAMATICALLY REDUCED BY SPATIAL FILTERING OF SURFACE ELECTROMYOGRAPHY .....	25
4 SPIKE SORTING PARADIGM FOR CLASSIFICATION OF MULTI-CHANNEL RECORDED FASCICULATION POTENTIALS .....	30
4.1 INTRODUCTION .....	31
4.2 MATERIALS AND METHODS .....	33
4.2.1 Experiments .....	33
4.2.2 FP Classification Program Description .....	34
4.2.2.1 Database of Detected FPs .....	35
4.2.2.2 Feature Extraction .....	36
4.2.2.3 Unsupervised Clustering Strategy for FP Classification .....	37
4.2.2.4 Visually Aided Evaluation and Refinement .....	38
4.2.2.5 Final Supervised Classification.....	41
4.2.2.6 Quantitative Evaluation of Relative Class Consistency .....	42
4.2.2.7 Examination of Reproducibility; Two-source Method Comparison .....	42
4.3 RESULTS .....	43
4.4 DISCUSSION .....	46
4.4.1 Presence of Voluntary Activity.....	47
4.4.2 FP Classification vs. EMG Decomposition .....	47
4.4.3 Previous Works.....	49

## TABLE OF CONTENTS (continued...)

<u>CHAPTER</u>	<u>PAGE</u>
4.4.4 <i>Choice of Unsupervised Clustering Technique</i> .....	50
4.4.5 <i>Feature Extraction</i> .....	51
4.4.6 <i>Applications of FP Classification</i> .....	51
4.4.7 <i>Time Consumption to Provide Accurate Results</i> .....	52
4.4.8 <i>Visually-aided Classification</i> .....	53
4.5 SUMMARY.....	54
4.6 ACKNOWLEDGEMENT .....	55
5 INNERVATION ZONE ANALYSIS OF FASCICULATING MOTOR UNITS IN ALS USING A LINEAR ELECTRODE ARRAY .....	56
5.1 INTRODUCTION .....	57
5.1.1 <i>Motor Unit and Motor Unit Potential</i> .....	57
5.1.2 <i>Multi-channel Recording of MUP and Innervation Zone</i> .....	58
5.1.3 <i>Work Plan</i> .....	60
5.2 MATERIAL AND METHODS .....	61
5.2.1 <i>Experiments</i> .....	61
5.2.2 <i>Determining the IZ</i> .....	62
5.2.3 <i>Statistical tests</i> .....	64
5.3 RESULTS .....	64
5.4 DISCUSSION .....	69
5.4.1 <i>Motor Neuron Degenerative Diseases and ALS</i> .....	69
5.4.2 <i>IZ in Fasciculating Motor Units</i> .....	70
5.4.3 <i>Fasciculating Motor Unit IZ distribution in Biceps</i> .....	70
5.4.4 <i>Difficulties in Finding the IZ</i> .....	71
5.4.5 <i>Increased Aging and Increased Variability in IZ Length</i> .....	71
6 A PRACTICE OF CAUTION: ACTION POTENTIAL SPIKES OR NOISE? .....	72
7 EMG-FORCE RELATION IN THE FIRST DORSAL INTEROSSEOUS MUSCLE OF PATIENTS WITH AMYOTROPHIC LATERAL SCLEROSIS .....	79
7.1 INTRODUCTION .....	80
7.2 METHODS .....	82
7.2.1 <i>Subjects</i> .....	82
7.2.2 <i>Experimental Design</i> .....	82
7.3 RESULTS .....	85
7.4 DISCUSSION .....	89
8 CHARACTERIZATION OF MOTOR UNIT FIRING BEHAVIOR IN THE FIRST DORSAL INTEROSSEOUS MUSCLE OF PATIENTS WITH AMYOTROPHIC LATERAL SCLEROSIS .....	92
8.1 INTRODUCTION .....	93
8.2 EXPERIMENTS .....	94
8.2.1 <i>Experimental Design and Subject Population</i> .....	94
8.2.2 <i>EMG Decomposition and Firing Rate Calculation</i> .....	97
8.3 RESULTS .....	99
8.4 DISCUSSION .....	103
8.5 ACKNOWLEDGEMENTS .....	106
9 FUTURE DIRECTIONS .....	107
9.1 DETECTION OF FIBRILLATION POTENTIALS.....	107

## TABLE OF CONTENTS (continued...)

<u>CHAPTER</u>	<u>PAGE</u>
9.2 MOTOR UNIT RECRUITMENT PATTERNS .....	108
9.3 MOTOR UNIT NUMBER ESTIMATION .....	108
9.4 STUDY OF ABNORMAL PROPAGATION PATTERNS – A SIMULATION STUDY .....	109
9.5 WITHIN-MOTOR UNIT INNERVATION ZONE ANALYSIS.....	109
9.6 FASCICULATION POTENTIAL ANALYSIS ON THE 8×8 GRID ELECTRODE.....	109
9.7 COMPLEMENT SURFACE EMG WITH OTHER TECHNIQUES THAT MEASURE SUBCUTANEOUS TISSUE AND SKIN LAYER PARAMETERS .....	110
REFERENCES .....	111
VITA .....	128
APPENDIX .....	131

# LIST OF FIGURES

<u>FIGURE</u>	<u>PAGE</u>
Figure 1: The linear electrode array used in this study. ....	13
Figure 2: An overview of 100 s spontaneous surface electromyogram (EMG) signals recorded with the linear electrode array, and the oneV and soneV signals. An enlarged version of a selected signal segment is also shown (with only 9zz channels), in which 4 fasciculation potentials are detected. ....	16
Figure 3: Demonstration of different situations of spontaneous spike detection. (a) the most typical case; (b) detection of two close spontaneous spikes; (c) detection of a complex spontaneous spike; (4) detection of a low amplitude spontaneous spike; (4) a false detection with the soneV signal which can be corrected by examining the raw signals of all the channels. ....	18
Figure 4: Sample raster plot of the detected spontaneous spikes from the biceps brachii muscle on an amyotrophic lateral sclerosis (ALS) subject using the linear electrode array. The occurrence time and the maximum peak- to-peak amplitude are indicated on the top of each spike. ....	20
Figure 5: A demonstration of the firing time, duration and amplitude of the detected spontaneous spikes in several 100-second signal segments selected from a 1500-second recording. The bottom right panel shows the amplitude and duration of all the spikes from the entire recording. ....	21
Figure 6: (a) A schematic plot of the 20-channel linear electrode array used for the biceps brachii muscle recording. Each recording bar is 1 mm in width and 10 mm in length, and the inter-bar distance is 10 mm. (b) A schematic plot of the 2D flexible electrode array used for the FDI or thenar muscle recording. Each recording probe is 1.2 mm in diameter, and the center to center distance between two adjacent probes is 4 mm for both horizontal and vertical directions. (c) A comparison of fasciculation potentials recorded from biceps brachii muscle of an ALS subject using the initial mode, the bipolar and double differential configurations, respectively. ....	28
Figure 7: Summary of the spike detection process. (A) shows a sample raw EMG. Half-second EMG epochs containing only 9 channels are shown here. (B) shows an example of amplitude thresholding. The bottom two lines (in blue) are EMG. The spikes on these channels are FPs. FPs are apparent on the rectified black line above that shows the one-dimensional signal. The magenta dashed line crossing the black line is the user-selected threshold. Amplitude thresholding on the black line provides the start and end times of each FP. (C) shows an example portion of a database of extracted FP. Each column represents one FP, where each row represents one channel of recording. ‘FT’ and ‘Amp’ refer to “firing time” and “maximum amplitude”, respectively. ....	35
Figure 8: (A) Sample plot of ‘Interactive Class Refinement’ module. FPs are plotted side-by-side. Each column represents one FP. Four options are integrated in the screen by the four regions. In this example, three samples (in different color) can be identified with inconsistent waveform shapes (case of superimposition). Clicking in region2 would exclude them from computing the template of this class, and clicking in region3 would remove their membership and assign them to L-0. (B) Sample plot of templates proposed to be similar to the template of the class of interest (in magenta color). (C) Up to five samples from the to-be-merged classes are plotted side by side, providing a visual aid for the user to determine whether to combine the two classes or not. (D) A multi panel plot. Each panel shows the to-be-classified sample (in green, left) along with the template of candidate class (in blue, right). Amplitude information is also included. The sample may be assigned to one of the classes, be left unassigned, be sent to Trash, or open a new class. ....	40



## LIST OF FIGURES (continued...)

<u>FIGURE</u>	<u>PAGE</u>
Figure 9: Single channel raw EMG corresponding to data presented in the result section. Each trace shows 100 s. Total recording time is 900 s. ....	43
Figure 10: An illustration of outcome results in a classification process. (A) shows an example outcome of spike detection. (B) refers to feature space. (C) shows the first three principal components of whole feature space. (D) shows the result of initial clustering algorithm (color coded) after evaluation and refinement of classes. (E) shows parts of the FP templates in their waveform shape. (F) shows groups of sample FPs assigned to each class. Further analysis of FP shape and firing pattern can start from here. ..	45
Figure 11: Schematic of a MU. Distribution of NMJs along muscle fibers is shown. On top of the skin surface, an array of tiny electrodes is located. Motor unit potential can be recorded simultaneously on multiple channels. ....	58
Figure 12: Raster plots of simulated MFAPs and a final MUP. This plot shows the concept of MUP generation obtained from summation of single MFAPs on multichannel electrodes. The Innervation Zone can be detected from the multichannel MUP. In reality, single MFAPs are not detectable by surface electrodes. ....	59
Figure 13: A simulated MUP. On the left, raster plot of MUP waveform is depicted (y axis is voltage with arbitrary unit (au) and x-axis is time duration (au)). On the right, the plot of Points of Extrema are presented (y-axis represents the time and corresponds to x-axis of the raster plot, and x-axis represent channel number). The sites of minimum are marked with green circles and the maximum points at each channel are marked with red squares. In the raster plot, the site of IZ is located at the center (channel 10). The troughs (both for the points of min and max) on the right panels, also occur at x=10. ....	63
Figure 14: Raster plots of nine sample prototype shape of FPs belonging to one subject. Class index, number of members of that class (how many samples assigned to it), and its amplitude is reported on the top. C2 has a strange straight propagation, with no time lags between the channels. In C5, two IZs were detected, indicating for either a doubly innervated MU or two superimposed FPs. The heavy black lines indicate of IZs. ....	65
Figure 16: Longitudinal study of IZ scatter for three ALS subjects. Statistical test was performed on STD of IZs. The asterisks indicate for statistical difference. ....	67
Figure 17: Variation of IZ within a muscle in control subjects with respect to their age. A linear trend can be observed. ....	68
<i>Figure 18:</i> An example of (a) an artifactual spike and (b) the distorted waveform after processing with a causal filter. ....	74
<i>Figure 19:</i> Signal distribution among 19 channels of the linear electrode array for: (a) an artifactual spike; (b) fasciculation potentials of biceps muscle of an ALS subject. ....	75
<i>Figure 20:</i> An example of repetitive spikes from one channel of electrode arrays. (a) Multiplets or myokymic discharges from the thenar muscle of an ALS subject; (b) Neuromyotonic discharges from the same muscle; (c) Repetitive artifactual spikes induced by external stimuli. ....	76

## LIST OF FIGURES (continued...)

<u>FIGURE</u>	<u>PAGE</u>
<i>Figure 21:</i> Signal distribution among different channels of the electrode array for: (a) repetitive artifactual spikes; (b) multiplets from the thenar muscle of an ALS subject. ....	77
Figure 22: Experimental setup for surface EMG and contraction force recordings from the FDI muscle. 83	
Figure 23: Examples of surface EMG and force signals recorded at two different contraction levels from a healthy individual. Each contraction lasted around 10 seconds. Six EMG channels are shown here in the upper panels. The lower panels show force profiles. Both fore directions in abduction (Fx) and flexion (Fy) are shown. The abduction force level in the left trial is about 1.7 N and in the right trial is 8.4 N. ...	86
Figure 24: The linear fitting of the EMG-force relation for each of the healthy control subjects. ....	87
Figure 25: The linear fitting of the EMG-force relation for each of the ALS subjects. ....	87
Figure 26: An 8×8 grid of surface EMG electrode placed over FDI muscle. ....	96
Figure 27: Discharge patterns of MUs extracted through EMG Decomposition, at 1 Newton of force. The data on the right panel belongs to a healthy subject, and on the left panel belongs to an ALS subject. Pulse per second is reperted at the end of each pattern. ....	99
Figure 28: averaged firing rates for each individual. The top row shows the results from ALS population, and the bottom row presents the results from healthy subjects. In each panel, x-axis indicates force (in absolute Newton value), and y-axis shows firing rate (pulse per seconds). Each sample represents the average firing rates of all the motor units extracted from EMG at each level of contraction. ....	100
Figure 29: the (fitted) linear relationship between firing rate and force levels (in Newton). ....	101
Figure 30: Plot of slope and initial firing rate values for the three groups (H: Healthy, G1: ALS with weak FDI, G2: ALS with normal FDI). On the left, distributions of A and B are depicted individually. On the right, a feature space of the data (x-axis: A, y-axis: B) is presented. The contours are dividing the feature space into three regions. The middle region contains all the H and G2 samples are clustered. The up and bottom regions include three and two samples from the G1. ....	102
Figure 31: A-B feature space divided (arbitrarily) into two regions. ....	105

## LIST OF TABLES

<u>TABLE</u>	<u>PAGE</u>
Table 1: Variable description.....	38
Table 2: Summary of classification outcome.....	46
Table 3: Measures of IZ distribution among FPs compared with MUPs in control and ALS subjects.....	65
Table 4: Longitudinal data of length of IZs within a muscle.....	67

## LIST OF ABBREVIATIONS

ALS	Amyotrophic Lateral Sclerosis
AP	Action Potential
EMG	Electromyography
FP	Fasciculation Potential
FR	Firing Rate
IDI	Inter-Discharge Interval
IFR	Instantaneous Firing Rate
IZ	Innervation Zone
LMN	Lower Motor Neuron
MFAP	Muscle Fiber Action Potential
MU	Motor Unit
MUP	Motor Unit Potential
MVC	Maximum Voluntary Contraction
NMJ	Neuromuscular Junction
STD	Standard Deviation
UMN	Upper Motor Neuron

## SUMMARY

Electromyogram signals were recorded and analyzed from subjects with Amyotrophic Lateral Sclerosis. In contrast to routine needle clinical examinations, we used surface electrodes (High Density surface EMG, HDsEMG) in an attempt to show the feasibility of muscle assessment using a non-invasive approach. The study started by examining Fasciculation Potentials, a crucial electrodiagnostic feature of ALS. The feasibility of the proposed surface recording for their detection was soon established, so the fasciculation potentials were then further explored in order to understand the nature of their spontaneous discharges, when compared with regular motor unit discharges.. Due to a lack of software applications to analyze the signals from HDsEMG electrodes, a number of new techniques were designed and implemented to extract these potentials from raw EMG, and to classify them based on their shapes. Taking advantage of advanced multi-channel recording technologies, we explored Fasciculation Potentials with respect to the ‘Innervation Zones’ of their sites of origin, where signs of muscle reorganization were observed. In addition to their non-invasive nature and their comfort for the patients, HDsEMGs were proposed as potentially more suitable in monitoring the progress of the disease. Preliminary results were presented on this theme. Muscle functional capacity was also assessed, by measuring the slope of the EMG-force relation. Abnormal EMG-force slopes in some of the ALS subjects were recorded. In addition to global EMG analysis, single motor units were also extracted in a collaborative project which provided EMG decomposition outcome. We studied discharge behavior of single motor units in hand muscles of ALS subjects, during isometric voluntary contractions. Overall, we concluded that HDsEMG can substitute for many electrodiagnostic practices in clinics, and can provide supplementary information about the muscle which is not attainable using single needle recording.

# 1 Overview

## 1.1 Amyotrophic Lateral Sclerosis

Amyotrophic Lateral Sclerosis (ALS) is a fatal progressive form of motor neuron disease leading to death of spinal and/or bulbar motor neurons. When these motor neurons die, there is a loss of connection between the muscle fibers and the CNS. In advanced cases, patients will experience increasing difficulty moving, swallowing, and speaking, depending on the site of motor neuron loss. Muscle atrophy, paralysis and respiratory system malfunctioning will follow. The root cause of ALS remains unclear, and varies from familial (in which there are strong genetic contributors) to idiopathic or sporadic. The disease causes degeneration of the lower motor neurons (LMN), located in the ventral horn of the spinal cord, and that innervate the muscles. There is usually associated loss of the upper (cortical) neurons (UMN) that provide descending input to the lower motor neurons. Thus, ALS patients typically experience symptoms and signs of both UMN (including spasticity and hyperreflexia) and LMN (including muscle weakness, muscle twitches and muscle atrophy) dysfunction.

To date, there is no unique diagnostic test for ALS. The “definitive” diagnosis is made by the presence and progression of both UMN and LMN symptoms and signs in three of four possible anatomical regions (bulbar, cervical, thoracic, and lumbosacral), and supported by findings of active denervation and reinnervation using clinical electromyography (EMG). Other appropriate imaging and blood tests are performed to exclude other “mimic” conditions (e.g., cervical spondylosis, inclusion body myositis, Lyme disease, etc.).

## **1.2 Electromyography**

The initiation of muscle contraction requires the movement of ions across the muscle fiber membrane. The gradient of these charges across the membrane creates electrical fields. An electrical field can be detected by recording from surface or intramuscular electrodes. This technique is called Electromyography (EMG). Due to the close interconnection of muscle and nerves, the EMG can be seen as a window to understand the functions of the nervous system. Consequently, the EMG has a significant role as an electrodiagnostic tool in neurological disorders.

One essential component of the nomenclature in this thesis is the concept of the Motor Unit (MU). The MUs are functional building blocks of a skeletal muscle. Muscles are connected to the nervous system (innervation) by means of specialized neurons called motor neurons. An  $\alpha$  motor neuron innervates a number of muscle fibers, which are not usually adjacent. A MU refers to the set of muscle fibers innervated by one motor neuron. The definition of the “motor unit” usually includes the motor neuron (its soma in the spinal cord, its axon, and its terminal branches), and corresponding muscle fibers. MUs’ territories within a muscle are overlapping, allowing them to function with the support of other units.

## **1.3 Muscle Fiber Action Potentials and Motor Unit Potentials**

An action potential is a short disturbance to the electrical resting potential of a nerve membrane. Once an electrical stimulus is greater than a threshold, it initiates an inflow of sodium ions toward the interior of the cell, called depolarization phase, followed by the outflow of potassium ions to the exterior of the cell, the repolarization phase, and finally returning to its resting potential, the refractory phase. An Action Potential (AP) refers to the series of the three

phases. APs are the key electrical means for transformation of information throughout the nervous system. While the stimulated point on the fiber is returning to its resting potential, adjacent points on both sides get stimulated, initiating their excitation. This way, the signal transfers toward the fiber endings on both sides.

The mechanism of voluntary muscle contraction is also initiated by APs. Originating in central nervous system, they reach to the soma of  $\alpha$  motor neurons in the ventral horn of spinal cord. The APs propagate along a motor axon and toward the terminal branches at the end of the nerve. At each axon branch end, there is a synaptic cleft, where the nerve ending is connected to (likely) the middle of a muscle fiber. This is called a Neuromuscular Junction (NMJ).

An AP in the presynaptic membrane causes activation of a key neurotransmitter (acetylcholine), which in turn launches an AP on the postsynaptic muscle fiber membrane. APs on muscle fibers are called Muscle Fiber Action Potentials or MFAPs. Since an  $\alpha$  motor neuron is connected to a number of muscle fibers (up to several hundreds, depending on the muscle), all the innervating muscle fibers are potentially excited at the same time. If there exist a means of electrical activity recording (an EMG electrode), summation of all MFAPs will be recorded at the same time, forming Motor Unit Potentials (MUPs).

## **1.4 Force Generation**

MFAPs propagate the same way as AP spread on nerve fibers. They travel along the fibers.. Their activation causes calcium release from the sarcoplasmic reticulum, which in brief makes the sarcomere, the contractile unit of the muscle fiber contract. The myofilaments (their subunits) slide together, leading to fiber contraction. In skeletal muscles, and at their ending, the muscle fibers are usually connected to tendon fibers, through which the generated force is transferred to



a bone. The nervous system controls a voluntary contraction by using two main strategies: MU recruitment and rate coding. The order of MUs activations and their firing rate modulation are the key factors that define the mechanism of a movement.

A body of research has been dedicated to investigate these phenomena by means of Electromyography (Burke, 1968; De Luca et al., 1982; Fuglevand et al, 1993; Farina et al., 2002; Zhou and Rymer, 2004). Along with this understanding, there comes the ability to detect potential abnormalities and define electrodiagnostic features.

## **1.5 High Density surface EMG**

Characterization of an EMG signal depends critically on electrode properties, including size, charge transfer properties, orientation with respect to muscle fibers/fascicles, and configuration (monopolar, differential etc.) . Indwelling micro and macro needle electrodes, fine wires, and surface electrodes provide a spectrum of invasive and non-invasive approaches, each used for a specific application.

Needle EMG examination is routinely used as the major diagnostic and confirmatory tool for identifying ALS in clinical practice. Surface EMG provides non-invasive examination of electrical activity of muscle, but has been viewed as being unsuitable for single MU analysis despite some promising clinical applications. This perceived role is due to its lack of sensitivity to small motor unit activities recorded from the surface of the skin. However, development of HDsEMG techniques has opened new avenues in reliable, noninvasive methods of EMG decomposition. Flexible surface electrode arrays (or grids) can be easily attached to the skin and can record long-lasting muscle activities noninvasively.

The HDsEMG technique is especially helpful when inserting a needle electrode could be painful (such as in facial muscles or tongue) and may cause discomfort for sensitive subjects. In HDsEMG, the lack of sensitivity (due to low pass filtering effect) is compensated by the additional spatial information added to temporal data. Multi-channel electrodes cover a large area of muscle, and can thus record more motor unit activities, while intramuscular EMG records from only a small volume of the muscle. This fact makes High-density surface EMG, HDsEMG, electrodes more appropriate for tracking the changes in the muscle for an individual over time, since inserting a needle at the exact same place inside the muscle is difficult if not impossible. Furthermore, HDsEMG electrodes can yield some information that cannot be obtained using single channel EMG, such as an estimate of motor unit end plate or muscle fiber conduction velocity.

## **1.6 Overall Objective**

In spite of more than a decade of investigations, HDsEMG recording still is in a research stage, and has yet to show its value in clinics. Accordingly, this work aims to investigate application of surface EMG data for subjects with ALS, and to facilitate data analysis, which can be helpful in extracting useful information for the sake of clinical diagnosis, as well as for scientific research. The overall goal of this project is to demonstrate the utility of surface EMG in the assessment of ALS.

## **1.7 Work Plan**

Most ALS diagnostic and tracking criteria require intramuscular recordings, to show presence of fibrillation potentials, fasciculation potentials (FPs), evidence for reinnervation in

motor unit potentials, and MU loss revealed by motor unit number estimation (MUNE). If surface EMG recordings are to be comparably useful, it will be necessary to demonstrate the feasibility of monitoring several aspects of the above-listed key electrodiagnostic features of ALS using multi-channel surface EMG recordings.

#### 1.7.1 Aim1: To detect and analyze abnormal spontaneous EMG activity

Loss of LMN is equivalent to decrease of neural input to a muscle, and this is called denervation. A major sign of active denervation is the presence of abnormal spontaneous electrical activities. Abnormal spontaneous firings include fibrillation potentials (an action potential fired from a single denervated muscle fiber) and fasciculation potentials (action potentials fired from a motor unit). Fibrillation potentials are essentially undetectable on the surface of skin, because they are at sub microvolt level. The focus in this aim (1) was on Fasciculation Potentials (FPs). The presence of FPs indicates the existence of abnormal membrane potential in the terminal of the motor axon (hyperexcitable) and if diffusely distributed, is a sign of denervation (De Carvalho et al., 2008). Presence of FPs is prominent in ALS.

Immediately after it became clear that FPs are detectable using HDsEMG technology, a lack of a proper software to analyze our EMG signal emerged. Available data analysis software (such as Spike2 and EMGLAB) have been proved inefficient for recordings of spontaneous activity of muscle, which requires hundreds of seconds of data recordings.

In this aim, the designs of clinically applicable programs for FP analysis are described. Chapters 2 to 4 are dedicated to this aim.

1.7.2 Aim2: To investigate the waveform of Fasciculation Potentials, in an effort to describe differences from a typical MU potential.

One of the novel features of multi-channel recordings is their ability to locate the innervation zone (IZ) of an individual MU. While other research groups have discussed fasciculation potentials based on their waveform potential complexity or their temporal information, we approached them based on their IZ distribution. Abnormal lengths for the collective neuromuscular junctions of a MU are discussed in Chapter 5.

1.7.3 Aim3: To Assess muscle function and its deficits by studying the relationship between surface EMG and joint torque

In order to understand the impact of the changes in the mechanism of MU recruitment and the resulting force generated, the EMG-force relationship has been extensively studied in the past in different neurological disorders, but rarely in subjects with ALS. We conducted a study where subjects with ALS were instructed to perform abduction contractions on FDI muscle at randomized different levels of force. EMG-force slope for ALS subjects were then compared with age matched healthy controls. Chapter 7 is dedicated to this project.

1.7.4 Aim4: To examine the motor unit firing rate behavior in ALS compared with aged matched controls.

MU firing rate refers to the rate of discharges of a recruited MU. Firing rate is one of the main factors in force generation. Changes in the rate coding strategy can help us to understand the underlying changes in the muscle, as an effect of the motor neuron degeneration disease.

Firing rate variations have also been associated with LMN or UMN lesions. This study is one of the first ones that address firing rate change in ALS using HDsEMG technology, while all the existing ones are made using intramuscular EMG. Chapter 8 is dedicated to this study.

## **2 A Clinically Applicable Approach for Detecting Spontaneous Action Potential Spikes in Amyotrophic Lateral Sclerosis with a Linear Electrode Array<sup>1</sup>**

Faezeh Jahanmiri-Nezhad, Xiaoyan Li, Paul E. Barkhaus, William Z. Rymer, Ping Zhou

Examination of spontaneous muscle activity is an important part of the routine electromyogram (EMG) in assessing neuromuscular diseases. The EMG is specifically valuable as a diagnostic test in supporting the diagnosis of amyotrophic lateral sclerosis (ALS). High density surface EMG (HDS EMG) is a relatively new technique that has until now been utilized in research, but has the potential for clinical application. This study presents a simple HDS EMG method for automatic detection of spontaneous action potentials from surface electrode array recordings of ALS patients. To reduce computational complexity while maintaining useful information from the electrode array recording, the multi-channel HDS EMG was transferred to single dimensional data by calculating the maximum difference across all channels of the electrode array. A spike detection threshold was then set in the single dimensional domain to identify the firing times of each spontaneous action potential spike while a spike extraction threshold was used to define the onset and offset of the spontaneous spikes. This data was used to extract the spontaneous spike waveforms from the electrode array EMG. A database of detected spontaneous spikes was thus obtained, including their waveforms, on all channels along with their corresponding firing times. This newly developed method makes use of the information from different channels of the electrode array EMG recording. It also has the primary feature of being simple and fast in implementation, with convenient parameter adjustment and user-computer interaction. Hence it has good possibilities for clinical application.

---

<sup>1</sup> Published in Journal of Clinical Neurophysiology 2014 Feb;31(1):35-40. doi: 0.1097/01.wnp.0000436896.02502.31 Wolters Kluwer Health Lippincott Williams & Wilkins© No modifications will be permitted.

## 2.1 Introduction

Diffuse, abundant spontaneous muscle activity may be a typical electrophysiological feature in many neuromuscular diseases. Various spontaneous electromyogram (EMG) signals collectively are the electrophysiological manifestation of widespread degeneration of the bulbar and spinal motoneurons (Brooks, 1994). This examination of spontaneous muscle activity is an important part of the routine EMG, particularly in supporting the diagnosis of amyotrophic lateral sclerosis (ALS). The electrophysiological diagnosis of ALS includes the detection of positive sharp waves or fibrillation potentials and the manifestation of reinnervation in the motor unit action potentials (MUAPs). These symptoms have to appear in three of four regions (bulbar, cervical, thoracic and lumbosacral) to confirm the diagnosis (Brooks, 1994). The presence of spontaneous EMG may portend lower motoneuron dysfunction prior to clinical symptoms such as weakness or muscle atrophy, possibly even before the onset of definite reinnervation changes in the MUAPs (de Carvalho and Swash 1998; Rosenfeld 2000; Barkhaus and Nandedkar 2005). Thus, enhanced detection of spontaneous EMG may be of great importance for early diagnosis of ALS. ALS is almost inevitably fatal in 3-5 years. With the introduction of potential new therapies (Swash, 2000), early diagnosis of ALS has become an extremely important issue in optimizing management. .

The intramuscular needle electrode is routinely used for detection of spontaneous muscle activity. It is generally accepted that the spontaneous activity of single muscle fibers such as fibrillation potentials or positive sharp waves can only be detected by such electrodes. Conversely, other spontaneous motor unit activity that may represent the collective activity of many muscle fibers (e.g. fasciculation potentials) can be recorded by both concentric needle electrodes as well as regular surface electrodes. While fibrillation potentials are considered to be the most important feature of active denervation such as seen in ALS, recent discussion has

revisited the potential application of fasciculation potentials to enhance the diagnostic sensitivity of ALS (de Carvalho 2000; de Carvalho et al. 2008; Benatar and Tandan, 2011; Noto et al. 2012).

In recent years, high density surface EMG (HDS EMG) techniques have been developed using electrode arrays comprised of a number of closely spaced, miniscule recording probes or bars (Zwarts and Stegeman 2003; Merletti et al. 2003; Rau et al. 2004; Lapatki et al, 2004; Pozzo et al. 2004; Merletti et al. 2009;). These electrode arrays cover a relatively large area of a muscle. Their noninvasive nature allows long recording times. The latter is required for a quantitative evaluation of the discharge patterns of spontaneous motor unit action potentials, which may vary from a few milliseconds to more than a minute (Howard and Murray, 1992). Because of the added value of the spatial information, such electrode arrays can facilitate further discrimination between spontaneous action potentials (Drost et al. 2007). These discharge patterns have been used to assess their different origins (Kleine et al. 2008; Kleine et al 2012). Although it has great potential to offer additional investigative and diagnostic information, HDS EMG has not been used as a clinical tool for evaluation of neuromuscular diseases (Drost et al., 2006). If new criteria are to be considered in using fasciculation potentials to facilitate earlier diagnosis of ALS (de Carvalho et al. 2008; Benatar and Tandan, 2011), it would be helpful to develop a clinically applicable method to optimize their detection. This work presents a simplified method to automatically detect action potential spikes from HDS EMG recordings in ALS patients, which is suitable for clinical assessment of fasciculation potentials. Our intent was not to develop complicated signal processing technique to discriminate between different spontaneous spikes. Our goal was to develop a clinically applicable method characterized by quick and convenient implementation for detecting the occurrence of spontaneous spikes, regardless of their motor unit origins (similar to the strategy used in routine needle EMG



examination). Development of such methods will promote clinical integration of HDS EMG in the evaluation of neuromuscular diseases.

## **2.2 2.2. Methods**

### **2.2.1 Testing Signals**

The testing data used in this study were recordings from 6 subjects with “Definite ALS” or “Probable ALS with Laboratory Support” based on El Escorial criteria from the third author’s institution. These patients had already been studied by conventional clinical EMG as part of their clinical evaluation (Brooks 1994). All subjects gave written, informed consent prior to participation in this study. This study was approved by the local Human Studies Committee.

Data collection protocol followed a spontaneous muscle activity paradigm. No disturbing sensory stimuli were allowed in the examination room. Each subject was positioned comfortably supine on an examination table with a pillow under their head. The tested arm was placed in its natural, resting position. The biceps brachii (BB) muscle was recorded with the elbow partially flexed and forearm in semi-pronation. A 20-channel linear bar electrode array (Figure 26), designed and fabricated in our laboratory, was used for all recordings. The distance between two consecutive recording bars is 5 mm, and each bar is 1 mm in width and 10 mm in length, arranged in a linear configuration. After placement of the linear electrode array from proximal to distal tendon junctions of the BB muscle, the subjects were asked to completely relax. Surface EMG signals were recorded for at least 10 minutes in a relaxed condition. The surface electrode array signals were amplified by the Refa EMG Recording System (TMS International BV, Enschede, The Netherlands) in a monopolar configuration, with a reference electrode located on the olecranon (each channel also has a common feedback subtraction of the average of all the

recording channels). The surface EMG signals were sampled at 2k Hz per channel, with a band pass filter setting of 20-500 Hz.



Figure 1: The linear electrode array used in this study.

### 2.2.2 Spontaneous Spike Detection

For an electrode array, a single channel EMG data is represented by a row vector  $\mathbf{d}_j = (x[1], x[2], \dots, x[N_s])$ , where  $j$  is the channel index and  $N_s$  is the total number of samples. The whole data set from the electrode array recording, represented as  $\hat{\mathbf{D}}$ , is a matrix of  $N_{ch}$  rows and  $N_s$  columns, where  $N_{ch}$  is the number of electrode channels ( $N_{ch}=20$  in this study). A spontaneous spike can be represented by a matrix of  $N_{ch}$  rows and  $M$  columns, where  $M$  is the duration of the spike. Six steps are involved in the spike detection algorithm from an electrode array.

Step 1: Select appropriate channels. One challenge with electrode array recording is to ensure the signal quality for all the channels (especially for electrode arrays comprised of a number of tiny recording probes). The minute skin-electrode contact area induces high skin-electrode impedance which is a major reason for high recording noise. Despite careful skin preparation, situations are sometimes encountered where the signal-to-noise ratio is poor in several channels of an electrode array. Thus in the first step, we reviewed all of the recording channels: those channels having poor recording quality were excluded from further analysis. If

all the channels have good signal quality, this step is unnecessary (this is usually the case for most of the liner bar electrode array recordings).

*Step 2: Signal segmentation.* Due to the lengthy recording period of the linear electrode array used in this study, it is not feasible to analyze the entire recording time or epoch. Thus, the signal was sequentially segmented into 100 s segments from beginning to end, with each segment being processed separately.

*Step 3: Creating a one-dimensional signal.* To facilitate convenient and fast spontaneous spike detection in the electrode array EMG recordings, a single dimensional signal, *oneV*, was constructed using signals from all the channels:

$$oneV = \max \hat{\mathbf{D}} - \min \hat{\mathbf{D}}$$

More specific,

$$oneV[i] = \max_{j=1:N_{Ch}} [x_{ij}] - \min_{j=1:N_{Ch}} [x_{ij}]$$

where  $\hat{\mathbf{D}} = [d_1, d_2, \dots, d_{N_{Ch}}] = [x_{ij}]_{N_{Ch} \times N_s}$ .

Thus, the amplitude of *oneV*[i] at each time equals the maximum difference across all channels of the array.

To reduce the high frequencies that induce error in the spike detection algorithm, a Hanning window was used to smooth the *oneV* signal, resulting in *soneV*:

$$soneV[i] = \frac{1}{n} \sum_{j=i-n}^{j=i+n} (oneV[i] * \omega[j]),$$

$$\omega[j] = 0.54 - 0.46 * \cos\left(\frac{2\pi}{n-1}j\right)$$

where *n* is the Hanning window size, which is user-adjustable depending on the raw EMG signal. Increasing *n* will result in more smoothed signal while concomitantly reducing the detection sensitivity. In this study, *n* was set to 20 *ms* as a compromise.

*Step 4: Spontaneous spike detection.* This step is to determine whether or not a spontaneous spike has occurred. A spike detection threshold was applied to the soneV signal, and any activity above this threshold indicates that a spontaneous spike occurred. The spike detection threshold was set as  $r \times \max(\text{soneV})$ , where  $0 < r < 1$ .  $r$  was set to be 0.2 in most cases of this study. A plot is provided in our program for a user to review the total soneV, as well as the preset threshold. This plot is a visual aid to the user to select the most appropriate level for spike detection threshold. In addition, the soneV signal can be plotted together, corresponding to all the available segments. The output of this step is the occurrence times of the peaks of the detected spontaneous spikes.

*Step 5: Onset and offset detection of spontaneous spikes.* This step extracts the beginning and end points of the detected spontaneous spikes in the previous step. To determine how long the data should be extracted for an individual spike, another threshold was set to determine the onset and offset of the spike. This threshold is called spike extraction threshold. In contrast to spike detection threshold, the spike extraction threshold is not fixed. In this study, the spike extraction threshold was set as 20% of the maximum peak amplitude of each detected spontaneous spike. The cross points of this threshold with the soneV signal determine the onset and offset of the detected spike. If the spike extraction threshold is lower than the baseline of the soneV signal (which may be the case for low amplitude spikes), the minima of the soneV signal is used to determine the onset (the first minima in the left lobe of the soneV signal) and the offset (the first minima in the right lobe of the soneV signal) of the spontaneous spike. The minima can be determined by the first zero crossing of the first order differentiation of the soneV signal.

*Step 6: Exaction of spontaneous spikes and database construction.* The temporal information obtained in step 4 and step 5 is used to extract multi-channel waveforms from the electrode array EMG recordings. This is the last step of our spike detection algorithm. The final

output is a database of individual detected spontaneous spikes, as well as the temporal information for each spike. It is noted that although each spike has its own duration, they are all stored with the same length, padded with zero when necessary.

## 2.3 Results

Figure 2 shows an example of an overall view of a 100 s spontaneous HDS EMG signal recorded from the BB muscle of an ALS subject, together with the converted one-dimensional signal, oneV, and its smoothed version, soneV. The bottom of the figure shows an enlarged version of a selected segment (only the first 11 channels are presented), in which four spontaneous spikes with different amplitude and duration are observed.

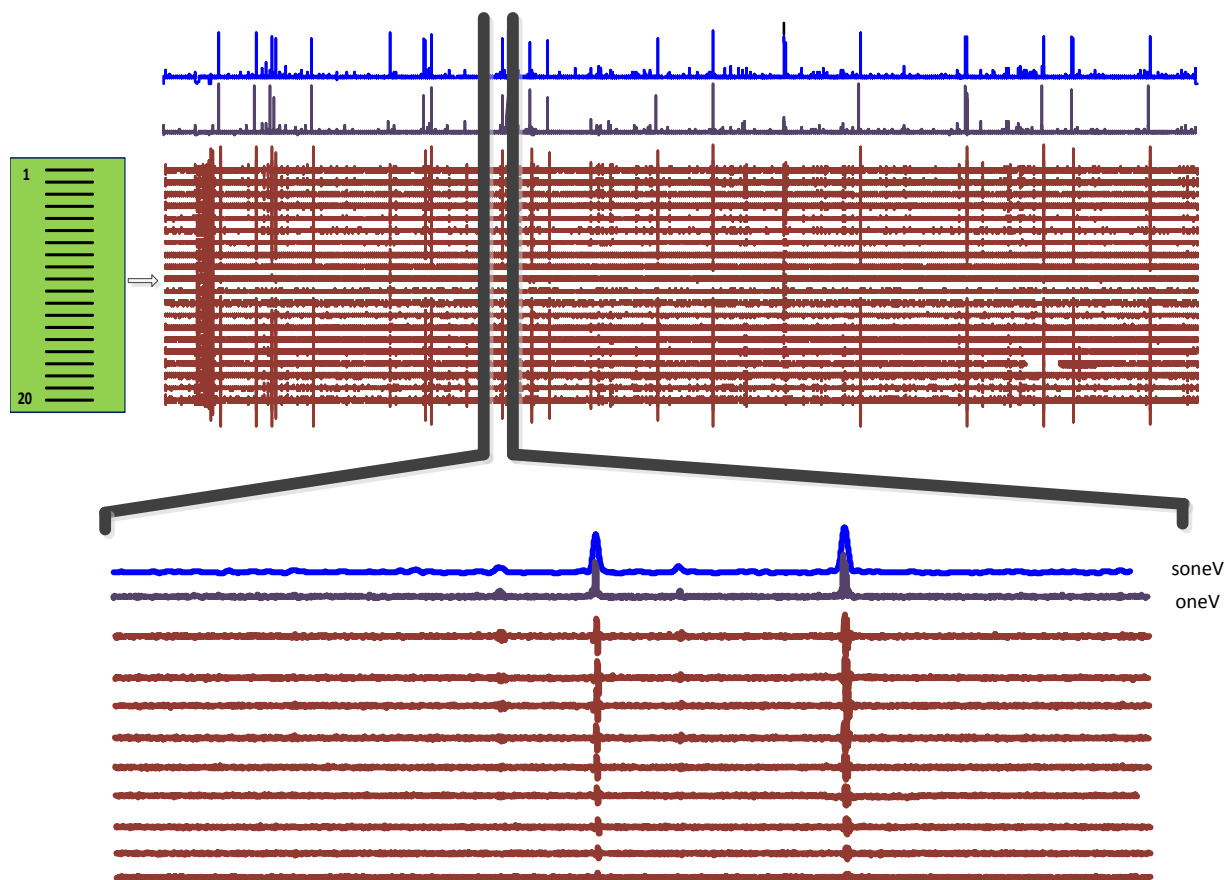


Figure 2: An overview of 100 s spontaneous surface electromyogram (EMG) signals recorded with the linear electrode array, and the oneV and soneV signals. An enlarged version of a selected signal segment is also shown (with only 9zz channels), in which 4 fasciculation potentials are detected.

Figure 3 demonstrates examples of spontaneous spike detection in different situations using our simplified method. Figure 3a shows the most typical case of the spike detection, where the segment of soneV signal is plotted with the spike detection threshold. The spike detection and extraction thresholds are marked as dotted and dashed horizontal lines, respectively. The onset and offset of the detected spikes are shown by the two vertical dashed lines. Beneath the soneV signal, the corresponding EMG data of selected channels are plotted. The duration of the detected spike is recorded on the top of the soneV signal.

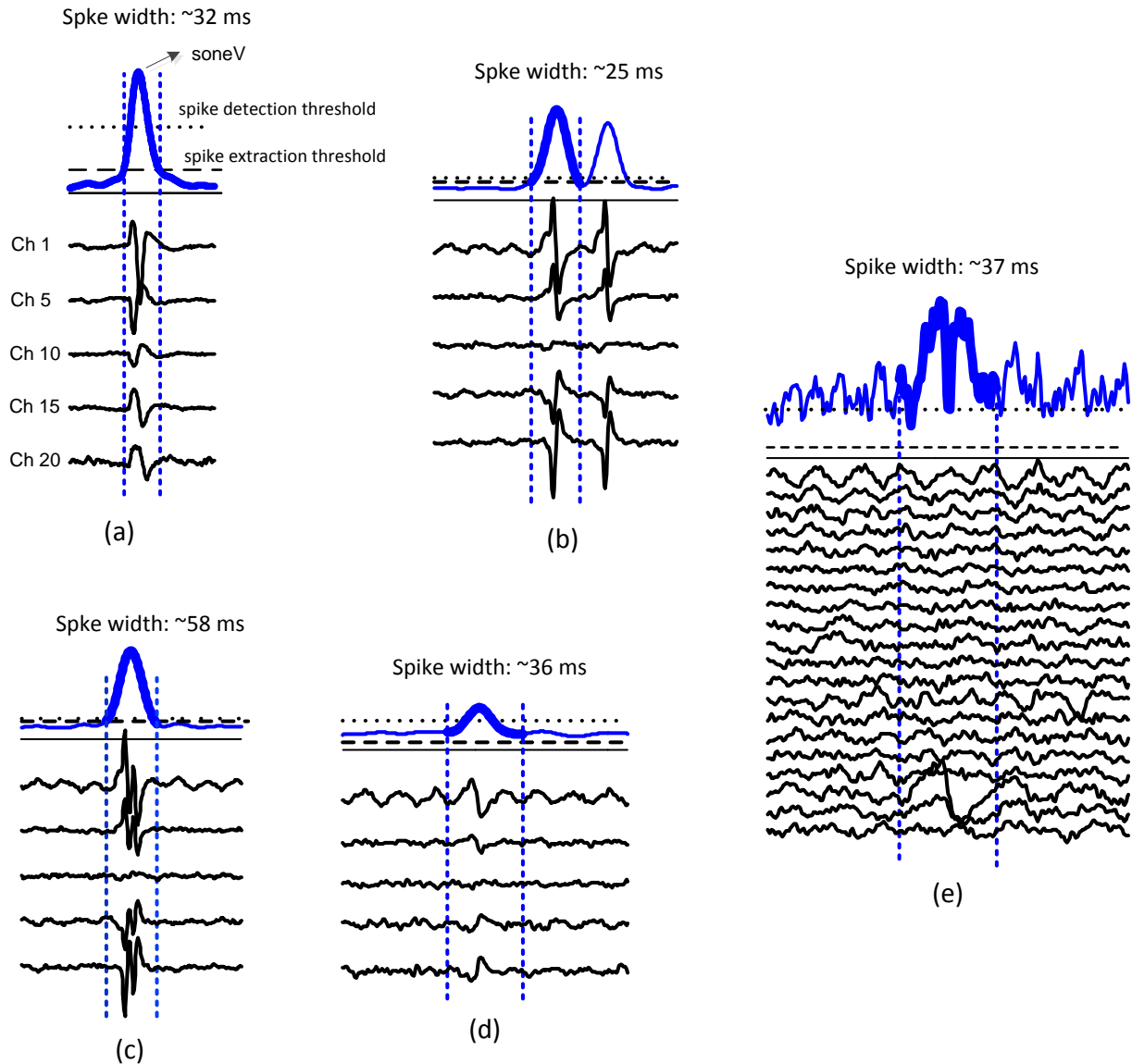


Figure 3: Demonstration of different situations of spontaneous spike detection. (a) the most typical case; (b) detection of two close spontaneous spikes; (c) detection of a complex spontaneous spike; (d) detection of a low amplitude spontaneous spike; (e) a false detection with the soneV signal which can be corrected by examining the raw signals of all the channels.

Figure 3b shows a similar example of two close spontaneous spikes, which can be detected from the soneV signal. Figure 3c shows an example of detection of a complex spontaneous spike. Figure 3d demonstrates that when the signal to noise ratio of the signal is low, the soneV can detect low amplitude spontaneous spikes (most likely originated from motor units deeper within the muscle). In this example, comparing the peak amplitude of the spike

with the spike detection threshold indicates that the detected spike has low amplitude. In addition, the spike extraction threshold, calculated as 20% of the maximum spike amplitude, is even lower than the soneV signal baseline. Thus, the first minima in the left and right lobes of the soneV signal were used to determine the onset and offset of the spike.

Figure 3e shows a false spike detection due to artifact that appeared on a specific channel of the electrode array (channel 18 in this example). Such false detection can be easily excluded by examining the soneV signal, together with the EMG signals on all the channels of the array: this is a function provided by our program.

Figure 4 shows an example of the final spontaneous spike database. Nine spikes out of more than 300 spontaneous spikes are present. In this figure each spontaneous spike is plotted in its own scale because of the large range in amplitude variation. Plotting all of the spontaneous spikes using the same scale would not lead to a comprehensive plot. It is worth noting the polarity changes across the channels, due to the common feedback in the recording system montage.

In general, we observed that the detected spontaneous spikes from ALS subjects have a wide range of amplitude and duration. Figure 5 shows an example of the spontaneous spike detection from several 100 s segments selected from a long recording of 1500 s. For each segment, the firing time, amplitude and duration of the detected spontaneous spikes are described in the 3-dimensional plots. A total of 263 spontaneous spikes were detected from the entire length of the recording, and their amplitude and duration distribution is presented in the right bottom panel of the figure. It is noted that the detected spikes may include slow and random fasciculation potentials, as well as some tonic spontaneous spikes with regular firing patterns.



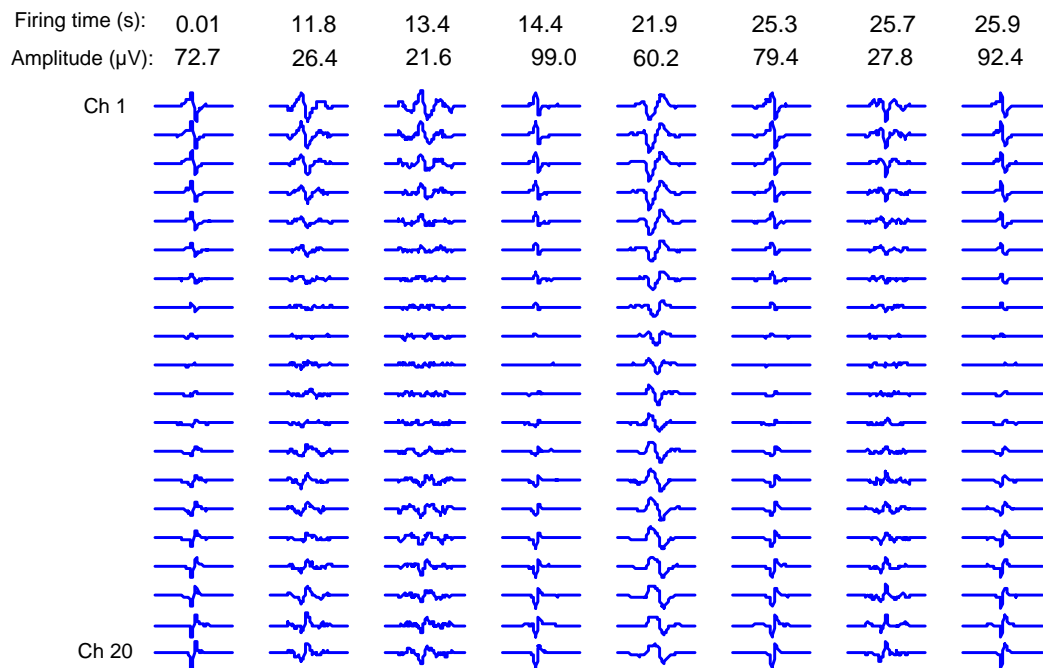


Figure 4: Sample raster plot of the detected spontaneous spikes from the biceps brachii muscle on an amyotrophic lateral sclerosis (ALS) subject using the linear electrode array. The occurrence time and the maximum peak- to-peak amplitude are indicated on the top of each spike.

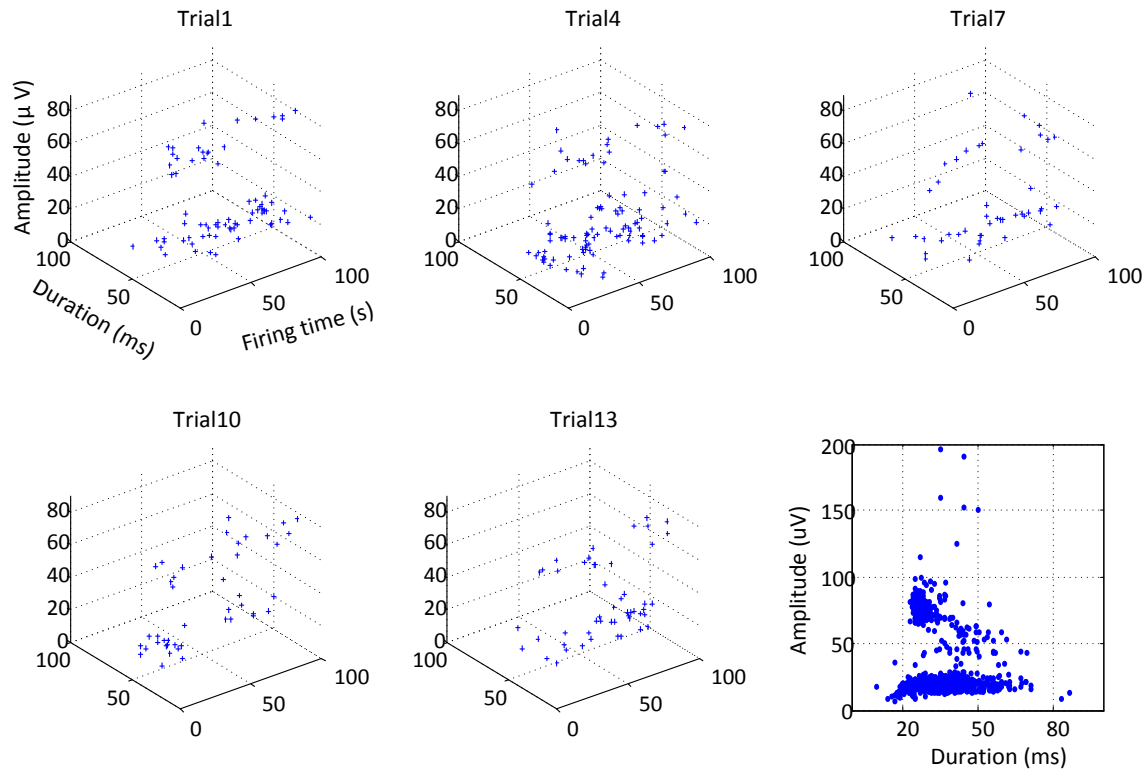


Figure 5: A demonstration of the firing time, duration and amplitude of the detected spontaneous spikes in several 100-second signal segments selected from a 1500-second recording. The bottom right panel shows the amplitude and duration of all the spikes from the entire recording.

## 2.4 Discussion

Since 1957, EMG examination has been routinely used as the primary electrodiagnostic and confirmatory tool for identifying ALS (Lambert and Mulder, 1957). Concentric needle EMG has been applied systematically and prospectively in diagnosing and evaluating ALS. HDS EMG has been emerging as a promising tool to offer additional investigative and diagnostic information (e.g., muscle fiber conduction velocity, motor unit territory, innervation zone localization) in the evaluation of neuromuscular disorders (Masuda and Sadoyama 1987; [Sun et al 1999](#); Zwarts and Stegeman 2003; Merletti et al. 2003; Rau et al. 2004; Merletti et al. 2008). To date it has seen relatively limited use as a clinical tool (Drost et al., 2006).

One major reason may be the complexity of the multiple channel processing imposed by the electrode montage. HDS EMG recording produces a large data set, causing inconvenience in data analysis in terms of memory space and time efficiency, thus constraining its clinical application even when recording from relaxed muscles. Although amplitude threshold based algorithms are often used for spike detection, application of such methods to HDS EMG is inconvenient. For example, thresholding using a specific channel of the array would have missed the spontaneous action potentials on other channels. Because of action potential propagation, the temporal information obtained in a specific channel may not be applicable to other channels. An alternative way is to apply thresholding to all the channels and assign those potentials with close timings to be of the same origin. For a HDS EMG recording this method is not efficient as one would need to repeat the detection process for all the channels.

To promote clinical application of HDS EMG, this study presents a convenient and fast approach for automatic detection and analysis of spontaneous action potential spikes from electrode array recordings in ALS patients. The primary feature of the study was to handle HDS EMG recordings in a simplified manner while preserving the advantage of multiple channel recordings. This was accomplished by transferring the multi-channel data matrix to single dimensional data via calculating the maximum differences across channels of the electrode array. For a differential recording which usually demonstrates polarity changes among the electrodes (as demonstrated in our data because of the common feedback subtraction of the average of all the recording channels), this can emphasize the occurrence of spontaneous spikes. The temporal difference due to action potential propagation along muscle fibers can also be reflected in the constructed one dimensional signal. By this means, our method takes advantage of the electrode array while avoiding computational burden and complexity imposed by multi-channel recordings. From the one-dimensional data, a spike detection threshold can be set to identify

firing times of each spontaneous spike while a spike extraction threshold can be used to define the onset and offset of the spikes. Such information is sufficient to extract the spontaneous spike waveforms from HDS EMG.

To facilitate clinical application, our program also provides convenient user-computer interaction. For example, at the signal preprocessing stage, a user is able to review the overall EMG segment, and exclude any segments with voluntary EMG activity or severe noise contamination. A user can set different threshold levels, according to the specific spike amplitude level of interest. At each step of the spike detection process, the program also provides plots allowing the user to view the results. At the end of spike detection from the last segment of a trial, the plot of final residual signal is provided by setting the detected spikes to zero. Before storing the spikes in the final database, a user can review the soneV signal together with the raw EMG signals on different channels to ascertain that the spontaneous spikes consistently occur on these channels rather than on a specific channel (as typically in the case of artifacts).

The output of our algorithm is a database of extracted multi-channel spikes along with their firing times. In parallel to the needle EMG examination, our algorithm detects the occurrence of spontaneous action potential spikes regardless of their motor unit origins since these would have the same diagnostic significance. The goal in this project was not to develop novel or advanced methods for classifying spontaneous spike waveforms. Instead, we wanted to develop a clinically applicable method to apply HDS EMG. Such a method would promote the clinical utility of HDS EMG. Although classification of action potentials or separation of superimposed waveforms is beyond the scope of this work, the database obtained from this study could be used as the first step for such a purpose. The developed spike detection method can also be applied to voluntary EMG to acquire candidate MUAPs for signal decomposition. The data

presented in this study are from spontaneous muscle recordings from ALS subjects.

Nevertheless, the spike detection algorithm can also be applied to examine spontaneous EMG activity from other patient populations (such as hemiparetic stroke or spinal cord injury).

Finally, although this study used a long recording time to test our method, such a long recording time is usually not required in routine clinical application. With clear conventional evidence of denervation (i.e., fibrillation potentials) in a muscle, detection of a small number of fasciculation potentials may be sufficient to further support the possibility of ALS. Conversely, when clinical and conventional EMG abnormality is limited, a longer duration recording time may be necessary. Thus, the recording time for detecting fasciculation potentials depends on the context of the clinical situation (Mills 2011; Zhou et al. 2012).

## **2.5 Acknowledgements**

This study was supported by the National Institute on Disability and Rehabilitation Research (NIDRR) of the U.S. Department of Education (H133G090093), and the National Institutes of Health (2R24HD050821).

### **3 Sensitivity of fasciculation potential detection is dramatically reduced by spatial filtering of surface electromyography<sup>2</sup>**

Faezeh Jahanmiri-Nezhad, Paul E Barkhaus, William Zev Rymer, Ping Zhou

Bipolar electrode configuration is most commonly used in surface electromyography (EMG) recording because a differential amplifier can eliminate any “common mode” components from the two closely placed recording surfaces. Higher order spatial filtering of surface EMG with an electrode array can further highlight activity of superficial motor units and thus provides a useful approach for single motor unit active y detection using surface EMG (Farina et al., 2003).

However, in this letter we demonstrate that to achieve the best capacity for fasciculation potential detection, as may be used to investigate amyotrophic lateral sclerosis (ALS), a monopolar surface electrode configuration provides a more accurate approach.

Fasciculation potentials may be an important marker in studying ALS (Mills, 2011). They can also contribute to help diagnosis of ALS according to recent consensus of the Awaji criteria (De Carvalho et al., 2008). Fasciculation potentials can be recorded readily by concentric needle and conventional bipolar surface electrodes (Howard and Murray, 1992), which are routinely available in clinical EMG laboratories. Recently, high-density surface electrode arrays comprised

---

<sup>2</sup> Published in Clinical Neurophysiology 125 (2014) 1496–1500

of a number of closely placed tiny recording probes have achieved increasing applications for research laboratory based investigation of neuromuscular diseases, including examination of fasciculation potentials from ALS patients (Drost et al., 2007; Kleine et al., 2008, 2012; Zhou et al., 2011, 2012; Zhang et al., 2013). It is important to optimize the detection of fasciculation potentials for such investigations. In this letter we attempt to quantify the effects of different spatial filtering techniques (which are often used for electrode array surface EMG recordings) on sensitivity of fasciculation potential detection, with the view toward determining the most appropriate electrode configuration.

Eight subjects ( $57 \pm 9$  years; 6 males, 2 females) with definite ALS or probable ALS with laboratory support participated in this study. The study was approved by the local Human Studies Committee, and all the subjects gave their written informed consent. Fasciculation potentials were recorded using surface electrode arrays from 18 muscles in total. These include 10 biceps brachii muscles, 4 first dorsal interosseous (FDI) muscles, and 4 thenar muscles. During the recording, subjects were asked to completely relax their tested arm. After skin preparation, a 20-channel linear electrode array (Fig. 1a), designed and fabricated in our laboratory, was used for biceps brachii muscle recording. The electrode array was placed on the middle of the muscle belly from proximal to distal tendons along muscle fiber direction. For the FDI and thenar muscles, a 64-channel 2D flexible surface electrode array (Fig. 1b, TMS international BV, the Netherlands) was used for recording. The electrode array was placed with one column along the muscle fiber direction. The duration of the resting muscle recording maintained at least 200 s for the biceps brachii muscle and 300 s for the FDI or thenar muscle. The signals were amplified by the Refa128 EMG system (TMS International BV, the Netherlands). Reference electrode was placed near the elbow. The signal was sampled at 2 kHz per channel, with a band pass filter setting of 20–500 Hz. It is noted that for each channel a

common feedback subtraction (average of all the recording channels) was imposed by the system. Because of this system feedback, in this letter, we call such a setting as initial mode (instead of usually called “monopolar configuration”). However, such a common feedback would not have any influence on implementing different linear spatial filters.

All the signal processing was performed offline using Matlab (MathWorks, Natick, MA).

Fasciculation potentials were detected using a previously described algorithm (Jahanmiri-Nezhad et al., 2014). In brief, the algorithm transforms the multi-channel signal to a single-dimensional data by calculating the maximum difference across all channels of the electrode array. Such processing can reduce computational complexity, yet maintain useful information from the electrode array recording as much as possible. A spike detection threshold was applied to the one-dimensional signal (smoothed by a Hamming window) to identify the firing times of each fasciculation potential. In this study, the spike detection threshold was set as 20% of the maximum amplitude of the smoothed one-dimensional signal.

The number of fasciculation potentials was first obtained in the initial mode. Then, different spatial filters were applied. For the linear electrode array, a longitudinal single differential (bipolar) filter and a longitudinal double differential (DD) filter were used for processing. For the 2-D electrode array, a longitudinal bipolar filter and a Laplace filter was tested. Each spatial filter corresponded to an electrode configuration comprised of several neighboring electrodes with different weights, as demonstrated in Fig. 6(a) and (b). The spatially filtered signal was obtained by weighted summation of neighboring electrode recording. The number of the fasciculation potentials was then identified for each spatial filter configuration. Fig. 1c shows an example of EMG recordings using different electrode configurations, which demonstrates that some fasciculation potentials recorded in the initial mode were not observable after the spatial



filtering. Because of this, the number of fasciculation potentials detected was dramatically reduced by spatial filtering of surface EMG.

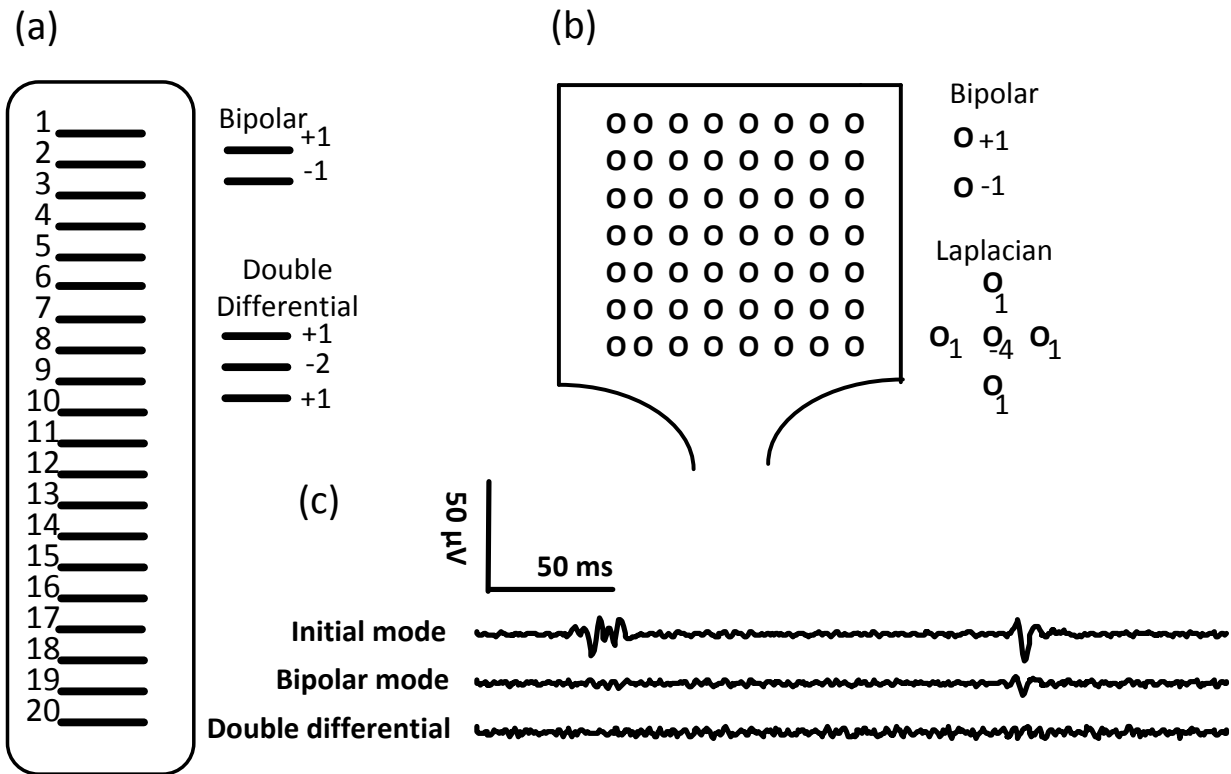


Figure 6: (a) A schematic plot of the 20-channel linear electrode array used for the biceps brachii muscle recording. Each recording bar is 1 mm in width and 10 mm in length, and the inter-bar distance is 10 mm. (b) A schematic plot of the 2D flexible electrode array used for the FDI or thenar muscle recording. Each recording probe is 1.2 mm in diameter, and the center to center distance between two adjacent probes is 4 mm for both horizontal and vertical directions. (c) A comparison of fasciculation potentials recorded from biceps brachii muscle of an ALS subject using the initial mode, the bipolar and double differential configurations, respectively.

For the 10 biceps brachii muscles, the average number of fasciculation potentials detected per 100 s was 149 (range: 13–407). After the bipolar filtering, this number was reduced to 28 (range: 1–75). Calculation of the reduction rate for each muscle indicates that on average 73.7% of the fasciculation potentials recorded in the initial mode could not be captured with the bipolar electrode configuration. The average detection rate per muscle was further reduced by 84.3%

with double differentiation compared with the initial mode. For the 4 thenar muscles, the average number of detected fasciculation potentials per 100 s was 264 (range: 10–545).

Calculation of the reduction rate for each muscle indicates that the average reduction rate of fasciculation potential detection was 53% for the bipolar electrode configuration, and 70.3% for the Laplace electrode configuration, respectively, compared with the initial mode. Similar findings were also observed from the FDI muscle. The average reduction rate of fasciculation potentials per FDI muscle was 47% for the bipolar configuration, and 86.4% for the Laplace configuration, respectively, compared with the initial mode.

We conclude that for robust detection of fasciculation potentials in ALS, spatial filtering of surface EMG dramatically reduces the detection sensitivity and thus should not be applied. The electrode configuration is of the user's construction, and the EMG signal as recorded is influenced by our choice of different electrode configuration methods. How to determine the most appropriate electrode configuration depends on the investigatory objective of the recording. For best capacity of fasciculation potential detection using surface EMG, our analysis indicates monopolar surface electrode configuration should be used.

## **Funding**

This work was supported in part by the National Institute on Disability and Rehabilitation Research of the U.S. Department of Education under Grant H133G090093, in part by the National Institutes of Health of the U.S. Department of Health and Human Services under Grant 2R24HD050821 and Grant 1R21NS075463.

## 4 Spike Sorting Paradigm for Classification of Multi-channel Recorded Fasciculation Potentials<sup>3</sup>

Faezeh Jahanmiri-Nezhad, Paul E. Barkhaus, William Z. Rymer, Ping Zhou

**Background:** Fasciculation potentials (FPs) are important in supporting the electrodiagnosis of Amyotrophic Lateral Sclerosis (ALS). If classified shaped-wise, FPs can also be very informative for laboratory-based neurophysiological investigations of the motor units.

**Methods:** This study proposes a Matlab program for classification of FPs recorded by multi-channel surface electromyography (EMG) electrodes. The program applies Principal Component Analysis on a set of features measured from all channels. Then, it registers unsupervised and supervised classification algorithms to sort the FP samples. Qualitative and quantitative evaluation of the results is provided for the operator to assess the outcome. The algorithm facilitates manual interactive modification of the results. Classification accuracy can be improved toward satisfaction. The program makes no assumption based on occurrence times of the spikes, in accordance with the sporadic and irregular nature of FP firings.

**Results:** Ten sets of experimental data recorded from subjects with ALS using a 20-channel surface electrode array were tested. A total of 11891 FPs were detected and classified into a sum of 235 prototype template waveforms. Evaluation and correction of classification outcome of a dataset with over 6000 FPs can be achieved within 1-2 days. Facilitated interactive evaluation and modification could expedite the process of gaining accurate final results.

**Conclusion:** The developed Matlab program is an efficient toolbox for classification of FPs.

*Keywords*— Amyotrophic Lateral Sclerosis, Fasciculation Potential, Feature Extraction, Principal Component Analysis, Unsupervised Clustering, Supervised Classification.

---

<sup>3</sup> Submitted to Computers in Biology and Medicine

## 4.1 Introduction

Amyotrophic Lateral Sclerosis (ALS) is a progressive, degenerative disorder that affects both upper and lower motor neurons. There is currently no unique marker to diagnose ALS. The crucial factor in ascertaining the diagnosis of ALS is to observe the clinical progression of motor neuron loss from the region(s) of onset, as it spreads to other regions in the body (M. de Carvalho et al., 2008). Active denervation is reflected by abnormal spontaneous activity in affected muscle, which includes fasciculation potentials (FPs), generated from single or multiple motor units (MUs). FPs are detectable by conventional clinical electromyography (EMG). While not necessarily an indicator of denervation, frequent occurrence of FPs in association with changes in motor unit potentials (reflecting MU reinnervation) has been recognized as an important supportive evidence for the electrodiagnosis of ALS (M. de Carvalho et al., 2008; de Carvalho & Swash, 2012, 2013).

Needle electrodes are used to detect spontaneous muscle activity in routine clinical EMG studies. Conventional surface electrodes are limited by their non-selective measurement of the electrical activity of a muscle that may be attenuated by their large size. In the last decade, High Density surface EMG (HDsEMG) electrode arrays have been developed (Drost, Kleine, Stegeman, van Engelen, & Zwarts, 2007; Howard & Murray, 1992; Merletti et al., 2010). This technique has attracted much attention in laboratory-based investigations including examination of FPs, (Drost et al., 2007; Howard & Murray, 1992; Merletti et al., 2010). A HDsEMG electrode contains an array of miniscule recording surfaces spaced closely to one another. The muscle's electrical activity can then be simultaneously recorded by a number of channels. This multi-channel electrode array enhances temporal and adds spatial information and selectivity that conventional surface electrodes lack. A thorough review of surface electrode array EMG analysis and its

advantages compared with concentric needle EMG is described by Farina et al (Farina, Holobar, Merletti, & Enoka, 2010). Zhou et al recently demonstrated that a HDsEMG array can be more sensitive than a needle electrode in capturing FPs from the superficial muscles in ALS patients (P. Zhou, Li, Jahanmiri-Nezhad, Rymer, & Barkhaus, 2012).

Although different FPs, regardless of waveform or motor unit origin, would have the same clinical diagnostic significance, it would be helpful to classify the FPs for laboratory-based investigations. Results of FP classification can be further analyzed to characterize the firing pattern and action potential waveform of fasciculating MUs. Potential applications may include (but not limited to) indirect discovery of their site of origin and distinguishing between FPs that are encountered in the normal population and those associated with pathological processes such as ALS (Fermont et al., 2010; Mills, 2010). These pieces of information can be obtained through classification of FPs into groups of similar waveform shapes.

The task of FP classification is somewhat similar to the task of EMG decomposition, which is the process of breaking down an epoch of voluntary EMG signal to derive its constituent single MU potential firings. In the past several decades, much effort has been focused on EMG decomposition, traditionally with intramuscular needle electrodes. The concept and methods of decomposition in clinical EMG have been reviewed by Stashuk [32]. In recent years, there have been numerous studies on EMG decomposition using surface electrode (Chauvet et al., 2003; Christodoulou and Pattichis, 1999; De Luca et al., 2006; Garcia et al., 2005; Glaser et al., 2013; Holobar et al., 2009; Holobar et al., 2010; Holobar and Zazula, 2004; Kleine et al., 2007; Marateb et al., 2011; Merletti et al., 2008; Nawab et al., 2010; Zennaro et al., 2003; Zouridakis and Tam, 2000). However, available EMG decomposition software, such as Spike2 (Cambridge Electronic Design Limited, Cambridge, England) or EMGLab (McGill et al., 2005) are not

applicable for FP classification, due to different characteristics of spontaneously fired spikes compared with voluntarily firing MUs.

The objective of this study is to design a spike sorting program specific to the unique features of FPs. Some routines in EMG decomposition are adopted for FP classification. However, our classification strategy does not rely on MU firing rate information because of the sporadic character of FPs. In this program, robust unsupervised and supervised classification techniques are combined with facilitated interactive decision making modules. Throughout this process, automatically classified FPs are evaluated in several steps. Erroneous assignments are corrected interactively. Consistency of waveforms in each class is visually examined. In addition to qualitative evaluation, quantitative within-class distance and between-class distances are also examined for the sake of class accuracy estimation. Moreover, performance of the classification is examined using the concept of “two-source” method by applying independently to two non-overlapping sets of channels divided from an array recording. The classification program is tested with FP data sets of ALS patients. Both advantages and limitations of the program are discussed.

## **4.2 Materials and Methods**

### **4.2.1 Experiments**

FPs recorded from subjects with Definite ALS or Probable ALS with Laboratory Support based on El Escorial criteria (Brooks, Miller, Swash, Munsat, & World Federation of Neurology Research Group on Motor Neuron, 2000) are used to test the classification program. Data recording is performed at the second author’s institution and had the approval of the local Human Studies Committee. All subjects are given written informed consent prior to their participation. Subjects are seated comfortably in a regular chair or in their wheelchair, with their

elbow partially flexed and forearm semi-pronated. Subjects are asked to completely relax.

A linear array of 20-channel HDsEMG electrode, designed and fabricated in our laboratory, is used for the recording of FPs in the biceps brachii muscle. The electrode is oriented along the long axis of the muscle fibers such that the center of the electrode array is close to the center of the muscle belly, with the proximal edge oriented toward the muscle's origin and the distal edge oriented toward the muscle's tendinous insertion. Each bar of electrode is 1mm in width and 10 mm in length. The inter electrode distance is 5 mm. The signals are amplified by the Refa128 EMG Recording System (TMS International BV, the Netherlands). The reference electrode is placed on the ipsilateral elbow. Sampling rate is 2 kHz per channel. Band pass filter is set for 20–500 Hz, which can slightly smooth out waveform shapes, but does not affect classification performance. Hardware-based common feedback (average of all available channels) is subtracted from each channel.

In this study, ten data sets of FPs recorded from the biceps brachii muscles of five ALS subjects ( $56 \pm 10$  years; 4 males, 1 female) are presented. The duration of recording ranges from F300 to 2500 seconds, with an average of approximately 1000 s.

#### 4.2.2 FP Classification Program Description

The FP classification program includes the following steps or modules. Prolonged recordings of spontaneous muscle activity are broken down into 100-second epochs. Spike detection algorithm (Jahanmiri-Nezhad, (in press)) is applied to the EMG signal. Extracted FPs are stored in a database along with information of their firing time. Below, we describe the feature extraction, spike sorting, evaluation and interactive modification processes. All programs are coded in Matlab version 7.12 (R2011), the MathWorks Inc.

#### 4.2.2.1 Database of Detected FPs

Prior to classification, FPs are detected using a modification of the algorithm described by (Jahanmiri-Nezhad et al., 2013). This algorithm starts by transforming the HDsEMG multi-dimensional signal into a one-dimensional signal. Amplitude thresholding is then applied to the one-dimensional signal to determine the timings of individual spikes. To construct the one-dimensional signal, the difference between maximum and minimum voltage values across all the channels is used to make a new data point at each time sample. In this study, we use the standard deviation of the EMG data at each sample time across all channels.

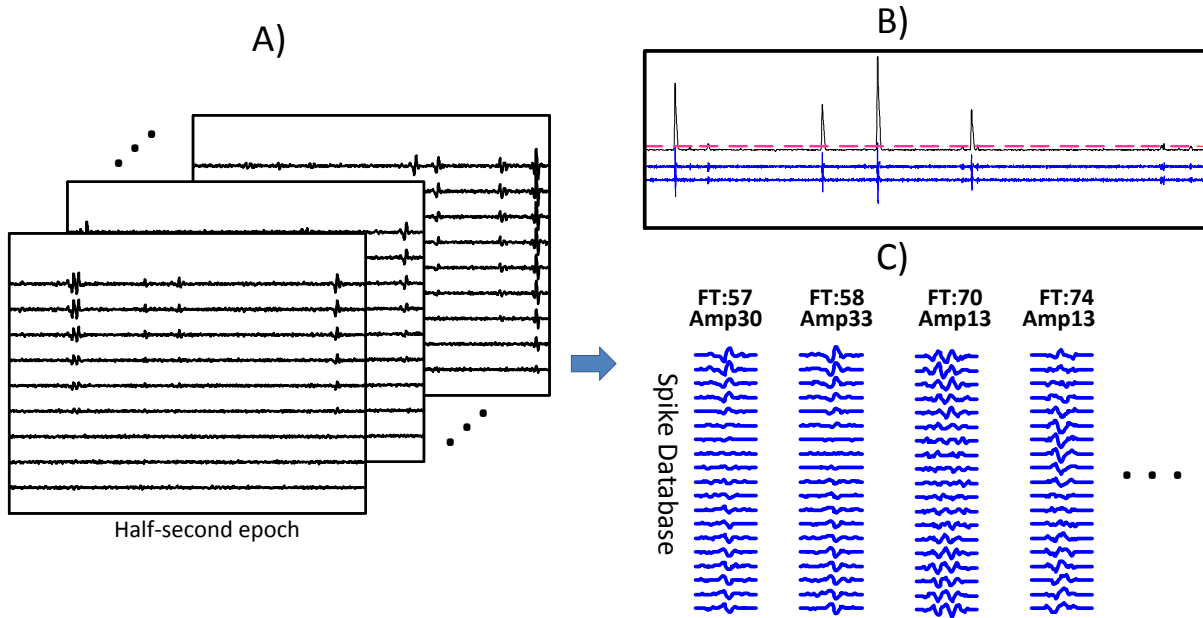


Figure 7: Summary of the spike detection process. (A) shows a sample raw EMG. Half-second EMG epochs containing only 9 channels are shown here. (B) shows an example of amplitude thresholding. The bottom two lines (in blue) are EMG. The spikes on these channels are FPs. FPs are apparent on the rectified black line above that shows the one-dimensional signal. The magenta dashed line crossing the black line is the user-selected threshold. Amplitude thresholding on the black line provides the start and end times of each FP. (C) shows an example portion of a database of extracted FP. Each column represents one FP, where each row represents one channel of recording. 'FT' and 'Amp' refer to "firing time" and "maximum amplitude", respectively.

Although it is a common practice to apply spatial filtering on multichannel EMG data in order to improve the quality of the signal (Merletti et al., 2008), we deliberately refuse to do so,



since it has been shown that sensitivity of FP detection is dramatically reduced after spatial filtering, (Jahanmiri-Nezhad et al., 2014). Figure 7 illustrates the procedure for FP extraction, starting from raw EMG (recorded at rest) at left. At the right panel, a sample database of FPs recorded by the 20-channel electrode array is shown. Firing times and maximum peak-to-peak amplitude across all channels are also reported.

#### 4.2.2.2 Feature Extraction

Regardless of electrode configuration, a matrix ( $[ ]_{nCh \times w}$ ) is used to represent a spike, where ‘nCh’ is the number of channels and ‘w’ is the duration of the waveform (in this work:  $[ ]_{20 \times 55}$ ). Two features from each channel are measured: 1) peak to peak amplitude (polarity considered). Amplitude ‘polarity’ is positive when the negative peak of the waveform comes prior to the positive peak; 2) area under the curve (sum of absolute values). An FP is ‘nf’-dimensional vector, where  $nf = nCh \times 2$ . To increase the efficiency of the feature domain, Principal Component Analysis (PCA) is applied. By selecting only a number of principal components, we can reduce the dimensionality of the feature space, and thus reduce the complexity of the processing. This is especially helpful in HDsEMG recordings where the number of recorded channels is large, or when the sample size for classification is relatively small. In general, in parametric methods (i.e. methods involving any type of Expectation-Maximization, including Kmeans and Gaussian mixture model estimation), relative number of samples to number of parameters has to be sufficiently large for reliable density estimation. However, in experimental data, the number of samples is usually limited. Efficient dimension reduction strategies are very helpful in this regard. For PCA implementation, first the dataset in feature space is built as a matrix  $feat-Data = [ ]_{N \times nf}$ , with N number of FP samples. Covariance matrix of ‘feat-Data’ matrix is computed,  $cov_{feat-Data} = [ ]_{nf \times nf}$ . Eigen-decomposition is applied on the covariance matrix. Data

samples transformed by the eigenvector corresponding to the largest eigenvalue hold the highest variance. This can be the most discriminative feature for classification purpose. We can choose one, two, or ‘nf’ principals to transform the data. As the dimensionality of feature space increases, the condition number of  $\text{cov}_{\text{feat-Data}}$  matrix is checked. A too large condition number will lead to an ill-conditioned covariance matrix, which in turn impairs the reliability of PCA. In theory, a ‘too large’ condition number is defined when the logarithm of the condition number is larger than precision of entry data. In this study, to optimize the PCA, the dimensionality of feature space does not exceed a value that causes the condition number to surpass 1000. A five dimensional space is usually chosen for the 20-channel data in this work.

#### 4.2.2.3 *Unsupervised Clustering Strategy for FP Classification*

The K-means technique (built in Matlab Statistics Toolbox) is used for the initial attempt of spike sorting. Number of classes and initial seeds (initial estimate of class templates) are required. To assist with the estimation of number of classes, FPs are plotted in 3D space using the first three principal components (an example is shown in Figure 4, Panel C). The plot (partially) demonstrates how the data are scattered, so the number of clusters may be estimated. Overestimation is preferable to underestimation at this stage. The former can be adjusted later by cluster combination. ‘Underestimation’ would lead to erroneous classes, which is undesirable. The initial seeds can be picked randomly (default) or selected manually. Once K-means is applied, the first set of clustered FPs is ready. The members of each class are then visualized in their waveform format, in separate plots. A good performance would be easily recognizable by overall consistency in waveform shapes within each class. If the overall outcome is poor for most of the classes, input parameters, which may include feature set dimension, initial estimate of class numbers, or distance metric, are modified. Then, the clustering step is repeated until the

overall output is reasonable. The variables ‘Cluster’ and ‘Label’ are adjusted accordingly afterwards. The variables are described in table 1.

Table 1 \_ Variable description

Variable	Description
$K$	Number of classes. This number gets updated throughout the process.
<i>Cluster</i>	Type: ‘structure’. It stores member indices assigned to each class. It also flags which indices may be used for measuring the template of the class.
<i>Label</i>	A vector storing class index of each FP.
<i>Label-0</i>	Refers to unlabeled FPs.
<i>Label-1</i>	Trash Bin. Refers to erroneous samples detected as FP, or waveforms with too small SNR.
<i>Template</i>	Prototype waveform shape of a class.
<i>template</i>	Prototype of a class in feature space.

#### 4.2.2.4 Visually Aided Evaluation and Refinement

The objective of this step is to make each class as accurate as possible. For this purpose, each class is visually examined and refinements are made as necessary. Class examination starts by first illustrating members of each class by their waveform shape. A class is either overall accurate (members’ waveform shapes are consistent) or inaccurate (there are too many inconsistencies). In the latter instance, if there are too many low-SNR or erroneous waveform shapes, the whole class is assigned to Label-1. If the cluster is composed of two or more patterns of data, then that class requires another round of clustering.

When the class is overall accurate and the number of erroneous assignments is minimal, ‘Interactive Class Refinement’ module is called up to remove inconsistent assigned samples. In

this module, there are four possible options to modify the status of each assignment. For each assigned member, the four options include: 1) accept and include in class template measurement; 2) accept but not include for class template; 3) move it to Label-0 group; or 4) move it to Label-1. The second option refers to correctly assigned members that for some reason (e.g., superimposition with other waveforms, unexpected noise on some channels, or misalignment of the waveforms compared to other members of a class) are excluded from computing class template shape. Figure 8, panel A, shows a sample plot by this module. Waveforms belonging to one class are plotted side by side. Members of a class are illustrated in a default number of 25-sample group at a time. The entire group can be Accepted/ Rejected, or individual samples can be modified one-by-one. For this purpose, the screen is divided into four regions by dotted lines, corresponding to options 1 to 4. The user can click in a particular region to select the appropriate option for a sample. The program will re-adjust the 'Cluster' and 'Label' variables accordingly. .

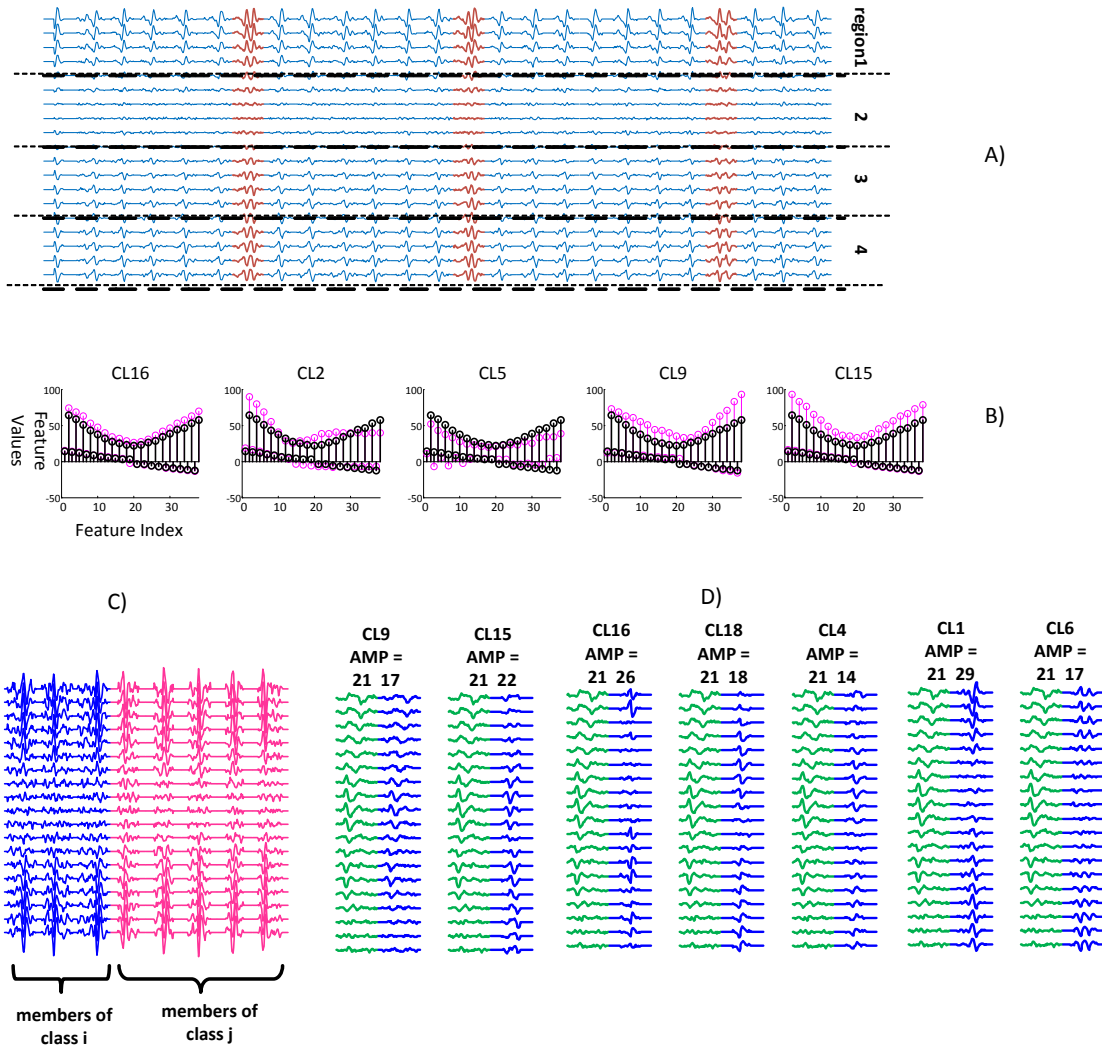


Figure 8: (A) Sample plot of 'Interactive Class Refinement' module. FPs are plotted side-by-side. Each column represents one FP. Four options are integrated in the screen by the four regions. In this example, three samples (in different color) can be identified with inconsistent waveform shapes (case of superimposition). Clicking in region2 would exclude them from computing the template of this class, and clicking in region3 would remove their membership and assign them to L-0. (B) Sample plot of templates proposed to be similar to the template of the class of interest (in magenta color). (C) Up to five samples from the to-be-merged classes are plotted side by side, providing a visual aid for the user to determine whether to combine the two classes or not. (D) A multi panel plot. Each panel shows the to-be-classified sample (in green, left) along with the template of candidate class (in blue, right). Amplitude information is also included. The sample may be assigned to one of the classes, be left unassigned, be sent to Trash, or open a new class.

After modifying classification results, it is usual to find two or more classes with almost identical waveform templates. This is primarily due to the initial overestimation of class number and presence of noise. Such classes need to be merged. Inter-cluster distance matrix is used to provide an initial list of potential twin classes. A plot of potential twin classes, in feature space, is provided which assists to narrow down the list, such as in Figure 8 panel B. Furthermore, the candidates are investigated in their waveform shape format to make a firm decision about merging, such as in Figure 8, Panel C. Variables ‘K’, ‘Cluster’ and ‘Label’ are updated, if a change has occurred. Another round of ‘Interactive Class Refinement’ module is called up for final refinement of the combined classes.

#### *4.2.2.5 Final Supervised Classification*

In the previous step, the goal is to make each class as accurate as possible. Uncertain samples are left unassigned. Now in this final step, classification decisions are made for the remaining unlabeled samples. In this step, class templates are known, whereas in step 1 (unsupervised clustering) such knowledge is unavailable. Therefore, the assignment of remaining samples can be made through supervised classification. A classifier is trained based on discriminant analysis (linear or quadratic) technique using thus far classified samples as training data. Theoretically a sample should be assigned to the closest class (minimum distance). However, since we deal with ‘difficult to classify’ spikes in this step, the waveform shapes of a sample and the candidate class template are visualized before any decision is made.

The algorithm pulls samples with Label-0, and finds the closest classes to each sample. In a first attempt, a few waveforms from each class along with all of the potentially new members are plotted side by side. The user can interactively “accept” or “reject” the classification (as shown in Figure 10). In a second attempt, yet unlabeled samples are examined

individually. An FP waveform is plotted along with candidate class templates, such as in Figure 8 panel D.

#### *4.2.2.6 Quantitative Evaluation of Relative Class Consistency*

A quantitative measurement is provided to the user, as a supplement to qualitative visual evaluation. As a measure of internal consistency in each class, within-class distance ( $S_W$ ) is measured and compared to between-class distances ( $S_B$ ). An ideal classification has a large  $S_B$  compared to  $S_W$ . This means that the classes are well separated from each other, while members of a class are compactly close to its center (i.e., similarity between members of a group is relatively high and similarity of members of different groups is small). Euclidean distance between members of a class and class template are measured and averaged, leading to  $S_W$ . Euclidean distance between templates of all possible pairs of classes are also measured and stored in the matrix  $S_B$ . For each class, a more-than-unity ratio of  $S_B/S_W$  is desired.

#### *4.2.2.7 Examination of Reproducibility; Two-source Method Comparison*

The program involves the operator in modification of the outcome. In an attempt to evaluate the reproducibility of the final outcome, the set of 20-channels data is divided to two non-overlapping 10-channels sets. Set1 refers to data on channels 1-10, and set2 refers to channels 11-20. The program is applied on set1 and set2, and the results are compared. The number of clusters might vary between the two sets. This is partially because of possibly high similarity of different waveforms, when the number of channels is reduced. Class labels of corresponding samples do not necessarily match. The only known variable is the index of class members. For each class, from the set of results with lower number of classes, we examine the corresponding labels from the other set of results. The most frequent label is determined,  $L_f$ . We

quantify the accuracy of the result for that class, by the ratio of number of members with  $L_f$  to the total number of members. At the end, we average the accuracy ratios of all the classes.

### 4.3 Results

FPs are extracted from spontaneous electrical activity in the biceps brachii muscle recorded by linear array HDsEMG electrode from subjects with ALS. The extracted spikes are stored in a database along with their firing times. Feature selection, initial unsupervised clustering, interactive evaluation and refinement, and final supervised classification steps are applied to the FP database.

One example set of results, on dataset ‘5-2’ in Table 2, is partially presented in Figure 10. The raw EMG of this data set -on a single channel- is presented in Figure 9. It is essential for the user to examine the whole length of recording to ensure that there is no unwanted voluntary muscle activity. Further discussion on presence of voluntary activity during spontaneous activity recording is presented in section 4.1. Illustration of the whole length EMG on all the channels is not feasible. Only one channel (where amplitude is high) is depicted here.

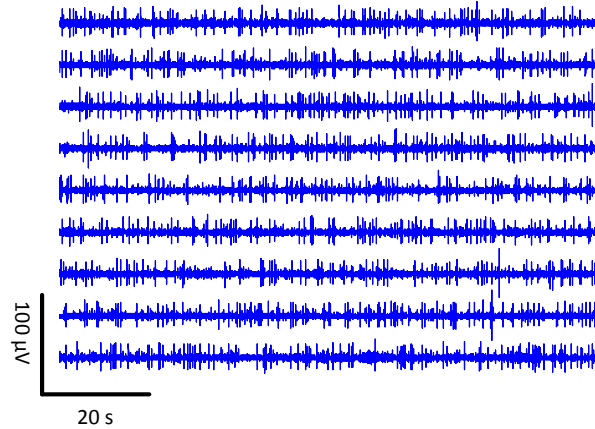


Figure 9: Single channel raw EMG corresponding to data presented in the result section. Each trace shows 100 s. Total recording time is 900 s.



The outcome of each step described in the method section is illustrated in Figure 4. A total of 749 FPs are detected. Panel A shows an FP in its waveform format, a sample outcome of spike detection algorithm. Panel B shows selected feature values. From each available trace of a multichannel FP, the peak-to-peak amplitude and area under the curve are measured. The blue thin circles represent the amplitude and the thick dark circles represent ‘area’ under the curve. Whole feature space in the first three components after PCA is depicted in panel C. Panel D refers to the same dataset after initial clustering and its refinement. Not all samples are included here. Panel E shows templates of each class (not all classes included). Panel F shows the final outcome of classification.

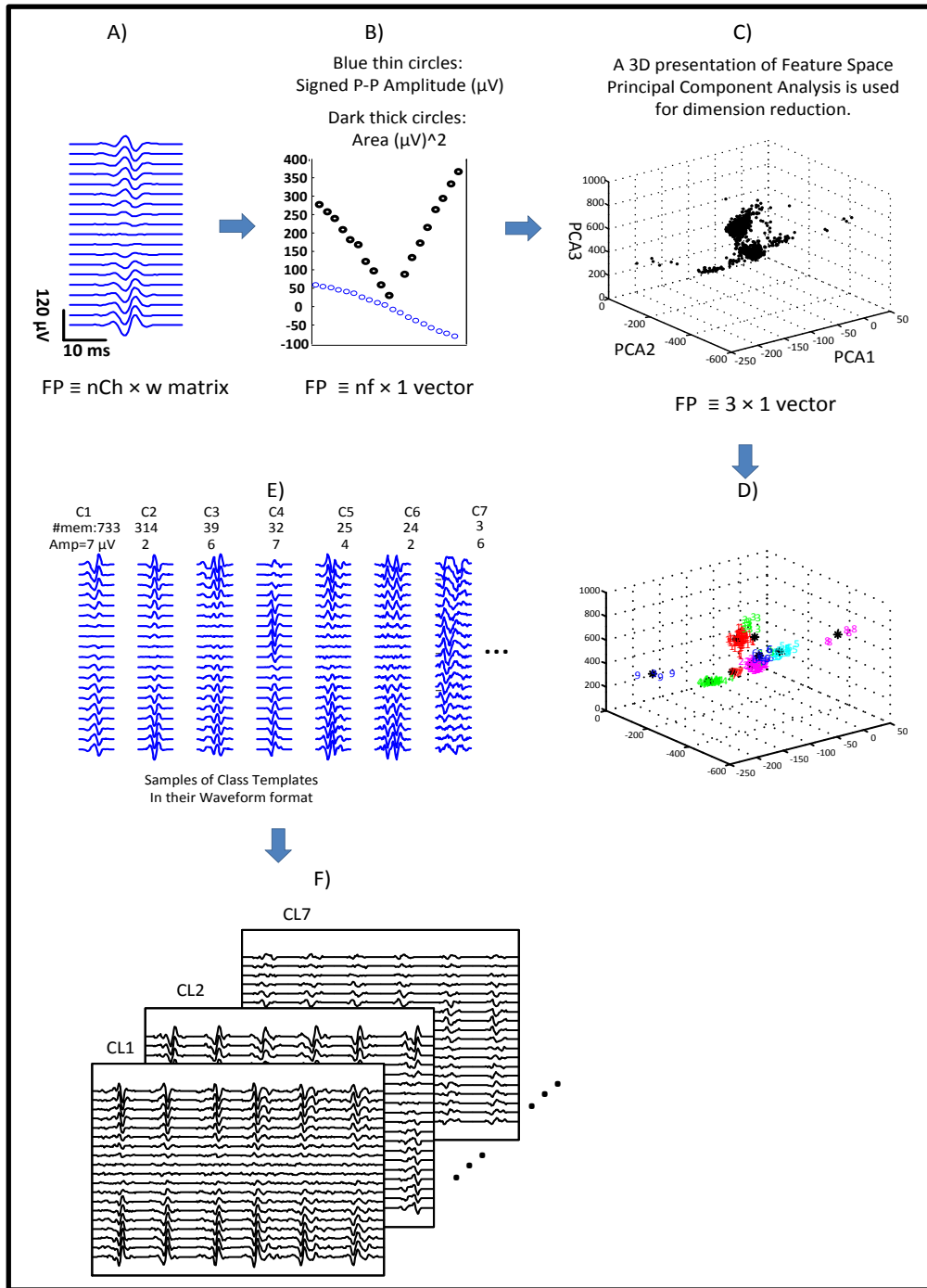


Figure 10: An illustration of outcome results in a classification process. (A) shows an example outcome of spike detection. (B) refers to feature space. (C) shows the first three principal components of whole feature space. (D) shows the result of initial clustering algorithm (color coded) after evaluation and refinement of classes. (E) shows parts of the FP templates in their waveform shape. (F) shows groups of sample FPs assigned to each class. Further analysis of FP shape and firing pattern can start from here.

Quantitative evaluation of classification performance is also computed. Averaged SB/SW for each class with respect to all other classes are measured. The averaged mean is again

averaged across all classes and reported in Table 2. Furthermore, averaged accuracy following two-source method is reported along with yielded number of classes.

Table 2 \_ Summary of classification outcome

DataSet (Subject index)	Duration in seconds	# of sample	# of Label-1	# of class	Ave S <sub>B</sub> / S <sub>w</sub>	2source Method Consistency( %)
1	900	479	2	24	21	89
2	900	632	30	57	33	80
3	500	583	196	33	29	70
4-1	300	205	2	12	9	94
4-2	900	1234	0	13	9	96
4-3	2500	6894	21	58	2	62
4-4	800	657	8	8	9	93
5-1	700	209	8	13	67	97
5-2	900	749	5	18	7	95
5-3	1500	249	1	3	9	99
Total: 10	Ave: 990± 615	Ave: 1189± 2028	–	–	Ave: 19.5± 19.5	Ave: 87.5 %± 12.6

Overall, the number of waveform classes varied from 3 to 57. A large number of classes refers to high variability of FP shapes and might indicate for very unstable membrane potentials at multiple locations. Within-class to Between-class distance ratio is always above 1, and the average value ranges from 2 to 67. Reproducibility of the outcome is tested with two source method, and accuracy ranges from 62 to 99%, with an average of 87.5%.

#### 4.4 Discussion

Ten sets of fasciculation potentials, collected from subjects with ALS, are tested for spike sorting with our proposed program.

The results reveal that on average only one or two classes are continually firing over the course of recording. The frequency of most other classes is much lower. This fact might explain the complexity of the classification problem from a mathematical point of view. To partially show the heterogeneity of class sizes in FP data, the FP classes are categorized to single classes, classes with 2-9 members, classes with 10 to 99 members, and classes with above 100 members. A summary of class size shows that, on average, there are 7 classes with only one member, 9 with 2-9 members, 6 with 10-99 members, and only 2 classes with above 100 members. Further investigation is needed to understand this phenomenon, which may or may not be related to the site of origin of FPs.

#### 4.4.1 Presence of Voluntary Activity

It is very common that over the long period of spontaneous EMG recording, short periods of voluntary activities show up, due to slight movements of the subject. Before deriving any conclusion over firing pattern of an FP class, it is necessary to examine the inter-discharge interval histogram of the class. Interval histogram can be cautiously inspected for any evidence of voluntary recruitment. Corresponding potentials should be excluded from further analysis of FPs. As Figure 9 shows an example, in this study, raw EMG is inspected before FP detection step. Any epoch of voluntary activity is excluded manually. Voluntary activity is usually easily recognizable from spontaneous activity. Unlike sporadic nature of FPs, voluntarily recruited motor units have a regular firing pattern.

#### 4.4.2 FP Classification vs. EMG Decomposition

EMG decomposition is an inverse process of EMG signal generation, which breaks down the EMG signal into the contributions of different MUs. For EMG decomposition, different

classes of waveform potentials indicate that they are from different MUs. In contrast, the number of different classes of FPs does not necessarily indicate that each class belongs to a different MU. This is primarily due to the fact that FPs may arise from different places at the distal branching near the muscle fibers, and hence have different shapes. In that case since they all share the same alpha motor neuron (same anterior horn cell), they belong to a single MU by definition. .

The concept and methods of EMG decomposition have been developed in the past 4 decades (see a review by Stashuk, 2001). The discharges of FPs are much less frequent than those of voluntarily activated MUs. Therefore, waveform potential superimposition is a less challenging problem. Template-based clustering is then appropriate for FP classification purpose. Conversely, as a consequence of lower firing frequency of FPs, a long duration of EMG recording time (in the order of minutes or longer) might be necessary to be able to capture a sufficient number of FPs. Analysis of long recordings with a large number of traces using HDsEMG is computationally costly, if performed on raw data, which is a common approach in many of the available EMG decomposition toolboxes. Also, a classification paradigm is needed that does not rely on firing time of spontaneous spikes. This is because FPs discharge randomly, in contrast with regular firing of voluntarily recruited MUs.

Furthermore, high variability in FP waveform shapes makes accurate classification hard. High variability in waveform shapes causes overlaps among different classes of FPs in feature space. It is known that even waveforms of voluntarily recruited MUs in healthy subjects vary over time, measured as jiggle (Stalberg and Sonoo, 1994). The variability in voluntary motor unit potential comes from slight variations in inter-discharge interval times of two consecutive muscle fiber action potentials. Since a motor unit potential is the summation of all muscle fiber potentials, consequently, the motor unit potential shape changes slightly as well. By ‘high variability of

waveform shapes among FPs', we refer to the fact that FPs come from (electrically) unstable membranes, and the site of instability might vary throughout time. FPs might fire from different dendrites' terminal branches at different times from within one single MU. These may lead to variation of waveform shapes even for FPs belonging to a single MU. From a classification perspective, the distribution of data may not have a clustered shape and data are spread all over the feature space. Visual interactive modification module designed in this work aims to help with difficult-to-classify samples.

#### 4.4.3 Previous Works

Although considerable work has been reported on decomposition of HDsEMG, classification of spontaneous spikes recorded for long duration of time has only been approached in limited number of studies. Drost et al.,(Drost et al., 2007), reported HDsEMG recorded FPs and illustrated the value of 2D spatial information in discriminating different waveforms. However in this work, only one set of data was analyzed using a previously developed EMG decomposition technique, (Kleine et al., 2007).

Another work of FP classification is performed by Winslow et al,2009, which focused on classification of 24hour-long EMG (at rest) from paralyzed hand muscles of subjects with spinal cord injury. However, their technique was designed for two-channel EMG data. An average of approximately 3000 spontaneous action potentials were detected, which required about 17 days to be fully classified, with 5 hours of segmentation, 1 day for clustering, 10 days for manual evaluation and 5 days for finalizing the classification. It was claimed that it would take up to two years for each dataset to be classified with a fully manual approach. In contrast, the current study demonstrates relatively good efficiency of FP classification time-wise. Spike detection and

first round of clustering take seconds to be complete. Modification of the results might take up to 1-2 days for a database with thousands of FPs.

#### 4.4.4 Choice of Unsupervised Clustering Technique

Unsupervised clustering (classification of a data set without *a priori* information about the number of classes or their shape) is applied to the data. Existing techniques for clustering are numerous, including parametric, non-parametric, iterative, or hierarchical methods (R.O. Duda, 2001). In general, no clear evidence exists about superiority of one clustering algorithm over another (B. Liu, 2007). Nevertheless, depending on the nature of the data, one technique might be preferable to others. Here, the K-means algorithm is selected for clustering the FPs. K-means technique has been widely used in many applications. It is computationally faster than hierarchical methods, when the number of variables is large. However, K-means has poor performance on non-hyper elliptical datasets (B. Liu, 2007). Feature selection plays a key role in performance of the clustering task. If the K-means method fails to correctly separate among the groups, then another approach needs to be sought for. We found Gaussian Mixture Model (GMM) clustering algorithm –also integrated in Matlab- very efficient in such cases. However, GMM fails to operate on classes with rather small sample size, especially if feature space dimension is large.

It is acknowledged that more automated clustering techniques needs to be attempted here. Combination of K-means with another clustering technique is one example, as shown by Takahashi et al., 2003, where each class obtained from the K-means is split and later (similar ones) are agglomerated to overcome the problem of overlapped classes. Meanwhile, a careful visual assessment of the results may always be necessary.

#### 4.4.5 Feature Extraction

Choosing discriminative features plays a key role in classification performance. In intramuscular needle recordings, features measured from motor unit potentials usually includes amplitude, duration, area, number of phases, number of turns, etc. (Sonoo & Stalberg, 1993). Those features are usually less useful for surface recordings, due to the low-pass filtering effect of the skin and subcutaneous body tissues on the EMG signal. Visually inspecting many experimental data, we believe that distributions of amplitude and area across all the channels are appropriate features.

#### 4.4.6 Applications of FP Classification

From a clinical electrodiagnosis perspective, the question of interest is solely presence or absence of FPs in an examined muscle. However, FPs are not yet fully understood, De Carvalho and Swash, 2012, as to their origin and pathophysiological significance. Hence further investigation of FPs is certainly warranted.

FPs firing pattern and waveform shapes can both provide additional diagnostic and investigatory information. A potential application is the discrimination between FPs observed in healthy population and those observed in pathological conditions such as ALS, for example as described by Mills, 2010. Discovering a discriminatory feature between the two groups would be very valuable, but first it necessitates understanding the origin site of these spontaneous activities. As described by Wettstein, 1979, these investigations go back to 1936, when Denny-Brown and Pennybacker defined FPs as originating from the anterior horn cell in the spinal cord. This finding has been challenged since then, and the body of research shows that FPs might arise from a cortical origin, as well as from the distal or proximal portions of the lower motor neuron. Some FPs are shown to be driven as by cortical magnetic stimulation (summarized by DeCarvalho and



Swash, 2012). Most of these studies use invasive techniques; however, HDsEMG has also been investigated to examine FPs (Drost et al., 2007; Kleine et al., 2008; Kleine et al., 2012). Kleine et al., 2008, investigated firing time of a (fasciculating) MU, specifically the Inter-Discharge Interval (IDI) histogram, believing that IDI histogram is a marker of membrane excitability property. The authors examined the IDI histograms of different FPs and concluded that both neuronal and axonal evidences exist among ALS population.

The waveform shapes are also discussed in terms of diagnosis by Drost et al., 2007, which still needs further investigation. FPs can be also studied in conjunction with drugs, since certain medication (e.g. cholinergic drugs) can affect their firing (Drost et al., 2007). FPs, as a neurologic symptom, are not limited to ALS and may also appear in different neuropathic disorders.

#### 4.4.7 Time Consumption to Provide Accurate Results

Our paradigm design applies the fast and simple K-means technique, which requires only seconds for even the longest dataset. The validation and refinement section takes the most time in this process. Usually for datasets of less than 500 samples, the refinement process may take up to one to two hours (depending on the signal's ambiguity). Usually, the required time for validation increases as the number of samples increases (i.e. above two or three thousand). Using this toolbox, and depending on the nature of dataset, it could take a user about 2 days to modify the results of classifications when the number of samples is greater than one or two thousand(s) spikes. This is still faster than the aforementioned 10 days by Winslow et al (Winslow, Dididze, & Thomas, 2009).

A major factor affecting the speed of modification step is the 'cleanliness' of the waveforms. Waveforms from a 'clean' EMG signal are typically more distinct from each other,

and consequently the initial results are more accurate and minimal further modification is required, if any. Recordings of low SNR, or presence of a considerable amount of superposition, will lead to greater uncertainty in classification. The “noisier” the signal, the greater the interference between corresponding samples of individual classes. This leads to feature space becoming non-hyper elliptical. This in turn leads to poor performance of the K-means algorithm, and prolongs the process of refinement.

Managing large data sets increases the evaluation and modification process, making it tedious. A large number of spikes in a dataset usually correlate with the detection of many small amplitude low SNR samples. Depending on the application of a study, such potentials may not be of interest and can be quickly excluded from the dataset. A reduction in data size simplifies analysis. However, when all the spikes need to be included, one approach dealing with large data size is to divide it into smaller sets. The results from each subset can then be combined and matched to provide the global output.

#### 4.4.8 Visually-aided Classification

A key advantage of this program is visualization of multi-channel waveforms to facilitate interactive decision making. A user is able to observe an unlabeled waveform along with other members of a class, and waveforms of other classes and make classification decisions.

Manual spike sorting is often used by a user expert in EMG techniques. Nevertheless, relying solely on observational or qualitative investigation can lead to erroneous classification due to human vision artifacts. Therefore, visually aided classification has both advantages and limitations. Human visual error typically occurs when two FP samples are very close in shape: comparison of waveforms across all channels is not always straightforward. One effective step to alleviate this issue is the sizing of displayed images of FPs on the screen. Default size of a figure

in Matlab has fixed square borders. If number of waveforms in a figure is relatively high, then waveform shapes will look compressed, and if number of waveforms is small, their shapes will look stretched out. In both cases, it is visually hard to assess the waveforms. So at each plot, the user would need to change the borders of the plot to change it to a proper size. To avoid this display problem, our toolbox automatically sets the size of a figure (width and height) based on a fixed maximum number of waveforms for each figure (width) and the number of channels (height). . This circumvents the risk of “visual artifact”, and expedites the evaluation process.

## **4.5 Summary**

This study tackles the problem of classification of fasciculation potentials (FPs), which are important for electrodiagnosis and investigation of Amyotrophic Lateral Sclerosis (ALS) or other neuromuscular diseases. Beside only their detection, examination of their detailed time course and waveform shape can shed light on their origins. A paradigm for classification of FPs was developed and tested with surface EMG data recorded from ALS patients using a 20-channel linear electrode array. The paradigm includes individual FP detection, feature extraction, and spike classification. The distributions of spike ‘amplitude’ and ‘area’ across all the existing channels were measured from FP waveforms to build the initial feature space. Principal component analysis was applied for the purpose of feature space dimension reduction. For spike sorting purpose, existing built-in Matlab unsupervised and supervised algorithms were used, such as Kmeans, GMM, and Linear Discriminant Analysis.

The key feature of our design was the development of visually-aided interactive modules for step-by-step evaluation and modification of classification results. The spike sorting process started by employing unsupervised ‘K-means’ clustering algorithm. The results were evaluated and modified through our facilitated user interactive modules. Supervised ‘Linear Discriminant’

function was then applied to classify thus-far unassigned samples, in a ‘controlled’-manner. Accuracy of classification was therefore visually inspected. Quantitative measure of class consistency was also provided.

Overall, accuracy of classification can potentially be improved toward satisfaction, through the interactive modification modules. From 10 sets of data, a total of 11891 FPs were detected, and classified into a sum of 235 prototype template waveforms. The final output was reproducible, tested by two-source method. Evaluation and correction of classification outcome of a dataset with over 6000 samples was achieved within 1-2 days. We observed that number of FP prototypes can be very large, but on average only 1-2 of the classes were continually firing over the course of recording. The result of this work facilitates further investigation on examination of FPs, such exploration of their site of origin.

## **4.6 Acknowledgement**

This study was supported by the National Institute on Disability and Rehabilitation Research of the U.S. Department of Education (Grant H133G 090093) and the National Institutes of Health (Grant 2R24HD050821).

## **5 Innervation Zone Analysis Of Fasciculating Motor Units In Als Using A Linear Electrode Array**

Faezeh Jahanmiri-Nezhad, Paul E Barkhaus, William Zev Rymer, Ping Zhou<sup>4</sup>

Abstract— In this study, fasciculation potentials recorded by linear array surface EMG from amyotrophic lateral sclerosis (ALS) subjects were examined. The Innervation Zones (IZ) of their originated motor units were estimated. The information was compared with that obtained from voluntarily recruited motor units in the same set of ALS subjects as well as in healthy controls. IZs within an ALS subject were found more scattered, versus more centrally clustered IZs in healthy subjects. IZs were even more scattered among fasciculating motor units. A more scattered IZ distributions among ALS subjects can be the result of muscle reorganization due to the ongoing denervation/reinnervation process. Three ALS subjects had repetitive visits, providing longitudinal data of FPs, where an increase of IZ distribution was observed for at least one instance in all the three subjects. Results and limitations of surface EMG are discussed.

---

<sup>4</sup> Ready for submission

## **5.1 Introduction**

### **5.1.1 Motor Unit and Motor Unit Potential**

An alpha motor neuron originates from spinal cord and innervates a number of muscle fibers via neuromuscular junctions. This framework is called a motor unit (MU). Motor units are structural and functional building blocks of a muscle. Central nervous system controls muscle contractions through different MU activation patterns. Information is transferred from the nervous system to a muscle via action potentials. An action potential is a wave of temporary ion transportation across cell membrane due to a stimulus impulse (or excitation) to the resting membrane potential. An order of muscle activation is delivered to the muscle when repetitive action potentials pass neuromuscular junction gap (NMJ) and reach the corresponding muscle fibers. Neuromuscular junction refers to the synapse between a nerve ending and the closest site of a muscle fiber membrane (called postsynaptic membrane). Neurotransmitters, mainly acetylcholine, are the main players for the depolarization of postsynaptic membrane, which in turn is the key factor to excite the muscle fiber. An action potential will fire on the muscle fiber at the site of NMJ and propagates along the muscle fiber in opposite direction toward the muscle tendons, as in Figure 11. Once there is a means of recording, the sum of all muscle fiber action potentials (MFAPs) within a MU will be recorded on the electrode, called a motor unit potential (MUP), as in Figure 12. Although the shape of an action potential (including MFAP) typically has depolarization, repolarization, and refractory period phases, during an Electromyography (EMG), at the site of detection, the shape of recorded waveforms depends on both physiological

and non-physiological factors [Farina] including the type of the electrode and its relative distance to origin site of excitation.

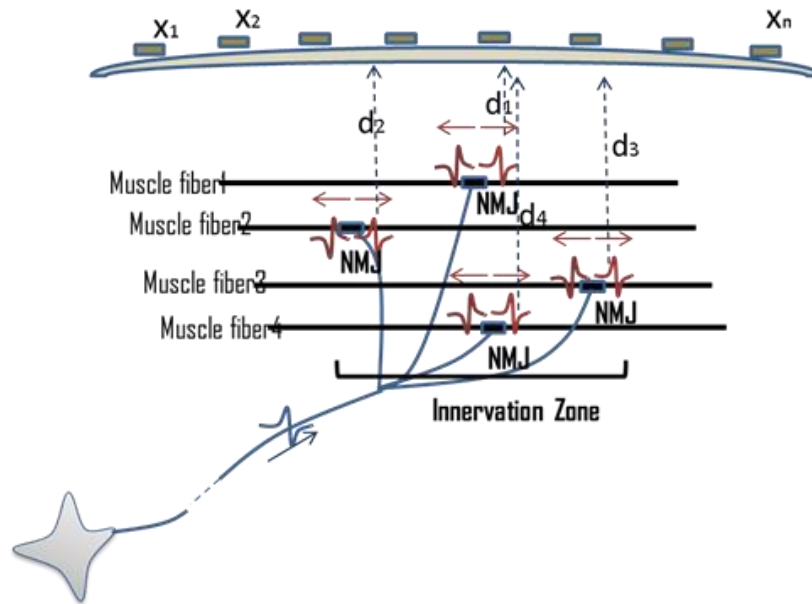


Figure 11: Schematic of a MU. Distribution of NMJs along muscle fibers is shown. On top of the skin surface, an array of tiny electrodes is located. Motor unit potential can be recorded simultaneously on multiple channels.

### 5.1.2 Multi-channel Recording of MUP and Innervation Zone

NMJ is usually defined for a single muscle fiber. A motor unit composed of hundreds of muscle fibers will have hundreds of NMJs. Long history of research reveals that in a parallel muscle such as Biceps Brachii, normally NMJs belonging to a single motor unit are usually clustered near the center of the muscle, as shown in Masouda et al, 1983. This fact allows us to determine an Innervation Zone (IZ) for a MU set. In this document, 'IZ length' or 'NMJ length' of a motor unit refer to the spatial length of NMJs spread along the muscle length, as shown in Figure 11. During last decade, technology for high density surface EMG recording with surface electrode arrays has emerged and well developed, allowing discovery of further information

about the architecture of a motor unit. For example, linear array surface EMG electrodes are found useful in determining the IZ of a motor unit, as shown in Merletti et al, 2003.

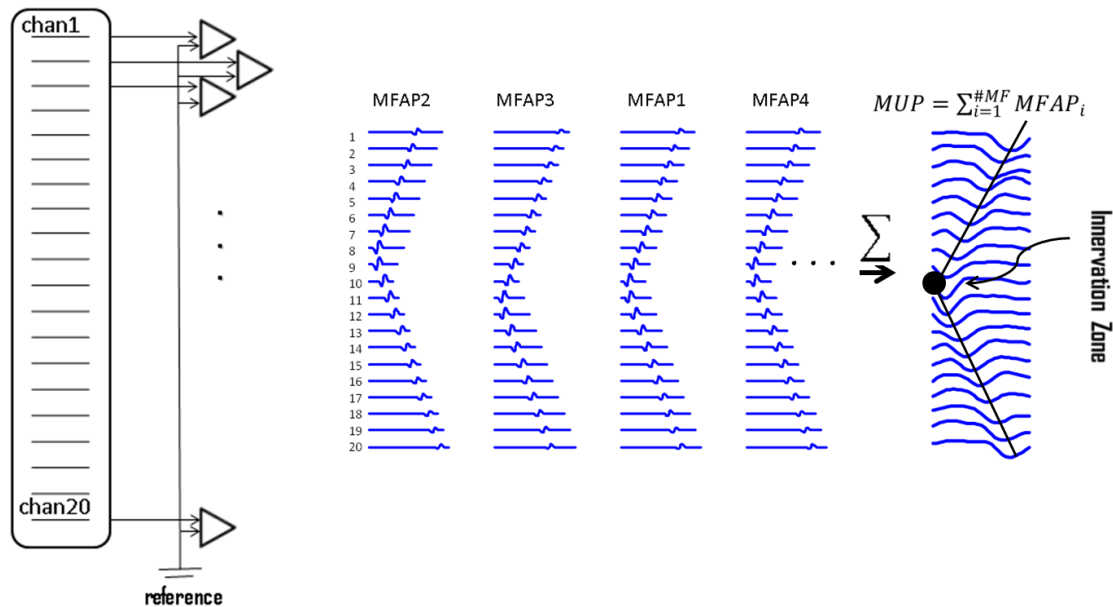


Figure 12: Raster plots of simulated MFAPs and a final MUP. This plot shows the concept of MUP generation obtained from summation of single MFAPs on multichannel electrodes. The Innervation Zone can be detected from the multichannel MUP. In reality, single MFAPs are not detectable by surface electrodes.

As shown in Figure 12, when a muscle fiber gets excited, the channel located right on top of the NMJ site is the one on which the waveform will appear first. The adjacent channels will receive the waveform with a time lag and this repeats for the rest of the channels until either the amplitude of the waveform diminishes in background noise (a sign to reach the end of fibers in a MU) or the last electrodes (distal or proximal or both) are reached. This propagation - accompanied with sequential time lags- builds a horizontal V-shape wave on the image of the multi-channel waveform, see Figure 12. The point, at which the two sides of the 'V' meet, is considered to be the IZ of that motor unit.



### 5.1.2. Fasciculation Potentials in ALS

Amyotrophic Lateral Sclerosis (ALS) is a fatally progressive motor neuron degenerative disease. Loss of neural drive to a muscle (called denervation) will lead to alteration in the muscle organization. Over the course of the degeneration process, one prominent electrophysiological abnormality is the emergence of spontaneous activities including Fibrillation Potentials and Positive Sharp Waves, and Fasciculation Potentials (FPs). The two former phenomena (Nandedkar et al., 2000) arise from single muscle fibers that are believed to be denervated (i.e., their corresponding axon branches have died). Due to their subtle amplitude, so far, Fibrillations are only detectable by means of intramuscular recordings, and cannot be seen on surface recordings. FPs, however, arise from a motor unit set, and are detectable on the surface of the skin. In contrary to a voluntarily recruited motor unit, firing of FPs is random and sporadic. Beside their clinical significance in diagnosis, FPs have been studied to understand their site of origin. An FP can potentially initiate anywhere: in a MU set (i.e. motor neuron soma in the spinal cord, along the motor axon, and at the end of terminal branches) or even supra-spinally. Many invasive and non-invasive approaches have been applied to tackle this question. Evidence of both central and peripheral origins and on a motor axon at both proximal and distal sites have been shown. A detailed history of these techniques can be found in De Carvalho and Swash, 2012. Among the established techniques, HDsEMG has also been used for this purpose (Drost et al, 2007; Kleine et al., 2012).

### 5.1.3 Work Plan

We explored the waveform shape of FPs, as well as voluntarily recruited MUPs both in ALS and age-matched healthy control subjects. We specifically examined their IZ and

propagation patterns, which have been proved helpful in understanding the MU organization in a muscle (Lateva and McGill, 2001; Lateva et al., 2002; Lateva et al, 2010). Results from different groups were compared and discussed.

## **5.2 Material and Methods**

### **5.2.1 Experiments**

Experimental EMG data were recorded from twelve neurologically intact subjects: 6 male and 6 female, age 20-70 years old, average age  $43 \pm 18$ . We also had seven subjects with ALS : 6 male and 1 female, age 48 to 71, average age  $56 \pm 10$ . The ALS subjects were diagnosed having “Definite ALS” or “Probable ALS with Laboratory Support” based on El Escorial criteria, Brooks, 1994. Three ALS subjects had multiple visits, and in total there were 14 datasets available from ALS. This study was approved by the local Human Studies Committee, and all the participants gave the informed consent.

The Biceps Brachii muscle was examined with the elbow partially flexed and forearm in semi-pronation. A custom-made 20-channel linear bar electrode array (Figure 12) was used for all experimental recordings. The distance between two consecutive recording bars was 5 mm, and each bar was 1 mm in width and 10 mm in length, arranged in a linear configuration. The linear electrode array was placed on the Biceps with its center on the belly of the muscle along muscle fibers. Channel 1 was on the proximal side and channel 20 covered the distal side of Biceps muscle. The signals are amplified by the Refa128 EMG Recording System (TMS International BV, the Netherlands). The reference electrode is placed on the ipsilateral elbow. Sampling rate is 2 kHz per channel. Band pass filter is set for 20–500 Hz, which can slightly smooth out waveform shapes, but does not affect classification performance. Hardware-based common feedback (average of all available channels) is subtracted from each channel.

### 5.2.2 Determining the IZ

Multichannel MUPs were extracted manually from low force levels of voluntary contraction EMG. FPs, however, were detected automatically using the software described in Jahanmiri-Nezhad et al., 2014. The algorithm first transformed the 20-dimensional signal to a 1-dimensional trace, and applied amplitude thresholding to detect a potential by recording its occurrence timing. The temporal information were then used to extract the multichannel waveforms from the 20-dimensional signal. Extracted FPs were stored in a database. The FPs were afterward clustered into classes of similar waveform shapes, by means of the toolbox described in Chapter 4.

IZ detection was performed semi-manually. A Matlab program was implemented to illustrate the points of extrema versus channel number. At each channel, the points of maxima and minima were determined and depicted in a figure (an example shown in Figure 13). Data in this figure can be divided to two ‘ascending’ and ‘descending’ sections. The point where these sections meet can be used to estimate the location of Innervation Zone. There may be no time-delay propagation around this point across several channels, and this clue can be used to estimate IZ length (through counting the number of channels where no MUP propagation pattern was observed). Channel number (x-axis) works as a ruler for muscle length.

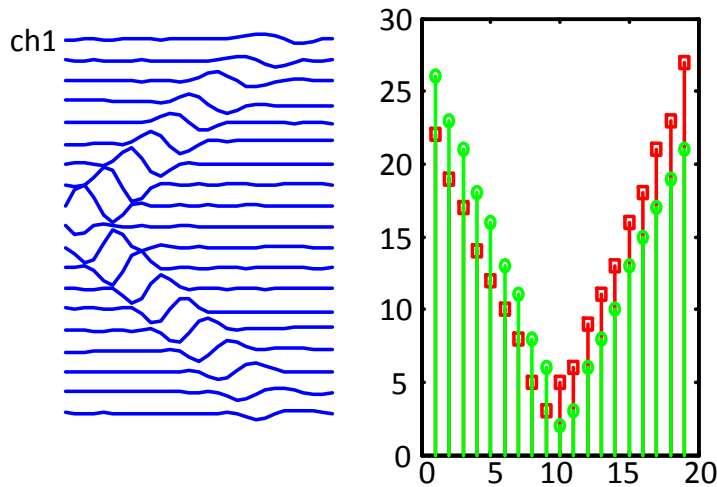


Figure 13: A simulated MUP. On the left, raster plot of MUP waveform is depicted (y axis is voltage with arbitrary unit (au) and x-axis is time duration (au)). On the right, the plot of Points of Extrema are presented (y-axis represents the time and corresponds to x-axis of the raster plot, and x-axis represent channel number). The sites of minimum are marked with green circles and the maximum points at each channel are marked with red squares. In the raster plot, the site of IZ is located at the center (channel 10). The troughs (both for the points of min and max) on the right panels, also occur at  $x=10$ .

The simulated waveforms in Figures 12 and 13 were synthesized by a single motor unit potential model (unpublished work), where we attempted to mimic the characteristics of biceps muscle and our experimental 20-channel linear array electrode. In this model number of fibers in a motor unit ('n'), depth of each fiber from the surface, transversal distance of a fiber from the center of the muscle, NMJ sites along the fiber length, longitudinal conductivity, and radial conductivity were determined. The spatial distribution of NMJs in a 3D Cartesian space was modeled by a random variable using random number generator.

For each examined muscle, distribution of IZs along the were determined by first its length (distance between the most proximal and the most distal IZ) and second by computing the variation (standard deviation, STD) of IZs. It is noted that even for a normal muscle, it is not unlike to spot an off-center IZ, but the hypothesis is that IZs are generally clustered at the center for normal muscles, so we expect to see small variations in IZs within a muscle of a healthy subject.

### 5.2.3 Statistical tests

Normality test (Jarque-bera test, built in Matlab) was performed before any t test comparison between the MUPs in ALS and healthy subjects. Where the test of normality failed, boxcox transformation was tried with different parameters, until the Normality assumption was met for the ttest. Power analysis (built-in Matlab) was also performed in order to estimate required sample size for a statistical test, although we were limited to the presented data.

## 5.3 Results

Four to nine MUPs (total of 69) were manually extracted from voluntary EMG trials, from 12 healthy subjects. The waveforms from each subject were visually examined so that each represented different MUs. Data from two of the subjects were excluded since their entire recording had no V-wave shape (propagation with time-lag) in them. An inspection of the EMG from these subject proved no time-lag across channels existed over the entire course of recording for these two subjects. From the remaining 59 waveforms, 10 MUPs were either noise, or had no clear IZ, and hence they were excluded too. This is worth mentioning, so that it is clear that abnormal patterns of propagation and no-clear IZ zone might be observed in control subjects as well, and is not always due to physiologic factors. As discussed later in this work, they may be result of a bad recording or due to superimposition of two or more MUPs (a prominent feature in surface recordings even at low force level EMG).

Likewise, three to nine voluntarily activated motor units (total of 47 MUPs) were manually extracted from 9 voluntary EMG recordings from ALS subjects (not all the 15 recordings, from ALS population, had voluntary trials from Biceps).

12630 FPs were automatically extracted from 15 trials of long duration of spontaneous activity recordings in 7 ALS subjects. Detected FPs from each set of recording were clustered

into a total of 375 classes of similar shape, using a program described in Chapter 4. Classified FPs were examined with regard to their IZ location, the same way as voluntary recruited MUPs. Figure 14 depicts a portion of different classes of FPs in one subject. Figure 15 presents the within-muscle distributions of IZs for the three groups of data. The results are summarized in Table 3.

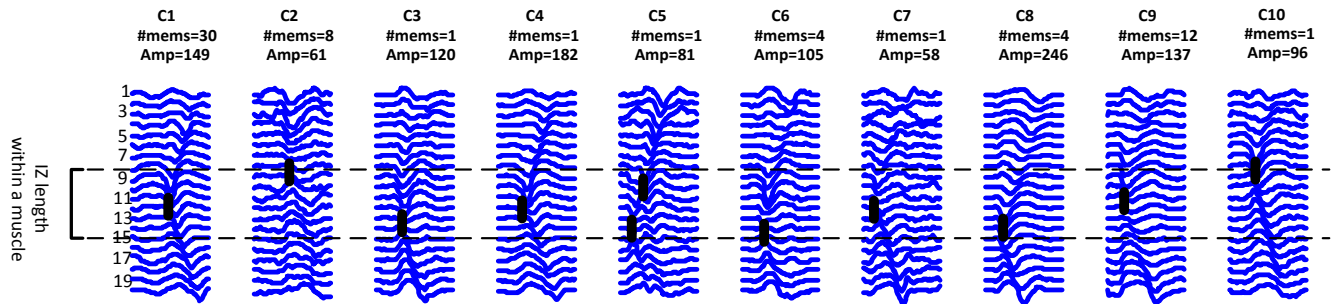


Figure 14: Raster plots of nine sample prototype shape of FPs belonging to one subject. Class index, number of members of that class (how many samples assigned to it), and its amplitude is reported on the top. C2 has a strange straight propagation, with no time lags between the channels. In C5, two IZs were detected, indicating for either a doubly innervated MU or two superimposed FPs. The heavy black lines indicate of IZs.

Table 3 – Measures of IZ distribution among FPs compared with MUPs in control and ALS subjects.

	MUPs ; healthy	MUPs; ALS	Fasciculation Potentials
IZ length within a muscle (mm)	2.5-25	5-42.5	12.5-75
Mean (mm)	10.2±8.1	19.2 ± 11.7	39.1 ±16.3
STD (IZs) (mm)	1.4 to 17.6	2.4 to 14	4 to 21
Mean (mm)	5.1±5	8.7±4.2	12.8±4.9

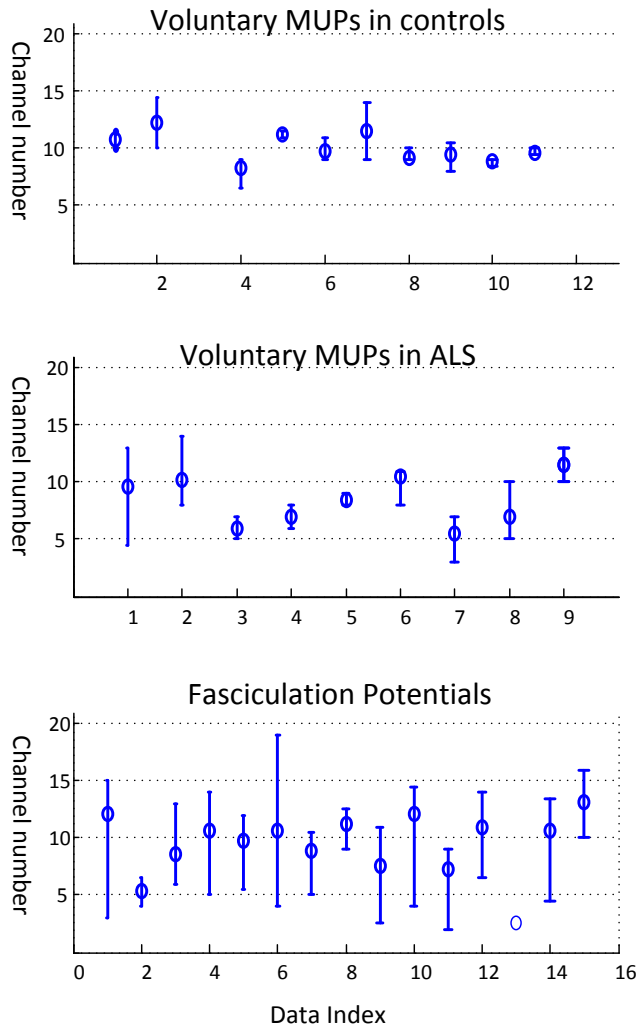


Figure 15: Plot of within-muscle IZ distribution.

The y-axis shows channel number, since IZ is determined based on 1:20 array electrode.

The x-axis represents each datasets.

Corresponding statistical comparisons are presented in Table 3.

Three subjects with ALS had multiple visits, as listed in Table 4. This allowed us to monitor their spontaneous discharge activities. Analysis of IZ distribution on FPs from these subjects are illustrated in Figure 16 and summarized in Table 4. In Figure 16, the x-axis is the index for each subject (S represents Subject, and V represents Visit). It is noted that the bars are just showing the extent of IZ distribution along the muscle, but the statistical tests (the ones who pass the tests are marked with asterisks), refer to standard deviation of IZs. The statistical tests showed significant differences from some of the visits in all three subjects. The zero length of IZ for the last visit of Subject 3, was the result of a very weakened muscle with only few classes of FPs with unclear IZs.

Table 4 \_ Longitudinal data of length of IZs within a muscle

IZ Length in mm	Jul 2009	Jun2011	Aug2011	Dec2011	Mar2012
Subject1	35	45	32.5	75	-
Subject2	-	27.5	17.5	42.5	52.5
Subject3	-	35	37.5	0	-

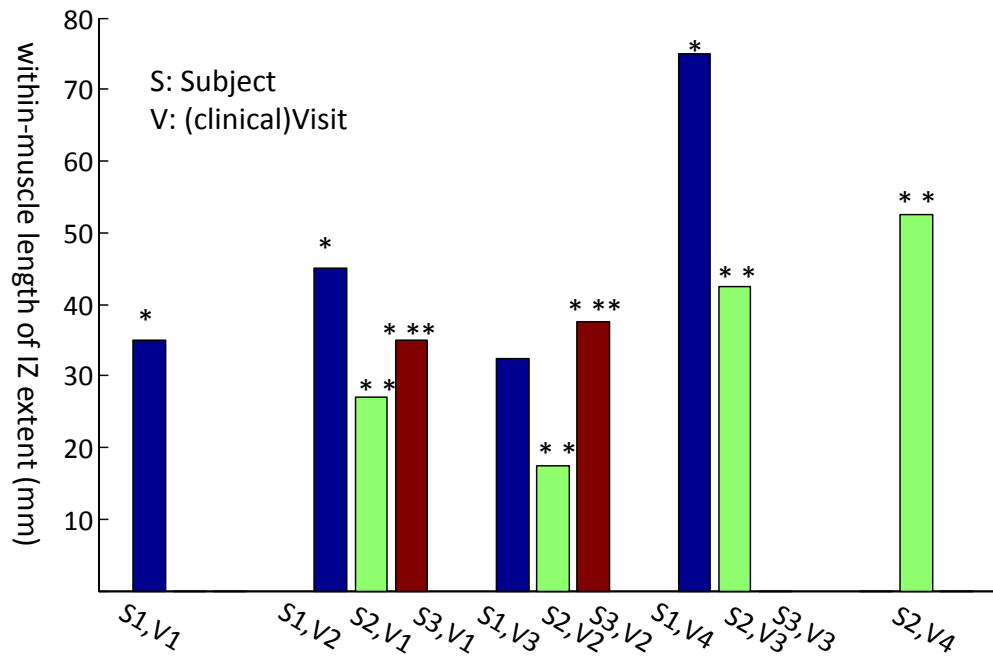


Figure 16: Longitudinal study of IZ scatter for three ALS subjects. Statistical test was performed on STD of IZs. The asterisks indicate for statistical difference.

It is not unlikely that more scattered IZs among healthy subjects would be correlated with age. In this regard, Figure 17 illustrates the IZ variation for the control population. A trend of increased IZ variation versus age can be seen.



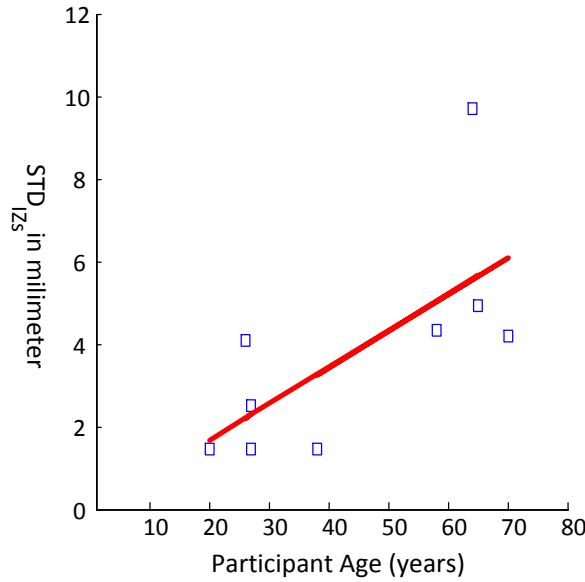


Figure 17: Variation of IZ within a muscle in control subjects with respect to their age. A linear trend can be observed.

In brief, scatter of IZs (IZ length) within a muscle had a larger extent among MUPs in ALS than in controls. However, statistical tests did not confirm it. A power analysis suggests that at least two more ALS samples are required for a statistical test. Meanwhile, it was proved that the variation of IZs (STD) within a muscle, in voluntary MUPs of ALS is statistically larger than in controls (p-value=6e-5). This quantity was also statistically larger among FPs than in voluntary MUPs in controls and ALS (p-values=5e-6, 0.052, respectively). It is acknowledged that the numbers of FP samples were significantly larger than the numbers of manually extracted MUPs, and higher variability of IZs also could be shown among MUPs if more data were available from voluntary EMG. Nevertheless, the fact that IZs have a narrow band around the center is in general an accepted hypothesis.

Enhanced variation of IZs location in the muscles with ALS can be an indicator of ongoing reorganization process of muscles under denervation caused by the motor neuron degenerative disease.

## 5.4 Discussion

This work is the first study for IZ analysis of fasciculating motor units. The study revealed the enlargement and scattered IZ of fasciculating motor units compared with voluntarily recruited motor units. The study also performed a preliminary IZ analysis for fasciculating motor units.

Longer length of IZ from could be related to the process of muscle fiber denervation/reinnervation. When a motor neuron dies, its corresponding muscle fibers become ‘orphans’, and will be ‘adopted’ by surviving motor units. Collateral sprouting and reinnervation process starts right after. It might be due to an non-optimum reinnervation process that myoneural junctions get more scattered. Verification of this hypothesis is beyond the scope of this work. It is also acknowledged that origin site of excitation causing FP potentials might be at terminal branches of an axon, rather than the motor neuron soma in the spinal cord. In other words, the 375 classes of FPs did not necessary from 375 different motor units. It remains unclear whether this fact can lead to abnormal site of IZ on FP waveforms.

### 5.4.1 Motor Neuron Degenerative Diseases and ALS

ALS is a type of motor neuron degeneration (MND) disease. There also exist other subtypes of MND. Primary Lateral Sclerosis (PLS) affects the lower motor neurons (LMNs), which are the neurons originating in the ventral horn of spinal cord and innervate the muscles. Primary Muscular Atrophy (PMA), in contrast, affects the upper motor neurons (UMNs), which are located in the cortex and provide descending input to LMNs. However, in ALS, both UMNs and LMNs are affected. An individual with ALS experience both the symptoms of UMN and LMN lesions. Symptoms of LMN lesion include muscle cramp, muscle weakness, muscle

twitches and muscle atrophy. Symptoms of UMN lesion usually include spasticity and hyperreflexia. In this work, the focus is on the fasciculation potentials, related to signs of LMN.

#### 5.4.2 IZ in Fasciculating Motor Units

Contrary to other studies on FPs using HDsEMG (Drost et al., 2007; Kleine et al., 2008; Kleine et al., 2012), we approached FPs by their IZ distribution. Determining the location of IZ in a motor unit by means of multi-channel EMG recording has more than 30 years of history (Masouda et al. 1983; Falla et al., 2002; Merletti et al., 2003; Mesin et al, 2008). In this work, distribution of motor unit IZs were studied, using an 20-array surface electrode on biceps muscles of ALS subjects. Longer extent of IZs within a muscle was observed among the FPs. The variation of IZ locations were statistically greater in ALS population, compared with the ones in healthy subjects.

#### 5.4.3 Fasciculating Motor Unit IZ distribution in Biceps

IZ distribution had been previously reported to have a narrow band in biceps of healthy subjects (Masouda et al. 1983; Masouda and Sayodama, 1986; Brown et al., 1988; Barbero et al., 2012). We showed that IZs are more scattered among fasciculating motor units in ALS. All the IZs within a muscle were extracted from a single trial of EMG recording from totally resting muscle, and without any voluntary contraction. Hence, the possibility of a shift in IZ location due to muscle contraction (as described in Martin and McIsaaz, 2006; Piitulainen et al., 2008; Nishihara 2010; Nishihara 2013) is ruled out.

This finding could be a result of muscle reorganization due to ongoing degeneration process.

#### 5.4.4 Difficulties in Finding the IZ

The relationship between MUP morphology and its corresponding anatomic factors is very interesting. An excellent example is presented in Lateva and McGill, 2010. Nevertheless, a need also emerges to know the non-physiologic factors that influence the motor unit waveform potentials and should be avoided to be interpreted as a neurophysiologic observation. With regard to IZ localization using surface recording, two major problems that complicate the analysis were encountered, including: improper electrode positioning and unresolved superimposed waveforms. Examples for the former include: 1) electrode was not positioned parallel to muscle fibers on the proximodistal axis of the muscle, and 2) improper use of electrode-skin gel making short cuts in between-electrode distance. An example of an anatomical factor aggravating IZ localization is presence of pennated fibers with regard to surface, as reported in detail in Barbero et al, 2012. This happens when muscle fibers in a motor unit are angled at one end of the muscle. Only few channels close to the superficial section of the fibers can record the potentials. The waveforms suddenly disappear and do not propagate along the muscle length, so IZ localization will be impossible.

#### 5.4.5 Increased Aging and Increased Variability in IZ Length

Although beyond the scope of this work, higher variation in IZ locations within a muscle was shown to be correlated with age among our control population, as shown in Figure 17. A systematic study is required to investigate the aging parameter in IZ distribution, in order to discriminate between this factor and that of progressive case of muscle denervation such as ALS.

## 6 A Practice of Caution: Action Potential Spikes or Noise?<sup>5</sup>

Faezeh Jahanmiri-Nezhad, Xiaoyan Li, William Zev Rymer, Ping Zhou

**Background.** High density surface electromyogram (EMG) techniques with electrode arrays have been used to record spontaneous muscle activity, which is an important aspect both for supporting the diagnosis of neuromuscular diseases and for laboratory based neurophysiological investigations. This short report presents a practical issue we have experienced during recording of spontaneous muscle activity using electrode arrays from subjects with neuromuscular disorders.

**Findings.** We show that recording artifacts can appear similar to spontaneous action potential spikes. Moreover, a causal filter may induce asymmetric distortions of an artifact and thus confuse it with a real action potential spike. For a single channel surface EMG recording, it might be difficult to judge whether such a spike is a real action potential or an artifact. Further investigation of the signal distributions among other channels of the array can be used to reach a more confident judgment.

**Conclusions.** During examination of spontaneous muscle activity using electrode arrays, caution is required for differentiation of physiological signals from artifactual spikes, which is important for extraction of accurate diagnostic or investigatory information.

---

<sup>5</sup> Submitted to Journal of Neuro Engineering and Rehabilitation

The examination of spontaneous muscle activity is an important aspect of electrodiagnostics both for supporting the diagnosis of neuromuscular diseases and for laboratory based neurophysiological investigations. The intramuscular needle electrode is routinely used for detection of spontaneous muscle activity. In recent years, high density surface electromyogram (EMG) techniques with electrode arrays comprised of a number of closely spaced, small recording probes or bars have been used to record spontaneous muscle activity (Drost et al., 2007; Jahanmiri-Nezhad et al., 2013; Kleine et al., 2008; Zhou et al., 2011; Kleine et al., 2012]. This brief report presents a practical issue we have experienced during recording of spontaneous muscle activity using these novel electrode arrays, from subjects with neuromuscular disorders (amyotrophic lateral sclerosis (ALS), hemiparetic stroke and spinal cord injury). We show that artifacts induced by external stimuli can appear similar to spontaneous action potential spikes. Therefore, such recordings should be judged with caution whether they are of physiological or non-physiological origins.

Below we demonstrate several typical examples and discuss the discrimination of artifactual spikes from real spontaneous action potentials. A 20-channel linear electrode array (custom made, each bar width 1 mm, length 1 cm, inter-bar-distance 5 mm) and a 64-channel flexible electrode array ( $8 \times 8$  square matrix, each electrode 1.2 mm in diameter, inter-electrode-distance 4 mm, TMS International BV, the Netherlands) were used for the spontaneous EMG activity recording of the hand and arm muscles. The surface electrode array signals were amplified by the Refa System (TMS International BV, the Netherlands), with a reference electrode located on the olecranon. Each channel also had a feedback subtraction of the mean of all the recording channels to reduce common mode noise. The surface EMG signals were sampled at 2 kHz per channel. All recordings were processed in a bipolar configuration by

calculating the differential signals between two consecutive electrodes or bars. All the experimental protocols were approved by the Institutional Review Board of Northwestern University (Chicago, USA), and the tested subjects gave written consent for participating in the study.

Figure 18 (a) shows an artifactual spike recorded by one channel of the linear electrode array. The spike was captured during recording of spontaneous EMG activity from the paretic biceps muscle of a stroke subject. Due to its monophasic and symmetric appearance, the spike can be recognized as an artifact. We note that after processing the signal with a causal filter (second order Butterworth high pass filter, cutoff frequency 10 Hz), the resultant waveform has a negative rebound (or positive rebound from clinical neurophysiology viewing with negative upwards) and a gradual return to the baseline (Figure 18b). Such asymmetric distortions of the artifact may be confused with a real action potential spike [Quian Quiroga, 2009]. For a single channel surface EMG recording, it remains difficult to judge whether such a spike is a real action potential or an artifact. Further investigation of the signal distributions among other channels of the array would be necessary to reach a more confident judgment.

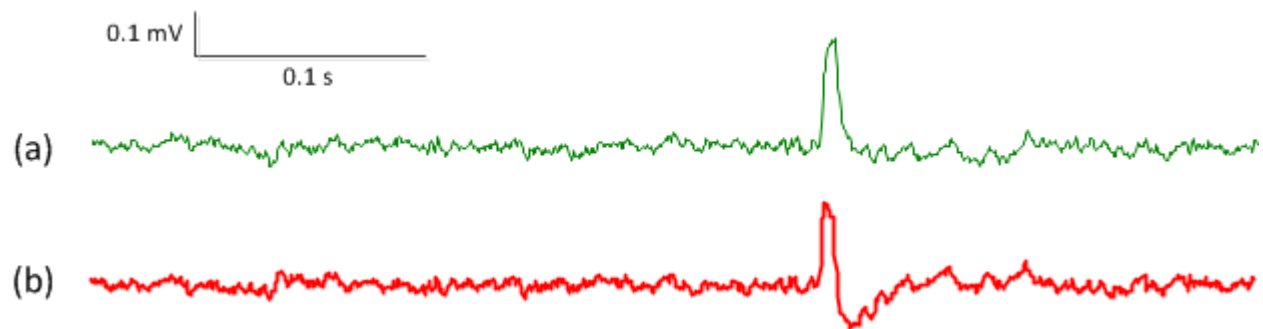


*Figure 18: An example of (a) an artifactual spike and (b) the distorted waveform after processing with a causal filter.*

Figure 2 shows such an example, where the distribution of the artifactual spike among the 19 bipolar channels of the linear electrode array (placed along muscle fibers) is demonstrated in

Figure 19a. It was observed that the artifactual spike only occurred in 2 adjacent bipolar channels at exactly the same time, suggesting their lack of physiological origin. As a comparison, Figure 19b shows three fasciculation potentials (two of them were from the same motor unit) recorded from the biceps muscle of an ALS subject, using the linear electrode array. Such fasciculation potentials were also confirmed by their reproducible occurrence during the long (> 10 minutes) recording period. Clear action potential propagation was observed from different channels along muscle fibers, demonstrating a V-shape propagation pattern. If calculating muscle fiber conduction velocities from inter-electrode-distance and time delay between the action potentials, a physiologically acceptable range (3-6 m/s) can be obtained.

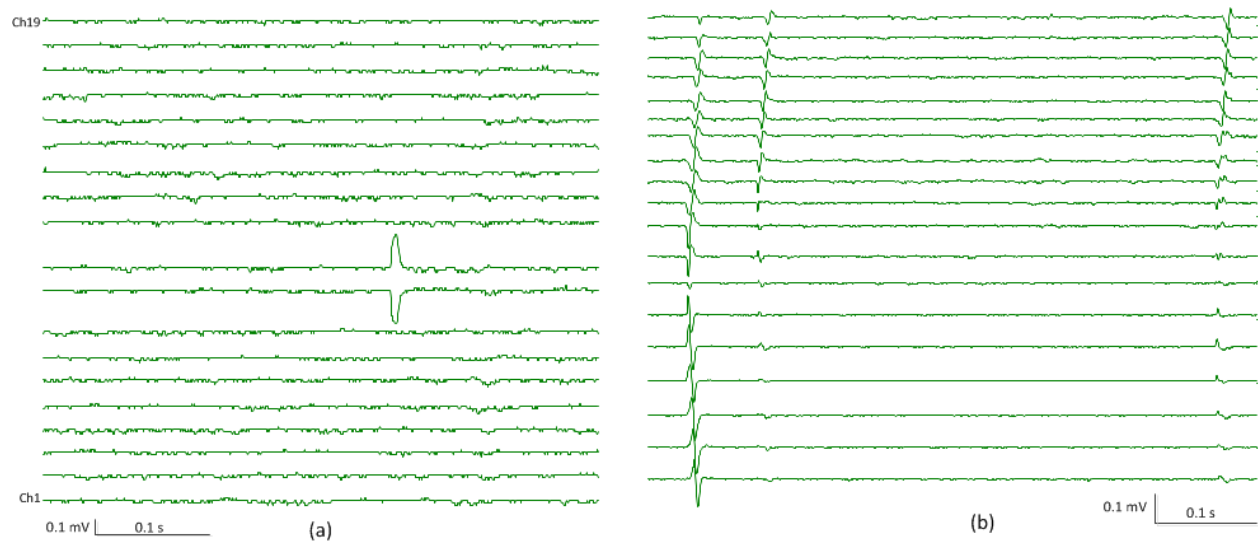


*Figure 19: Signal distribution among 19 channels of the linear electrode array for: (a) an artifactual spike; (b) fasciculation potentials of biceps muscle of an ALS subject.*

Figure 20 shows an example of repetitive spikes from one channel of electrode arrays, with physiological origins (multiplets, myokymic or neuromyotonic discharges (Gutmann and Gutmann, 2004; Whaley and Rubin, 2010)) or induced by external stimuli. The signals shown in Figure 3a and 3b were recorded from the thenar muscle of an ALS subject using the flexible



electrode array. Figure 20(a) shows brief bursts of single action potentials spikes. The spikes within multiplets discharged multiple times in rapid succession. These bursts discharged recurrently at regular or irregular intervals up to several minutes. Figure 20(b) shows an example of neuromyotonic discharges, which have similar characteristics but bursts are prolonged and the spike amplitude may wane. In contrast, Figure 20(c) shows an example of repetitive artifactual spikes, which have a similar pattern to myokymic discharges. Again, for a single channel surface EMG recording, it would be difficult to judge whether such repetitive spikes are of physiological origin or triggered by external stimuli.

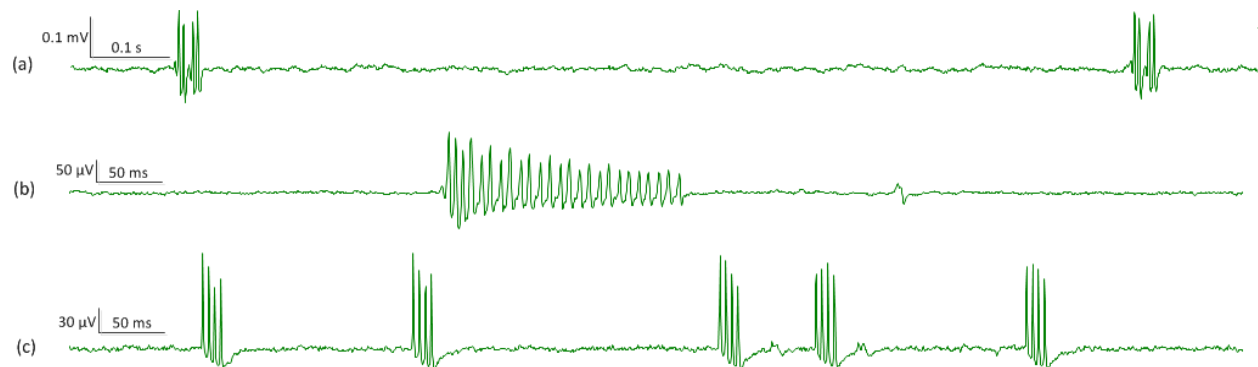


*Figure 20: An example of repetitive spikes from one channel of electrode arrays. (a) Multiplets or myokymic discharges from the thenar muscle of an ALS subject; (b) Neuromyotonic discharges from the same muscle; (c) Repetitive artifactual spikes induced by external stimuli.*

Figure 21 shows the distribution of the repetitive spikes on different channels of the electrode array. The non-physiological origins of the repetitive artifactual spikes (Figure 21a) can be determined from two observations. Firstly, each individual spike has monophasic and symmetric appearance. It is worth noting that causal filters commonly used for on-line spike detection might change such appearance and make artifacts look more similar to real action potentials. Secondly, the repetitive artifactual spikes occurred at exactly the same time with

random polarity change. In contrast, the repetitive action potential spikes demonstrate clear action potential propagation observed from different channels.

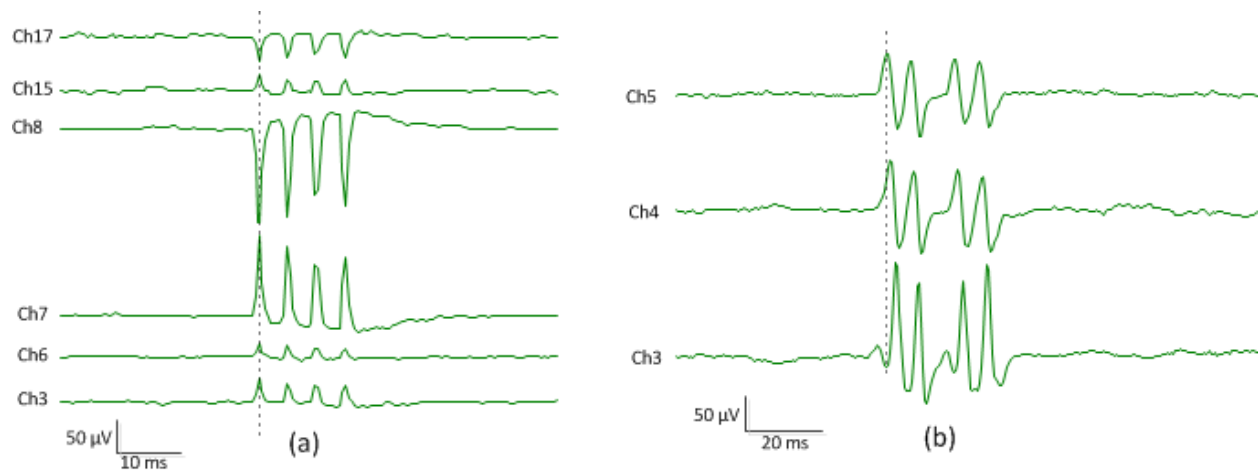


*Figure 21: Signal distribution among different channels of the electrode array for: (a) repetitive artifactual spikes; (b) multiplets from the thenar muscle of an ALS subject.*

Although examination of signal distribution over an electrode array is very helpful in differentiating artifactual spikes from real action potentials, it should be acknowledged that abnormal action potential propagation patterns do not necessarily mean artifactual spikes. For example, for deeper motor units, the action potential propagation tends to be blurred by the volume-conductor properties of overlying tissue (Mesin et al., 2011). Abnormal conduction velocities in the biceps brachii muscles have been reported in muscular dystrophy patients with the aid of a multichannel EMG system, suggesting pathological longitudinal spread of end-plates (Hilfiker and Meyer, 1984; Kumagai and Yamada, 1991). Thus, caution is required for differentiation of physiological signals from artifactual spikes, which is important for extraction of accurate diagnostic or investigatory information. It is also important to explore the cause of artifacts. For example, we found the repetitive artifactual spikes shown in Figure 20(c) can be triggered by connecting a cell phone, which should therefore be avoided during the recording.

This study was supported in part by the National Institute on Disability and Rehabilitation Research of the US Department of Education under Grant H133G090093, in part by the National Institutes of Health under Grant R24HD050821, and in part by the Memorial Hermann Foundation.

## 7 EMG-force Relation in the First Dorsal Interosseous Muscle of Patients with Amyotrophic Lateral Sclerosis<sup>6</sup>

Faezeh Jahanmiri-Nezhad, Xiaogang Hu, Nina Suresh, William Zev Rymer, Ping Zhou

*Background and Purpose:* The relationship between surface electromyography (EMG) and joint force is essential to assess muscle function and its deficits. However, few studies have explored the EMG-force relation in patients with amyotrophic lateral sclerosis (ALS). The purpose of this study was to examine the EMG-force relation in ALS subjects and its alteration in comparison with healthy control subjects.

*Methods:* Surface EMG and force signals were recorded while 10 ALS and 10 age-matched healthy control subjects produced isometric voluntary contraction in the first dorsal interosseous (FDI) muscle over the full range of activation. A linear fit of the EMG-force relation was evaluated through the normalized root mean square error (RMSE) between the experimental and predicted EMG amplitudes. The EMG-force relation was compared between the ALS and the healthy control subjects.

*Results:* With a linear fit, the normalized RMSE between the experimental and predicted EMG amplitudes was  $9.6 \pm 3.6\%$  for the healthy control subjects and  $12.3 \pm 8.0\%$  for the ALS subjects. The slope of the linear fit was  $2.9 \pm 2.2 \mu\text{VN-1}$  for the ALS subjects and was significantly shallower ( $p < 0.05$ ) than the control subjects ( $5.1 \pm 1.8 \mu\text{VN-1}$ ). However, after excluding the four ALS subjects who had very weak maximum force, the slope for the remaining ALS subjects was  $3.5 \pm 2.2 \mu\text{VN-1}$  and was not different from the control subjects ( $p > 0.05$ ).

*Conclusions:* A linear fit can be used to well describe the EMG-force relation for the FDI muscle of both ALS and healthy control subjects. A variety of processes may work together in ALS that can adversely affect the EMG-force relation.

---

<sup>6</sup> "Reprinted from IOS Press Journal of NeuroRehabilitation, DOI: 10.3233/NRE-141125, Copyright (2014), with permission from IOS Press."

## 7.1 Introduction

The relationship between surface electromyography (EMG) during muscle contraction and the resulting force has been extensively studied in the past(Perry J, 1981). A linear relation between force and EMG amplitude has been documented in small muscles with narrow motor unit recruitment force ranges, such as the first dorsal interosseous (FDI) muscle , while nonlinear EMG-force relations have also been reported for larger muscles (e.g. proximal leg or arm muscles) with wide motor unit recruitment force ranges(Basmajian & DeLuca, 1985; Lawrence & De Luca, 1983; Moritani & deVries, 1978; Solomonow, Baratta, Shoji, & D'Ambrosia, 1990; Woods & Bigland-Ritchie, 1983).

The investigation of EMG-force relation has various clinical applications. For example, based on the established EMG-force relation, the EMG signal can be used to predict muscular force which may otherwise be difficult to measure directly. The EMG-force relation can be a useful marker of changes in motor unit or motor neuron pool activation during muscle force generation. For example, imposition of the spinal cord section in animal preparations may induce a significant increase in the regression slope of the EMG-force relation indicating an inefficient use of the muscle(Blaschak, Powers, & Rymer, 1988). Due to pathophysiological changes in motor neuron pool and intrinsic muscle properties in patients with neurological disorders, the EMG-force relation can also be profoundly affected. Namely, diverse changes in EMG-force slopes have been reported in paretic muscles of stroke patients compared with contralateral or neurologically intact muscles(Gemperline, Allen, Walk, & Rymer, 1995; Tang & Rymer, 1981; P Zhou, Li, & Rymer, 2013).

In contrast to studies of EMG-force relation in neurological injuries such as stroke, it is presently unknown whether or how the EMG-force relations may be altered in patients with

motor neuron diseases such as amyotrophic lateral sclerosis (ALS). ALS (also known as Lou Gehrig's disease) is a progressive neurodegenerative disease that affects both upper and lower motor neurons. Intramuscular EMG examination has been routinely used for supporting the diagnosis of ALS (M De Carvalho et al., 2008). Motor unit number estimation (that relies on electrical stimulation and surface EMG recording) and its various forms of modification or improvement can provide a useful tool for assessing spinal motor neuron degeneration and tracking disease progress (X. Liu et al., 2009; Nandedkar, Barkhaus, & Stålberg, Nov 2010; Shefner & Gooch, 2002). The utility of interference surface EMG analysis has also been reported for supporting the diagnosis of the disease (Diószeghy, Egerházi, Molnár, & Mechler, Dec 1996).

To date, the EMG-force relation has not been systematically examined in ALS except for one study that was performed toward an estimation of muscle contraction levels using EMG amplitude in patients with neuromuscular disorders including ALS (Boe, Rice, & Doherty, April 2008). In addition to force estimation, a systematic analysis of the EMG-force relation in individuals diagnosed with ALS can provide valuable information to assist in the assessment of neural and muscular pathological changes. The objective of this study was then to examine EMG amplitude and force levels of the FDI muscle during voluntary isometric contractions tested in both neurologically intact and ALS subjects. First, we investigated whether a linear regression, as previously reported for the FDI muscle in healthy subjects, can be used to characterize the EMG-force relation for the ALS subjects. Second, the EMG-force relation observed from the ALS subjects was compared with the healthy control subjects to assess whether there was a systematic alteration in the relation.

## 7.2 Methods

### 7.2.1 Subjects

Ten subjects with confirmed ALS (7 male and 3 female;  $53 \pm 12$  years, range: 31 - 67 years; years from symptom onset: 1 - 6 years; years from diagnosis: <1 - 4 years) and 10 neurologically intact subjects (5 male and 5 female,  $52 \pm 15$  years, range: 25 - 80 years) participated in this study. The first dorsal interosseous (FDI) muscle of the stronger hand was tested in 9 ALS subjects, and for one ALS subject the test was performed bilaterally. Therefore, 11 datasets were available in total for the ALS group. For the control subjects, the test was performed on the dominant side. All subjects signed informed consent via protocols approved by the Institutional Review Board under the Office for the Protection of Human Subjects at Northwestern University (Chicago, USA).

### 7.2.2 Experimental Design

Subjects were seated in a Biodex chair in a standardized posture with the forearm resting on an arm base. As shown in Figure 1, the wrist and forearm were placed in an arm brace and secured to the supporting surface to avoid movement when the subject performed index finger isometric abduction. Extra foam was placed around the arm brace for further securing purpose to avoid force contamination on the FDI muscle. The proximal phalanx of the index finger was held in neutral position and placed in a firm cast inside a vise that was attached with a six degrees-of-freedom load cell (ATI-FT4006, ATI Inc, Garner, NC). The thumb angle relative to the index finger was held at 45 degrees. The three medial fingers were secured on specifically designed surfaces. Isometric force of the FDI muscle was measured at the 2<sup>nd</sup> metacarpophalangeal (MCP) joint (Figure 22).

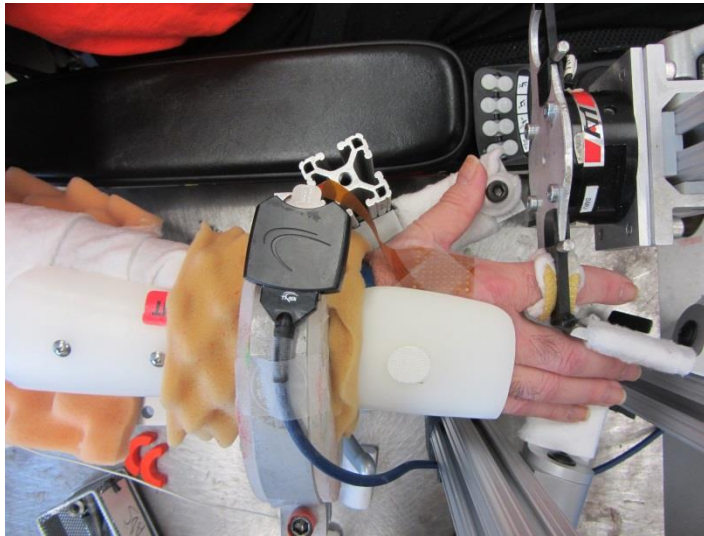


Figure 22: Experimental setup for surface EMG and contraction force recordings from the FDI muscle.

A flexible surface electrode array with 64 channels (8 rows and 8 columns, each recording probe 1.2 mm in diameter, inter-probe distance 4 mm for both directions) was used to measure electrical activity of the muscle through a 128-channel EMG system (Refa system, TMS International BV, Netherlands). The system has adjustable filter settings and real time display, providing visual feedback to the examiner to assess signal quality. The EMG signal was sampled at 2000 Hz per channel with a bandpass filter setting at 5-500 Hz. The auxiliary channels of the system were used to record muscle force. The force signal was sampled at 2000 Hz with a low pass filter at 20 Hz. The EMG and force recordings were synchronized during the experiment. All the data were stored in ASCII format for offline analysis.

The experimental protocol started by measuring the isometric maximum voluntary contraction (MVC) force of the FDI muscle for index finger adduction. Once the MVC was determined, the subject was asked to perform isometric contractions of the FDI muscle at 10%, 20%, 30%, 40%, 50%, 60%, and 70% of the MVC in different trials. For each trial, one level of



muscle contraction was performed. The subject was instructed to reach the target force and hold it for approximately 10 seconds. The order of contraction levels was randomized and each contraction level was repeated at least twice. Sufficient resting periods between trials were provided to the subject to minimize mental and muscle fatigue.

In order to guide the subject to perform a desired level of contraction, a home-designed Graphical User Interface (GUI) Matlab program was used to provide visual feedback. This GUI program shows a two dimensional Cartesian coordinate plane, where  $x$ -axis represents force on the horizontal direction ( $F_x$ , index finger abduction/adduction) and  $y$ -axis represents force on the vertical direction ( $F_y$ , index finger flexion/extension). A cursor in the shape of a triangle was used to indicate the current position of muscle contraction force in the  $x$ - $y$  plane, which is at the origin during rest. To perform each level of contraction, an open circle and a filled circle were used to represent the Target position and the Guide position, respectively. The filled circle can change colors from yellow to orange and then to green in order to indicate to the subject that a trial is about to start. The subject was asked to generate force by abducting the index finger to move the cursor to the Target, stay at the Target position for 10 s and then relax slowly until the cursor was back at the starting point.

### 7.2.3. Data Analysis

The segments of EMG signal during which the force was held constant were used for later analysis. To facilitate signal segmentation, a simple interface program was designed for the user to choose the most constant part of the force profile. Based on the timing of force signal segmentation, EMG signals were segmented as well. The average rectified value (ARV) of each channel's EMG was measured. Due to the fact that the electrode array is larger than the FDI muscle and the EMG channels on the edge of the array were off the muscle, the ARV values

from the 16 centered channels of the electrode array were averaged to represent the EMG amplitude of the FDI muscle.

A linear function in the form of  $y = ax + b$  was derived based on a 1<sup>st</sup> order polynomial least-square fit, where  $x$  represents force measurement,  $y$  represents EMG amplitude,  $a$  is the slope of the EMG-force relation, and  $b$  is the intercept. To evaluate the linear fit of the EMG-force relation, we calculated the normalized root mean square error ( $E_{n-rmse}$ ) between the experimental EMG amplitudes and those predicted by the linear fit from the force measurement.

The analysis was performed on all the ALS and healthy control subjects. Two-sample  $t$ -tests were used to examine the difference between the slopes of the EMG-force relation of ALS and healthy control subjects. Statistical significance was defined as  $p < 0.05$ .

## 7.3 Results

### 7.3.1. MVC force and EMG measurement

The MVC force in abduction was recorded for the FDI muscle of both ALS and healthy control subjects. As we expected, the MVC force of the ALS was systematically lower than that of the healthy control subjects. Across healthy control subjects the average MVC force was  $32 \pm 12$  N (range: 17 - 55N), which was significantly larger than the ALS subjects with an average MVC force of  $15 \pm 13$  N (range: 1.5-32 N) ( $p < 0.05$ ). It was also observed that the average EMG amplitude at the MVC was  $146 \pm 34$   $\mu$ V (range: 98 - 201  $\mu$ V) of healthy control subjects, which was significantly higher ( $p < 0.05$ ) than the maximum EMG amplitude of the ALS subjects [ $47 \pm 41$   $\mu$ V (range: 3 -132  $\mu$ V)].

### 7.3.2. EMG-force relation

Figure 23 shows the sample recordings of the EMG and force signals at two different muscle contraction levels from a healthy control subject. For each level, the force in directions of index finger abduction and flexion was measured. Among 64 channels of the electrode array, only 6 channels (channels 26 to 31) of data are shown to avoid complexity in the figure. Figure 24 and Figure 25 present the experimental EMG and force relation for all the healthy control and ALS subjects, respectively. The line drawn in each panel is the result of a 1<sup>st</sup> order polynomial least-square fit for the recorded sets of data points.

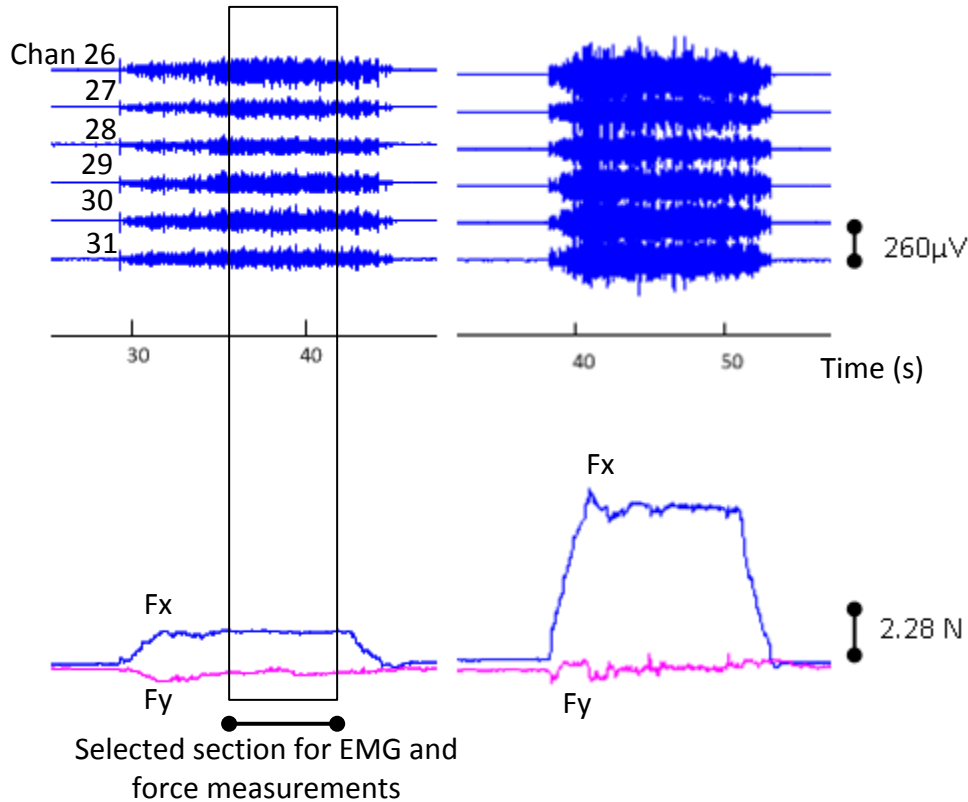


Figure 23: Examples of surface EMG and force signals recorded at two different contraction levels from a healthy individual. Each contraction lasted around 10 seconds. Six EMG channels are shown here in the upper panels. The lower panels show force profiles. Both fore directions in abduction (Fx) and flexion (Fy) are shown. The abduction force level in the left trial is about 1.7 N and in the right trial is 8.4 N.

It was evident that a linear fitting can be used to well describe the EMG-force relation for the FDI muscle of both ALS and healthy control subjects.

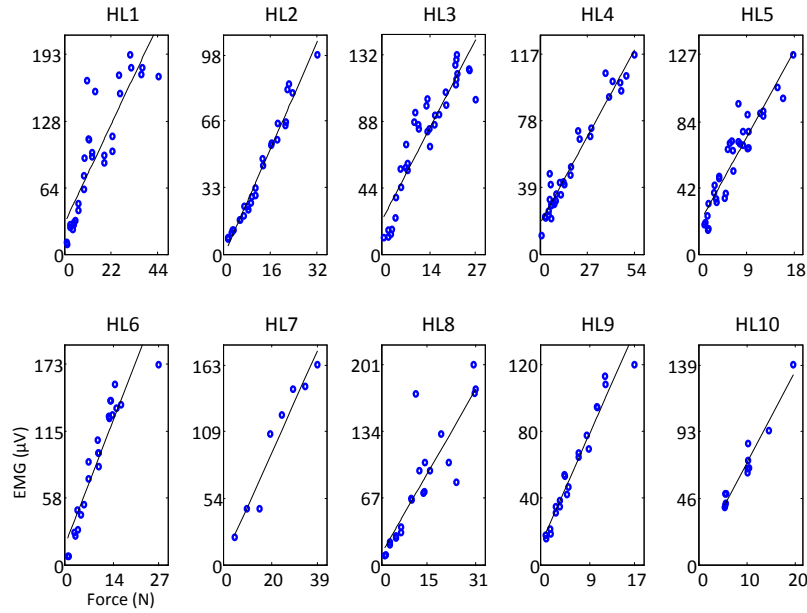


Figure 24: The linear fitting of the EMG-force relation for each of the healthy control subjects.

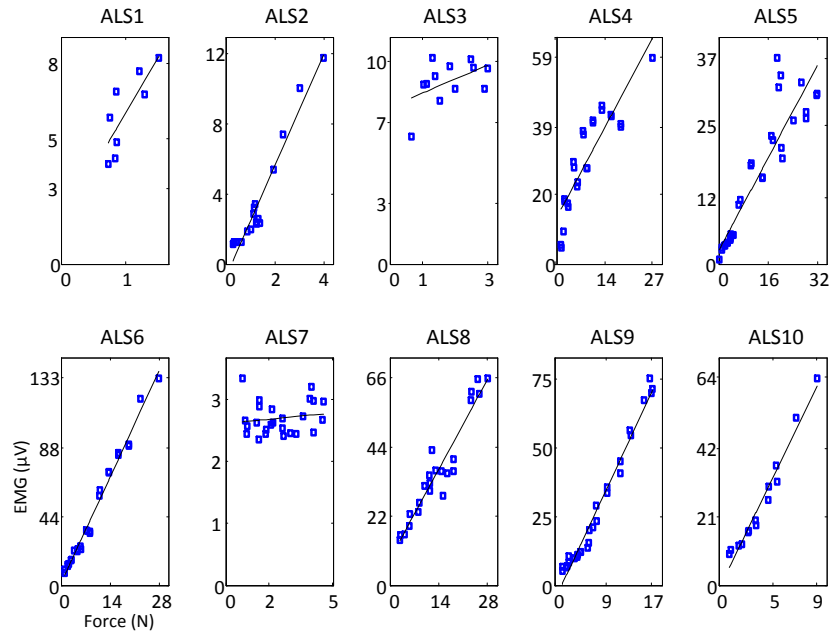


Figure 25: The linear fitting of the EMG-force relation for each of the ALS subjects.

For four ALS subjects (ALS 1, ALS 2, ALS 3, and ALS 7), the maximum force of the FDI muscle was very weak. Among this group, three subjects (ALS 1, ALS 3, and ALS 7) showed a more scattered sets of data points, with a linear trend still visible between the recorded EMG and force signals. Fitting a linear function into the experimental data, the normalized root mean square error (RMSE) value was  $9.6 \pm 3.6\%$  for the healthy control subjects and  $7.5\% \pm 3.5\%$  for the ALS subjects, after excluding the three subjects (ALS1, ALS3, and ALS 7) with scattered data points, and not difference was found between groups ( $p > 0.05$ ). Whereas including these three subjects, the normalized RMSE value was  $12.3 \pm 8.0\%$  for the ALS subjects, which was significantly higher than that of the healthy control subjects ( $p < 0.05$ ).

### 7.3.3. EMG-force slope comparison

The slope of the 1<sup>st</sup> order polynomial curve fit of the EMG-force relation was calculated and compared between the two groups. The slope was  $5.1 \pm 1.8 \mu\text{VN}^{-1}$  for the healthy control subjects and was significantly steeper than the ALS subjects ( $2.9 \pm 2.2 \mu\text{VN}^{-1}$ ) ( $p < 0.05$ ). It is noted that the slope for the ALS subjects with weak maximum contraction force (i.e., ALS 3 and ALS 7, Figure 25) was very small. After excluding the four subjects who had very weak force or scattered EMG-force data points (ALS 1, ALS 2, ALS 3, and ALS 7), the slope for the remaining ALS subjects was  $3.5 \pm 2.2 \mu\text{VN}^{-1}$ . A trend of slope reduction can still be observed when compared with healthy control subjects, but no statistical difference was found between the two groups ( $p > 0.05$ ).

## 7.4 Discussion

This study examined the alteration of the relation between the EMG amplitude of the FDI muscle and the corresponding isometric force during index finger abduction in individuals diagnosed with ALS. The observed relation was further compared with that of the healthy control subjects to assess neuromuscular deficits in ALS. A linear fit between the surface EMG amplitude and the muscle contraction force was confirmed to be valid for the FDI muscle of the healthy controls and the ALS subjects. A trend of decreased slope in the linear fit of the EMG-force relation was observed in the ALS subjects compared with healthy control subjects. But no significant difference was found between the two groups when the reduction of MVC was taken into account.

The findings of this study may be a result of various types of interactive processes in ALS patients that can impact the EMG-force relation in different ways. These may include spinal motor neuron degeneration, muscle fiber reinnervation following the degeneration process, impairment of motor unit control properties, and muscle fiber atrophy, etc. The influence of these processes on EMG-force relation has been investigated using a simulation of motor neuron pool activity (muscle force and surface EMG)(P Zhou, Suresh, & Rymer, Sept 2007). The decreased slope of EMG-force relation can arise from several factors such as a selective degeneration of high threshold motor units, increased motor unit firing rates, atrophy of muscle fibers, and muscle contractile property changes, which have been reported in ALS patients. For example, a weaker correlation was found between motor unit action potential and twitch force in the FDI muscle for rapidly progressing ALS subjects, compared with healthy controls or subjects with slowly progressive motor neuron degeneration such as spinal muscular atrophy(Dengler et al., June 1990; Vogt & Nix, 1997). This suggested degeneration of high threshold motor units,

resulting in prevalence of relatively a large number of slow motor units in the muscle. For ALS patients with dominant lower motor neuron dysfunction, elevated motor unit firing rates were also observed, possibly due to compensatory mechanisms to cope with the loss of motor units(Kasi et al.). With all these changes, surface EMG of the affected muscle involves summation of relatively a large number of motor unit action potentials with small amplitudes in order to reach a given force. Due to increased degree of action potential cancellation, the surface EMG amplitude in such a case would be lower. This effect would be more evident at higher force levels, resulting in a slope reduction in the EMG-force relation(P Zhou et al., Sept 2007).

On the other hand, factors increasing the slope of the EMG-force relation were also reported in ALS subjects, such as muscle fiber reinnervation following motor neuron degeneration. Decreased motor unit firing rate was also observed in patients with dominant upper motor neuron dysfunction possibly due to decreased central drive or intrinsic motor neuron property changes(Kasi et al.). It is noted that for motor neuron diseases such as ALS, a variety of processes may work together (for example, denervation and reinnervation of muscle fibers) at different stages of the disease, which in turn may affect the disease progress. Thus experimentally observed EMG-force slope variations in affected muscles of ALS subjects could be the overall effects of many different factors.

In this study, a non-invasive electrode array was used for EMG data recording. The advantage of high density surface EMG has been reported in (Staudenmann, Kingma, Daffertshofer, & Stegeman, April 2006) (Staudenmann, Daffertshofer, & Kingma, April 2007) for improving estimation or tracking of muscle force using principal component analysis and independent component analysis. In this study, the objective was to examine the EMG-force relation. We found that the EMG amplitude varied significantly on different channels even for a

specific level of contraction. As force increases, the pattern of amplitude variation versus force might be different from channel to channel. Thus we averaged the EMG amplitude of all the channels to have a more robust and comprehensive measurement of the EMG-force relation.

Finally, given recent advances in surface EMG decomposition using high density surface EMG(Holobar, Farina, Gazzoni, R, & Zazula, Mar 2009; Holobar & Zazula, 2007), it is feasible to decompose the EMG signals collected in this study, thus providing more definite information about motor unit alteration than that obtained from the EMG-force relation analysis. Indeed, this was the primary motivation of using high density surface EMG recording in this study. As an overall effect of many different factors, EMG-force relation analysis can provide a general estimation of motor unit changes in an affected muscle. To obtain more definite information, our future work will focus on decomposition based motor unit analysis (e.g., motor unit control property, quantitative motor unit action potential analysis, etc.) in ALS subjects.

## **7.5. Acknowledgment**

This work was supported in part by the National Institute on Disability and Rehabilitation Research of the U.S. Department of Education under Grant H133G090093, in part by the National Institutes of Health of the U.S. Department of Health and Human Services under Grant 2R24 HD050821, and in part by the 1000 Talent Plan Special Program of China (Recruitment Program of Global Experts).



## 8 Characterization of Motor Unit Firing Behavior in the First Dorsal Interosseous Muscle of Patients with Amyotrophic Lateral Sclerosis

Faezeh Jahanmiri-Nezhad, Ales Holobar, William Z. Rymer, Ping Zhou

### Abstract

The objective of this study was to examine motor unit discharge patterns in subjects with Amyotrophic Lateral Sclerosis (ALS), compared to a healthy control population. A flexible 8×8 grid of surface miniscule electrodes was used to record electromyographic (EMG) signals from the First Dorsal Interosseous (FDI) muscle of ten ALS subjects and ten age-matched neurologically healthy subjects. Motor units were recruited voluntarily during randomized series of isometric contraction at different force levels, ranging from 10% to 100% of Maximum Voluntary Contraction (MVC) at 10% increment. Segmented EMG signals were decomposed and single motor unit discharge patterns were identified. Mean firing rates were computed based on instantaneous firing rates (IFR) of each motor unit. The firing rates at each force level were analyzed for each individual by fitting a linear line in them and measuring the firing rate-force slope and initial firing rate values. The ALS subjects were divided to two groups based on their FDI weakness (measured by abduction force at maximum voluntary contraction). The ALS subject with normal FDI strength had no statistically difference with healthy subjects in their slope and initial firing rate, unlike the ALS subjects with severe FDI weakness.

## 8.1 Introduction

Motor unit firing rate refers to the rate of discharges of a recruited motor unit. Increase of firing rate, along with number of activated motor units, contributes to muscle force generation. Changes in firing rate, called as ‘rate coding’, can be considered as a strategy for the nervous system to adjust the mechanical output of a muscle, and have been extensively studied in animal models and humans (Burke, 1968; De Luca et al., 1982; Fuglevand et al, 1993; Farina et al., 2002; Zhou and Rymer, 2004; Hu et al., 2014).

In this work, we examined possible changes in motor unit firing behavior of individuals with Amyotrophic Lateral Sclerosis (ALS). ALS is a unique form of motor neuron disease caused by the progressive degeneration of the lower motor neurons (LMN) located in the ventral horn of the spinal cord that innervate the muscles, and the upper (cortical) motor neurons (UMN) that provide efferent input to the lower motor neurons.

So far it is not very clear whether or how motor unit firing rate would be altered in ALS patients. As one of the main factors in force generation, MU discharge behavior might be altered as a result of changes in neural control mechanisms for a muscle under denervation. Furthermore, altered MU firing rate might explain muscle weakness in an individual, and therefore may be considered a useful neurophysiologic factor in assessment of an individual in clinical trials.

In De Carvalho et al., 2005, review of published clinical trial designs for ALS, it was concluded that ALS-FRS (Functional Rating Scale), perhaps MUNE (MU number estimation), and Neurophysiological index (related to nerve conduction and excitability parameters) are the most effective measurements in providing guidelines for an individual treatment designs. The

latter two suggested neurophysiological measurements are focused at compound motor action potential amplitude and the number of MUs. Both parameters dwindle dramatically along with disease progression (Maathuis et al., 2013; Baumann et. al, 2012). However, motor unit discharge behavior is also a main factor in force generation, that can compensate for recruitment. Firing rate of MUs are critically valuable in examining muscle weakness in an individual and have been hardly studies in ALS in first dorsal interosseous muscle by Kasi 2009; and in tibialis anterior muscle by De Carvalho et al., 2012).

High Density surface EMG (HDsEMG) provides non-invasive examination of electrical activity of muscle. Multi-channel electrodes cover a large area of muscle, thus can record more activities, while intramuscular EMG records from only a small area of the muscle. This fact makes HDsEMG electrodes more appropriate for tracking the changes in the muscle for an individual over time, since insertion of a needle at the exact same place might be difficult if not impossible. For the study of firing rate, EMG and Force was recorded simultaneously from First Dorsal Interosseous (FDI). Techniques of multi-channel surface EMG decomposition and their adequate accuracy assessment has been previously established (Zhou and Rymer, 2004; Holobar et al., 2009; Holobar et al., 2010; Holobar et al., 2014).

## **8.2 Experiments**

### **8.2.1 Experimental Design and Subject Population**

Experimental data from ten healthy intact subjects (5 male, 5 female, age range 30 to 80 years, with mean  $51.2 \pm 15.3$ ) and ten subjects with ALS (7 make, 3 female, age range 31 to 67 years, with mean  $53.1 \pm 12.5$ ) are presented. All subjects signed informed consent via protocols approved by the Institutional Review Board under the Office for the Protective of Human

Subjects at Northwestern University (Chicago, USA). The experiments were performed at the Single Motor Unit lab of the Rehabilitation Institute of Chicago, IL, USA. The first dorsal interosseous (FDI) muscle was examined. For control subjects and ALS subjects with non-affected hand muscle, the dominant side was examined, and for the ALS subjects with very weak hand muscles the stronger side was tested.

All the ALS participants were taking Rilutek, with ALS 1, 8 and 9 as exceptions. Riluzole, the only drug approved for the treatment of ALS, has been reported to have no acute effects on motor unit parameters (Desai et al, 1998).

Subjects were seated in a Biodex chair. Forearm was resting on an arm base. The wrist and forearm were placed in an arm brace and secured to the supporting surface to avoid movement when the subject moved the index finger. Extra foam was placed around the arm brace to further firm the forearm, to avoid force contamination on the FDI muscle. The proximal phalanx of the index finger was held in neutral position and placed in a firm cast inside a vise. A six degrees-of-freedom load cell (ATI-FT4006, ATI Inc, Garner, NC) was attached to the vise. The thumb angle relative to the index finger was held at 45 degrees. The three medial fingers were secured on specifically designed surfaces. Isometric abduction force of the FDI muscle was measured at the 2<sup>nd</sup> metacarpophalangeal (MCP) joint.

A flexible surface electrode array with 64 channels (8 rows and 8 columns, each recording probe 1.2 mm in diameter, inter-probe distance 4 mm for both directions) was used to record EMG; see Figure 26. EMG was amplified by Refa system (TMS International BV, Netherlands). The system has integrated filter settings. Bandpass filtering with tuned for 5-500 Hz. Real time display provided visual feedback to the examiner to assess signal quality. The

EMG signal was sampled at 2000 Hz per channel. The auxiliary channels of the system were used to record muscle force. The force signal was sampled at 2000 Hz with a low pass filter at 20 Hz. The EMG and force recordings were synchronized during the experiment. All the data were stored in ASCII format for offline analysis in Matlab 7.12.0, The MathWorks Inc., Natick, MA, 2011.

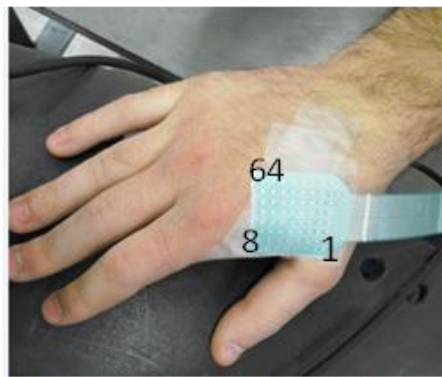
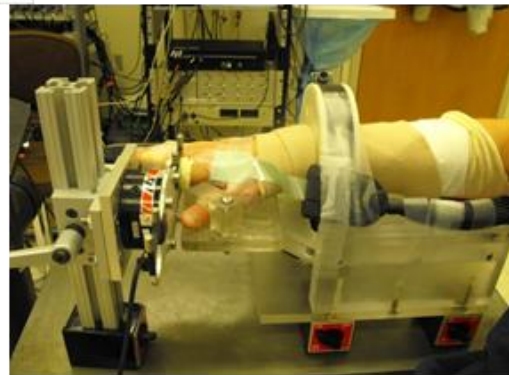


Figure 26: An 8×8 grid of surface EMG electrode placed over FDI muscle.



In order to guide the subject to perform a contraction at a certain level of force, a custom designed Graphical User Interface (GUI) Matlab program was used to provide visual feedback. This GUI program shows a two dimensional Cartesian coordinate plane, where  $x$ -axis represents force on the horizontal direction ( $F_x$ , index finger abduction/adduction) and  $y$ -axis represents force on the vertical direction ( $F_y$ , index finger flexion/extension). A cursor in the shape of a triangle was used to indicate the current position of muscle contraction force in the  $x$ - $y$  plane,

which is at the origin during rest. To perform each level of contraction, an open circle and a filled circle were used to represent the Target position and the Guide position, respectively. The filled circle can change colors from yellow to orange and then to green in order to indicate to the subject that a trial is about to start. The subject was asked to generate force by abducting the index finger to move the cursor to the Target, stay at the Target position for 10 s and then relax slowly until the cursor was back at the starting point.

The experimental protocol started by measuring the isometric maximum voluntary contraction (MVC) force of the FDI muscle for index finger adduction. Once the MVC was determined, the subject was asked to perform isometric contractions of the FDI muscle at 10%, 20%, ..., 100% of the MVC in different trials. If MVC level is large enough, minimal force levels such as 1N, 2N, ..., 5N were also tried. The order of contraction levels was randomized and each contraction level was repeated at least twice. Sufficient resting periods between trials were provided to the subject to minimize mental and muscle fatigue.

#### 8.2.2 EMG Decomposition and Firing Rate Calculation

The decomposition technique followed a blind source separation approach. Segments of EMG during constant force were decomposed using an existing software described in (Holobar et al., 2009; Holobar et al., 2010; Holobar et al., 2014), which takes Convolutional blind source separation strategy to decompose an interference pattern to individual motor unit potentials.

IDIs were computed from sequential firing times. Instantaneous firing rate (IFR) refers to the reciprocal of individual IDIs in a class. Mean firing rate was measured as the average of all IFRs, excluding 'too small' or 'too large' values. Such supposedly erroneous IDIs might be the result of false positive (causing too small IDI) and false negative (too large IDI) malfunctioning

of EMG decomposition. In this work, IDIs above 250 ms and less than 25 ms were excluded from the firing rate calculation, equivalent to a 4-40 pulse per second (pps) cutoffs.

Figure 27 shows two examples of EMG decomposition output at 1 Newton abduction force level. In both a) and b), the bottom trace shows one channel of EMG (selected from the center of the grid). The above traces on EMG is an illustration of discharge patterns for 4 and 9 MU activities extracted from the EMG trace in an ALS and a Healthy subject, respectively.

Furthermore, firing rate versus force values can be fitted into a linear line:  $y = Ax + B$ , where  $y$  refers to firing rate,  $A$  refers to the slope,  $x$  refers to force, and  $B$  refers to the constant value (the ordinate number at force = 0).

### 8.2.3. Statistical Tests

Student ttest was used for statistical comparison. Normality of data distribution for each side of the comparison was tested using a Jarque-Bera test (built in Statistical Toolbox of Matlab). This test makes no assumption about the mean and STD of data, in contrast to a Kolmogorov-Smirnov test. If a data set failed the normality test, we attempted to transform the data until the test did not reject the null hypothesis. A power function or a boxcox function was used to transform the data.

All the programs were coded in Matlab, MathWorks, Natick, Massachusetts, USA.

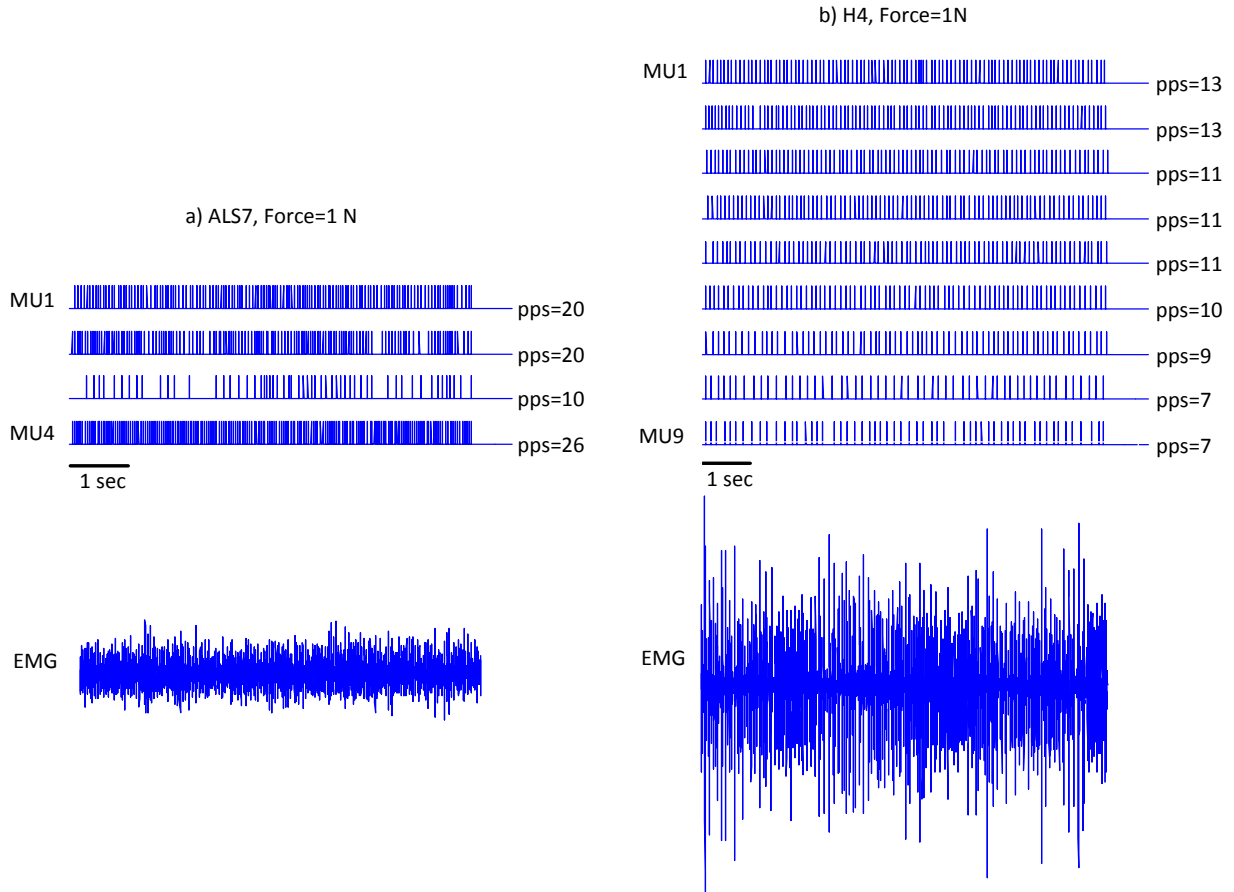


Figure 27: Discharge patterns of MUs extracted through EMG Decomposition, at 1 Newton of force. The data on the right panel belongs to a healthy subject, and on the left panel belongs to an ALS subject. Pulse per second is reported at the end of each pattern.

### 8.3 Results

Overall, 1038 motor units from the ten healthy subjects, and 675 units from the ALS group were extracted. Number of extracted MUs from a single trial, regardless of force level, ranged from 1 to 30 (averaged at  $12 \pm 5$ ), for intact group; and from 2 to 18 (averaged at  $7 \pm 4$ ) for ALS group. Averaged firing rates versus force (N) for each individual are illustrated in Figure 28. In general, a linear trend between firing rate and exerted force can be seen for the populations, excluding



subjects ALS1, 3, and 7. Subjects ALS1, 2, 3, and 7 have a very weak FDI ( $F_{MVC} < 5N$ ). Subject ALS10 had a mild level of weakness, with maximum force of 12N.

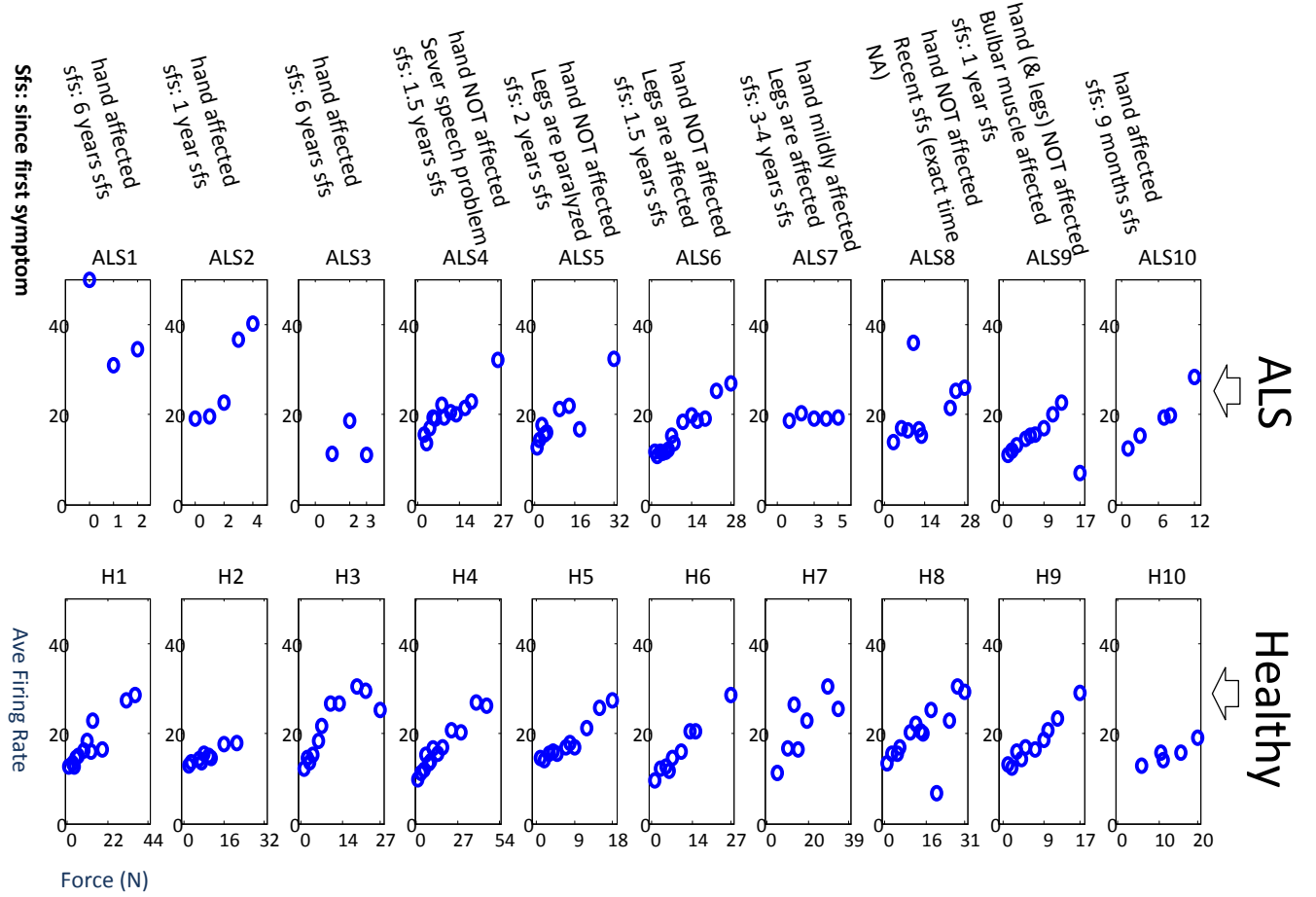


Figure 28: averaged firing rates for each individual. The top row shows the results from ALS population, and the bottom row presents the results from healthy subjects. In each panel, x-axis indicates force (in absolute Newton value), and y-axis shows firing rate (pulse per seconds). Each sample represents the average firing rates of all the motor units extracted from EMG at each level of contraction.

Due to high variability of force levels among ALS subjects, the data were grouped into three classes:  $H=\{H1-H10\}$ ,  $G1=\{ALS1,2,3,7,10\}$ , and  $G2=\{ALS4,5,6,8,9\}$ . For each individual, a line was fitted to the Firing Rate and Force quantities. Fitted lines are illustrated in Figure 29. In

this figure, we can see G2 overlaps with H. Large inconsistencies are seen among G1, with some level of force generation).

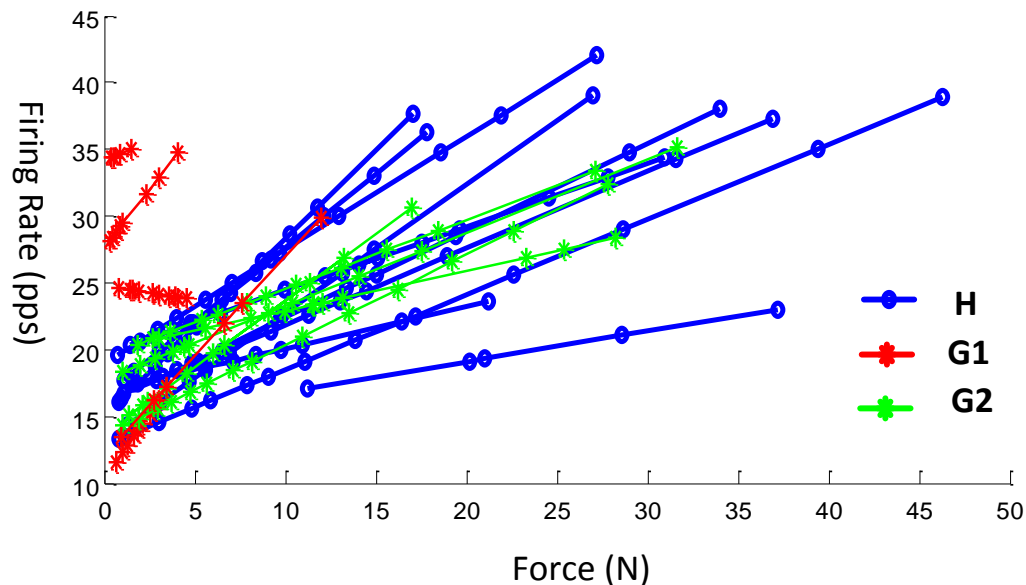


Figure 29: the (fitted) linear relationship between firing rate and force levels (in Newton).

From each fitted line  $y = Ax + B$ , two parameters A and B (slope and the constant value) can be derived. In Figure 30, the distributions of A and B belonging to each individual is depicted in each group. Variability among both A and B parameters is higher for data in G1 (weak muscles). To quantify it for example, the coefficient of variation ( $COV = \text{STD} / \text{Mean}$ ) of slopes in G1 is about two times larger than in H and G2 ( $COV = 0.49, 0.82, 0.42$  for H, G1, and G2, respectively). In same Figure 30, on the top right, a feature space is illustrated with both A and B values, with blue dots presenting healthy subjects, and red stars presenting the ALS subjects. The bottom right shows the same figure expanded. Three contours are dividing this

space to three regions. The middle region is where most of the data are clustered, mainly composed of H and G2 samples. The top and bottom regions are exclusively composed of G1.

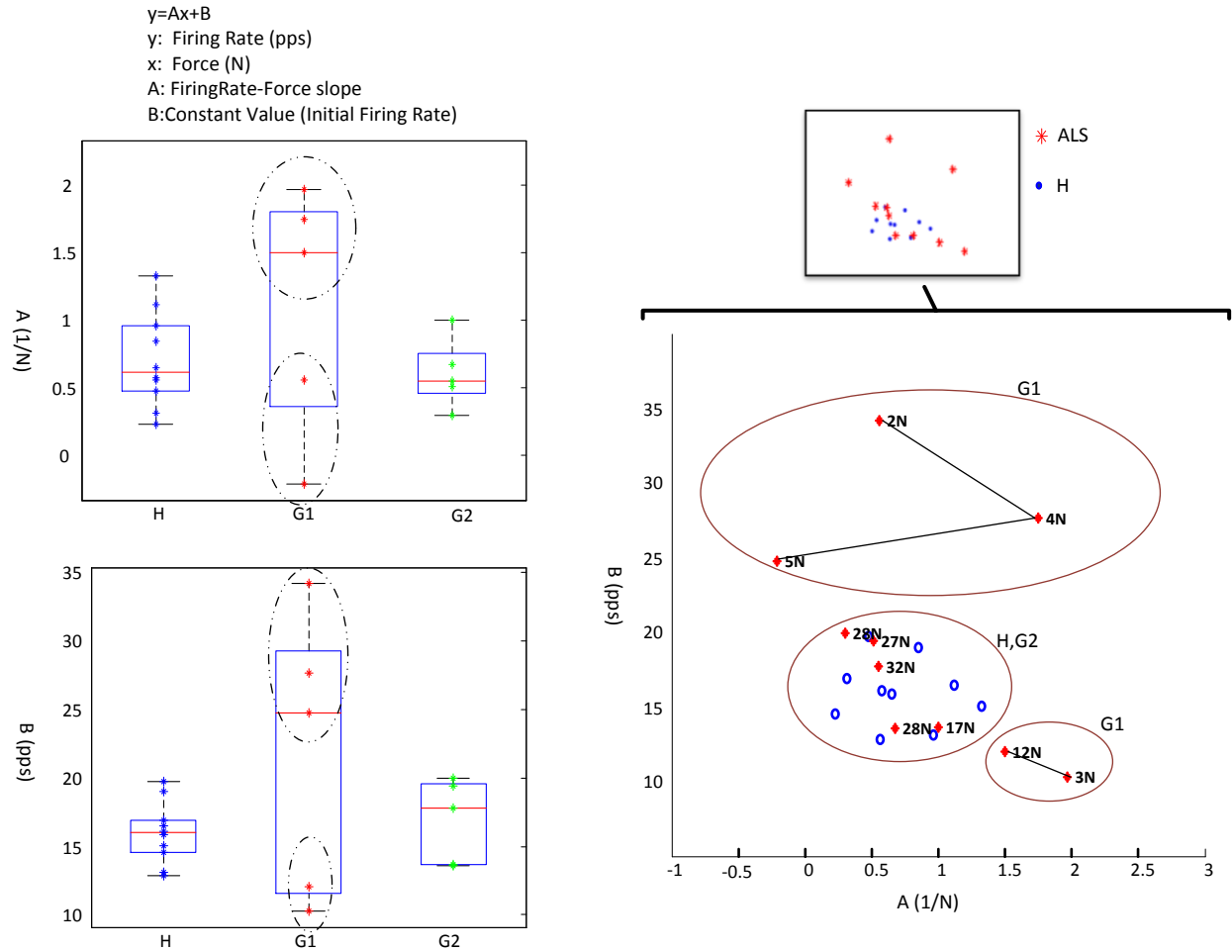


Figure 30: Plot of slope and initial firing rate values for the three groups (H: Healthy, G1: ALS with weak FDI, G2: ALS with normal FDI). On the left, distributions of A and B are depicted individually. On the right, a feature space of the data (x-axis: A, y-axis: B) is presented. The contours are dividing the feature space into three regions. The middle region contains all the H and G2 samples are clustered. The up and bottom regions include three and two samples from the G1.

## 8.4 Discussion

### 8.4.1. Analysis of Firing Rate

Monotonic increase of firing rate in FDI has been previously published by De Luca et al., 1982 (up to 80% of MVC); while, Conwit et al., 1999, reported a constant firing rate up to 30% of MVC and rate coding strategy playing an effective role only at high levels of force in quadriceps femoris muscle. High firing rates have been associated with lack of recurrent inhibitions Davey et al, 1993. Effect of synaptic noise on force steadiness (Dideriksen et al., 2012) -> may be irrelevant; but may also be related to Firing rate variability

### 8.4.2. Firing Rate Analysis and ALS

To date, diagnosis of ALS is not straightforward. It depends on clinical assessment and involves detection of both LMN and UMN symptoms, evidence of disease progress and spread to different regions, and eventually ruling out other mimic conditions (Higashihara and Sonoo, 2007; De Carvalho et al., 2011). Sonoo et al., 2011, emphasized on utility of EMG for detection of LMN symptoms in ALS diagnosis. Meanwhile, Vucic, 2012, pointed out the significance of UMN in early diagnosis of ALS. Both the functional transcranial magnetic stimulation and anatomic diffusion tensor imaging were mentioned as two highly sensitive detectors of UMN signs, yet they would require sophisticated costly technology which may not be available at all medical facilities. Nevertheless, motor unit discharge behavior of voluntary EMG, after accurate decomposition, can hint the presence of UMN signs. A significant reduction of coefficient of variation of instantaneous firing rates was observed in different groups of patients with marked spasticity including primary lateral sclerosis, as well as ALS, while the opposite happened for patients with dominant LMN lesions. Vucic et al. concluded that detection of abnormalities in firing rate especially when no sign of LMN symptoms exist would have important

pathophysiological importance and can help with an early diagnosis. The importance of MU firing rate measurements in detecting neuromuscular dysfunction had been also emphasized by Dorfman, et al., 1989.

#### 8.4.3. Firing Rate Analysis In Other Conditions

Firing rate modulation have also been studied in other conditions such as muscle fatigue, other neurologic disorders such as stroke and spinal cord injury (Andreassen and Rosenfalck, 1978; Thomas and del Valle, 2001; Kallenberg and Hermens; 2006; Zhou et al., 2007; Inglis et al., 2011; Chou et al., 2013; Watanabe et al, 2013; Mottram et al., 2014), and studies of aging (Patten et al., 2001; Kallio et al., 2012).

#### 8.4.4. Summary of the Results

Both ALS and Control subjects were using rate coding strategy during force generation. Based on figure 28, three ALS subjects with very weak muscle were exceptions (ALS1, 3 and 7). In order to characterize the results, a linear line was fitted into the firing rate and force values. The slope and the initial firing rate values were measured. Our results showed that ALS subjects with normal force generation abilities had a similar pattern of firing rate modulation versus force as in healthy subjects. However, the characteristics of ALS subjects with mild to severe weakness are scattered with some examples with high slopes and low initial firing rate, and some example with rather variant slope values and high initial firing rates.

The scattered results presented in Figure 30 can be interpreted in different ways. One other example is depicted in Figure 31, where the whole space is grouped into two regions, based on

the data in ALS, with a proposed trend in each group (ALS2 is considered as an outlier). The MVC force values, on the lines connecting the ALS samples, are interestingly declining as the lines move outwardly from the center. The In this new categorization, ALS1,4,5,7,8 are in one group, and ALS3,6,9, and 10 in another group. The members of the first set had rather low values of slope; and, as force declined, the initial firing rate increased. Meantime, the members of the latter had low values for initial firing rates; and, as force declined, the slope increased. This interpretation suggests two different mechanisms in rate coding as weakness progresses, but remains unproved at this stage of data analysis.

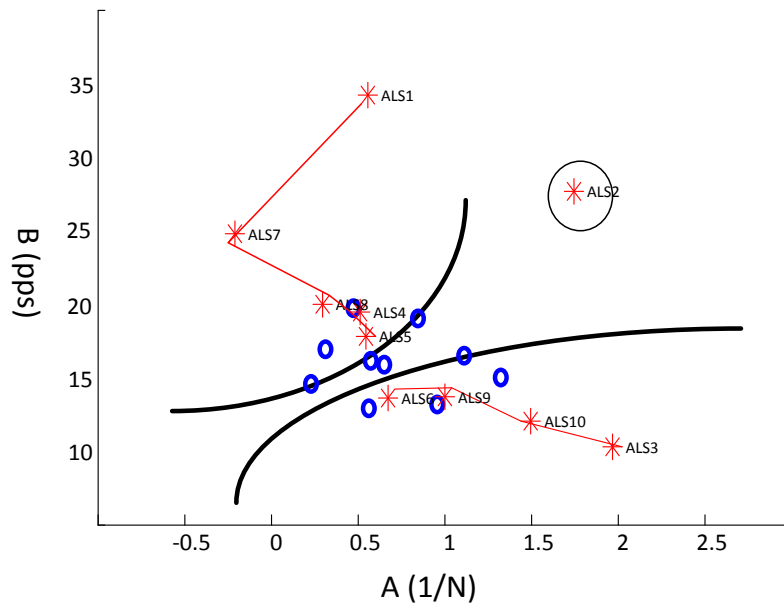


Figure 31: A-B feature space divided (arbitrarily) into two regions.

## **8.5 Acknowledgements**

The authors would like to sincerely thank Dr. Xiaogang Hu, Dr. Nina Suresh for their extensive help with data collection, as well as Dr. Sabrina Lee for the helpful discussions.

## 9 Future Directions

The series of work presented here are dedicated to surface electromyography (EMG) examination of subjects with a progressive motor neuron degenerative disease, ALS, using High Density Surface EMG electrodes. The developed data analysis techniques facilitate the potential clinical applications of surface EMG. In addition, they provide supplementary investigatory information, which is helpful for basic neurophysiological investigations (such as comprehending the organization of motor units in a muscle, examining the neural control strategies of muscle activation, etc.). The findings can ultimately be useful to detect the abnormality in the muscle and/or its neural drive as a result of the neurophysiologic disorder.

In this work, the examination of within-muscle Innervation Zone distributions, the analysis of EMG-force slope, and measuring single motor unit discharge behaviors were presented. Further studies can be followed up to explore potential applications of HDsEMG to study ALS. Suggested studies are listed, but not limited to the following:

### 9.1 Detection of Fibrillation Potentials

Fibrillation potentials are the hallmark of denervation. They arise on single muscle fibers that are believed to be denervated (lost connection to their corresponding motor axons). Their detection is so far only attainable through needle EMG (Nandedkar et al, 2000). It would be very helpful to examine the possibility of HDsEMG recording (which can cover larger area of a muscle), combined with advanced data analysis techniques, to discover these hidden rhythmic activities



on top of the skin, which might imply presence of fibrillation potentials. Attempts of finding differences between baseline EMG of control and ALS subjects reported in nonlinear dynamic domains (Zhang and Zhou, 2014). Nevertheless, no confirmed evidence exists so far whether the differences in such domains were specifically induced by underlying fibrillation potentials. A simultaneous recording of surface and intramuscular EMG is required to provide more definite information. By analyzing simultaneously recorded needle EMG, one will know whether an episode of surface recording contains fibrillation potentials or other abnormal discharges.

## **9.2 Motor unit recruitment patterns**

Motor unit recruitment and firing rate are the two motor unit control properties governing muscle force generation. In chapter 9, we investigated the firing rate behavior of single motor units in ALS. Analysis of motor unit recruitment patterns, in particular with respect to motor unit type and size, will be an essential complementary study. A different force protocol with slow ramp contractions will be more appropriate for motor unit recruitment investigations.

## **9.3 Motor Unit Number Estimation**

Another critical study commonly practiced in motor neuron degeneration disorders is the Motor Unit Number Estimation and its various modification forms such as motor unit number index estimation (MUNIX) (Nandedkar et al, 2004; Li et al., 2012; Zhou et al, 2014), which demand electrical stimulation of the nerve. The future studies in this area will be to examine whether an HDsEMG will have any advantage for motor unit number estimation compared with single channel surface EMG recording.

## **9.4 Study of abnormal propagation patterns – a simulation study**

We observed abnormal pattern of waveform propagation among some of the fasciculation potentials from the biceps muscle of ALS subjects. This abnormal pattern had also been reported previously but by very few people. It will be helpful to conduct a simulation study of motor unit potential with respect to its innervation properties, in an attempt to find the factors that can drive a multi-channel MUP waveform to resemble the abnormal patterns observed in experimental data. The results will be helpful to understand the experimentally observed abnormal propagation patterns.

## **9.5 Within-motor unit innervation zone analysis**

Chapter 6 is dedicated to ‘within-muscle’ innervation zone analysis. It is also suggested to examine the ‘within motor unit’ IZ analysis. We observed abnormally longer innervation zone length in fasciculating motor units of ALS subjects. The analysis was based on the collective measurements from the available motor units in each individual. Meanwhile, we observed that some waveform potentials have a long innervation zone. While the former project may indicate for a muscle reorganization, the latter will indicate for reinnervation occurring within a motor unit.

## **9.6 Fasciculation potential analysis on the 8×8 grid electrode**

Developed techniques of fasciculation potential detection and classification (Chapters 2 and 4) are easily extendable to data recorded by the grid electrode. Spontaneous EMG data from First Dorsal Interosseous (FDI) and Abductor Pollicis Brevis (APB) are available recorded by the grid electrodes from same population of ALS subjects, described in Chapter 6. Innervation zone

analysis can be repeated on these data. Comparison of the outcomes on distal muscles (the FDI and APB) and the more proximal muscle (the biceps) will be very interesting. The obstacle will be the anatomy of FDI and APB muscles. Unlike the straightforward parallel structure of muscle fibers in the biceps, the FDI and API muscles have a bipennate architecture. Estimation of their innervation zones would require cautions.

### **9.7 Complement surface EMG with other techniques that measure subcutaneous tissue and skin layer parameters**

The final but certainly not least in this list is the ‘notation’ that surface EMG should be carefully treated and not mistaken as an intramuscular EMG. This is significantly important, yet usually simply ignored. In an intramuscular EMG recording, an electrode is inserted into the muscle and directly records the electrical activity. A surface EMG, however, cannot collect the same signal as that from an intramuscular EMG electrode, being affected by the effects of the connective tissue around the muscle, the different skin layers, and also by the effect of the skin-electrode contact (if a conducting gel is applied). Both intramuscular and surface EMG recordings are affected by the electrode type (i.e. the electrode configuration, geometry, the recording surface area, etc.). In substituting an intramuscular electrode for a surface recording electrode, potential techniques should be looked for that may provide some estimation of the collective contribution of these factors. (Barkhaus and Nandedkar, 1994; Barkhaus et al, 2006).

## REFERENCES

- Andreassen, S., & Rosenfalck, A. (1978). Impaired regulation of the firing pattern of single motor units. *Muscle Nerve*, 1(5), 416-418. doi: 10.1002/mus.880010514
- Barbero, M., Merletti, R., & Rainoldi, A. (2012). *Generation, Propagation, and Extinction of Single-Fiber and Motor Unit Action Potentials*.
- Barkhaus, P. E., & Nandedkar, S. D. (2001). EMG Evaluation of the Motor Unit - The Electrophysiologic Biopsy. *eMedicine Journal (Neurology)* from <http://www.emedicine.com/neuro/topic610.htm>
- Barkhaus PE, Nandedkar SD: Recording characteristics of the surface EMG electrodes. *Muscle Nerve* 17:1317-23, 1994.
- Barkhaus PE, Collins MI, Nandedkar SD: Influence of the surface EMG electrode on the compound muscle action potential. *Electromyography & Clinical Neurophysiology*, 2006; 46:235-239.
- Basmajian, J. V., & De Luca, C. J. (1985). *Muscles Alive: Their Functions Revealed by Electromyography*. Baltimore, MD: Williams and Wilkins.
- Baumann, F., Henderson, R. D., Gareth Ridall, P., Pettitt, A. N., & McCombe, P. A. (2012). Quantitative studies of lower motor neuron degeneration in amyotrophic lateral sclerosis: evidence for exponential decay of motor unit numbers and greatest rate of loss at the site of onset. *Clin Neurophysiol*, 123(10), 2092-2098. doi: 10.1016/j.clinph.2012.03.007

- Benatar, M., & Tandan, R. (2011). The Awaji criteria for the diagnosis of amyotrophic lateral sclerosis: have we put the cart before the horse? *Muscle Nerve*, 43(4), 461-463. doi: 10.1002/mus.21942
- Blaschak, M. J., Powers, R. K., & Rymer, W. Z. (1988). Disturbances of motor output in a cat hindlimb muscle after acute dorsal spinal hemisection. *Exp Brain Res*, 71(2), 377-387.
- Boe, S. G., Rice, C. L., & Doherty, T. J. (2008). Estimating contraction level using root mean square amplitude in control subjects and patients with neuromuscular disorders. *Arch Phys Med Rehabil*, 89(4), 711-718. doi: 10.1016/j.apmr.2007.09.047
- Brooks, B. R. (1994). El Escorial World Federation of Neurology criteria for the diagnosis of amyotrophic lateral sclerosis. Subcommittee on Motor Neuron Diseases/Amyotrophic Lateral Sclerosis of the World Federation of Neurology Research Group on Neuromuscular Diseases and the El Escorial "Clinical limits of amyotrophic lateral sclerosis" workshop contributors. *J Neurol Sci*, 124 Suppl, 96-107.
- Brooks, B. R., Miller, R. G., Swash, M., Munsat, T. L., & World Federation of Neurology Research Group on Motor Neuron, D. (2000). El Escorial revisited: revised criteria for the diagnosis of amyotrophic lateral sclerosis. *Amyotroph Lateral Scler Other Motor Neuron Disord*, 1(5), 293-299.
- Brown, W. F., Strong, M. J., & Snow, R. (1988). Methods for estimating numbers of motor units in biceps-brachialis muscles and losses of motor units with aging. *Muscle Nerve*, 11(5), 423-432. doi: 10.1002/mus.880110503
- Burke, R. E. (1968). Firing patterns of gastrocnemius motor units in the decerebrate cat. *J Physiol*, 196(3), 631-654.

- Chou, L. W., Palmer, J. A., Binder-Macleod, S., & Knight, C. A. (2013). Motor unit rate coding is severely impaired during forceful and fast muscular contractions in individuals post stroke. *J Neurophysiol*, *109*(12), 2947-2954. doi: 10.1152/jn.00615.2012
- Conwit, R. A., Stashuk, D., Tracy, B., McHugh, M., Brown, W. F., & Metter, E. J. (1999). The relationship of motor unit size, firing rate and force. *Clin Neurophysiol*, *110*(7), 1270-1275.
- Cope, T. C., Webb, C. B., & Botterman, B. R. (1991). Control of motor-unit tension by rate modulation during sustained contractions in reinnervated cat muscle. *J Neurophysiol*, *65*(3), 648-656.
- Davey, N. J., Ellaway, P. H., Baker, J. R., & Friedland, C. L. (1993). Rhythmicity associated with a high degree of short-term synchrony of motor unit discharge in man. *Exp Physiol*, *78*(5), 649-661.
- de Carvalho, M. (2000). Pathophysiological significance of fasciculations in the early diagnosis of ALS. *Amyotroph Lateral Scler Other Motor Neuron Disord*, *1 Suppl 1*, S43-46.
- de Carvalho, M., Dengler, R., Eisen, A., England, J. D., Kaji, R., Kimura, J., . . . Swash, M. (2008). Electrodiagnostic criteria for diagnosis of ALS. *Clin Neurophysiol*, *119*(3), 497-503. doi: 10.1016/j.clinph.2007.09.143
- de Carvalho, M., Dengler, R., Eisen, A., England, J. D., Kaji, R., Kimura, J., . . . Swash, M. (2011). The Awaji criteria for diagnosis of ALS. *Muscle Nerve*, *44*(3), 456-457; author reply 457. doi: 10.1002/mus.22175
- de Carvalho, M., & Swash, M. (1998). Fasciculation potentials: a study of amyotrophic lateral sclerosis and other neurogenic disorders. *Muscle Nerve*, *21*(3), 336-344.

- de Carvalho, M., & Swash, M. (2012). Fasciculation potentials: still mysterious. *Clin Neurophysiol*, 123(2), 227-228. doi: 10.1016/j.clinph.2011.07.002
- de Carvalho, M., Turkman, A., & Swash, M. (2012). Motor unit firing in amyotrophic lateral sclerosis and other upper and lower motor neurone disorders. *Clin Neurophysiol*, 123(11), 2312-2318. doi: 10.1016/j.clinph.2012.04.016
- De Luca, C. J., LeFever, R. S., McCue, M. P., & Xenakis, A. P. (1982). Behaviour of human motor units in different muscles during linearly varying contractions. *J Physiol*, 329, 113-128.
- DeFreitas, J. M., Costa, P. B., Ryan, E. D., Herda, T. J., Cramer, J. T., & Beck, T. W. (2010). Innervation zone location of the biceps brachii, a comparison between genders and correlation with anthropometric measurements. *J Electromyogr Kinesiol*, 20(1), 76-80. doi: 10.1016/j.jelekin.2008.09.009
- Dengler, R., Konstanzer, A., Kuther, G., Hesse, S., Wolf, W., & Struppler, A. (1990). Amyotrophic lateral sclerosis: macro-EMG and twitch forces of single motor units. *Muscle Nerve*, 13(6), 545-550. doi: 10.1002/mus.880130612
- Desai, J., Sharief, M., & Swash, M. (1998). Riluzole has no acute effect on motor unit parameters in ALS. *J Neurol Sci*, 160 Suppl 1, S69-72.
- Dideriksen, J. L., Negro, F., Enoka, R. M., & Farina, D. (2012). Motor unit recruitment strategies and muscle properties determine the influence of synaptic noise on force steadiness. *J Neurophysiol*, 107(12), 3357-3369. doi: 10.1152/jn.00938.2011
- Dioszeghy, P., Egerhazi, A., Molnar, M., & Mechler, F. (1996). Turn-amplitude analysis in neuromuscular diseases. *Electromyogr Clin Neurophysiol*, 36(8), 463-468.

- Dorfman, L. J., Howard, J. E., & McGill, K. C. (1989). Motor unit firing rates and firing rate variability in the detection of neuromuscular disorders. *Electroencephalogr Clin Neurophysiol*, 73(3), 215-224.
- Drost, G., Kleine, B. U., Stegeman, D. F., van Engelen, B. G., & Zwarts, M. J. (2007). Fasciculation potentials in high-density surface EMG. *J Clin Neurophysiol*, 24(3), 301-307. doi: 10.1097/WNP.0b013e31803bba04
- Drost, G., Stegeman, D. F., van Engelen, B. G., & Zwarts, M. J. (2006). Clinical applications of high-density surface EMG: a systematic review. *J Electromyogr Kinesiol*, 16(6), 586-602. doi: 10.1016/j.jelekin.2006.09.005
- Enck, P., Franz, H., Azpiroz, F., Fernandez-Fraga, X., Hinninghofen, H., Kaske-Bretag, K., . . . Merletti, R. (2004). Innervation zones of the external anal sphincter in healthy male and female subjects. Preliminary results. *Digestion*, 69(2), 123-130. doi: 10.1159/000077878
- Falla, D., Dall'Alba, P., Rainoldi, A., Merletti, R., & Jull, G. (2002). Location of innervation zones of sternocleidomastoid and scalene muscles--a basis for clinical and research electromyography applications. *Clin Neurophysiol*, 113(1), 57-63.
- Farina, D., Fosci, M., & Merletti, R. (2002). Motor unit recruitment strategies investigated by surface EMG variables. *J Appl Physiol* (1985), 92(1), 235-247.
- Farina, D., Jiang, N., Rehbaum, H., Holobar, A., Graimann, B., Dietl, H., & Aszmann, O. C. (2014). The Extraction of Neural Information from the Surface EMG for the Control of Upper-Limb Prostheses: Emerging Avenues and Challenges. *IEEE Trans Neural Syst Rehabil Eng*, 22(4), 797-809. doi: 10.1109/TNSRE.2014.2305111



- Farina, D., & Merletti, R. (2003). A novel approach for estimating muscle fiber conduction velocity by spatial and temporal filtering of surface EMG signals. *IEEE Trans Biomed Eng*, 50(12), 1340-1351. doi: 10.1109/TBME.2003.819847
- Farina, D., Schulte, E., Merletti, R., Rau, G., & Disselhorst-Klug, C. (2003). Single motor unit analysis from spatially filtered surface electromyogram signals. Part I: spatial selectivity. *Med Biol Eng Comput*, 41(3), 330-337.
- Fuglevand, A. J., Winter, D. A., & Patla, A. E. (1993). Models of recruitment and rate coding organization in motor-unit pools. *J Neurophysiol*, 70(6), 2470-2488.
- Fuglevand, A. J., Winter, D. A., Patla, A. E., & Stashuk, D. (1992). Detection of motor unit action potentials with surface electrodes: influence of electrode size and spacing. *Biol Cybern*, 67(2), 143-153.
- Gemperline, J. J., Allen, S., Walk, D., & Rymer, W. Z. (1995). Characteristics of motor unit discharge in subjects with hemiparesis. *Muscle Nerve*, 18(10), 1101-1114. doi: 10.1002/mus.880181006
- Gutmann, L., & Gutmann, L. (2004). Myokymia and neuromyotonia 2004. *J Neurol*, 251(2), 138-142. doi: 10.1007/s00415-004-0331-5
- Higashihara, M., & Sonoo, M. (2007). [Electrodiagnosis of ALS]. *Brain Nerve*, 59(10), 1031-1041.
- Hilfiker, P., & Meyer, M. (1984). Normal and myopathic propagation of surface motor unit action potentials. *Electroencephalogr Clin Neurophysiol*, 57(1), 21-31.
- Holobar, A., Farina, D., Gazzoni, M., Merletti, R., & Zazula, D. (2009). Estimating motor unit discharge patterns from high-density surface electromyogram. *Clin Neurophysiol*, 120(3), 551-562. doi: 10.1016/j.clinph.2008.10.160

- Holobar, A., Minetto, M. A., Botter, A., Negro, F., & Farina, D. (2010). Experimental analysis of accuracy in the identification of motor unit spike trains from high-density surface EMG. *IEEE Trans Neural Syst Rehabil Eng*, 18(3), 221-229. doi: 10.1109/TNSRE.2010.2041593
- Holobar, A., Minetto, M. A., & Farina, D. (2014). Accurate identification of motor unit discharge patterns from high-density surface EMG and validation with a novel signal-based performance metric. *J Neural Eng*, 11(1), 016008.
- Holobar, A., & Zazula, D. (2007). *Multichannel blind source separation using convolution kernel compensation*. Paper presented at the IEEE Trans Signal Process.
- Howard, R. S., & Murray, N. M. (1992). Surface EMG in the recording of fasciculations. *Muscle Nerve*, 15(11), 1240-1245. doi: 10.1002/mus.880151104
- Hu, X., Rymer, W. Z., & Suresh, N. L. (2014). Motor unit firing rate patterns during voluntary muscle force generation: a simulation study. *J Neural Eng*, 11(2), 026015. doi: 10.1088/1741-2560/11/2/026015
- Inghilleri, M., & Iacovelli, E. (2011). Clinical neurophysiology in ALS. *Arch Ital Biol*, 149(1), 57-63. doi: 10.4449/aib.v149i1.1264
- Inglis, J. G., Howard, J., McIntosh, K., Gabriel, D. A., & Vandenboom, R. (2011). Decreased motor unit discharge rate in the potentiated human tibialis anterior muscle. *Acta Physiol (Oxf)*, 201(4), 483-492. doi: 10.1111/j.1748-1716.2010.02233.x
- Jahanmiri-Nezhad, F., Barkhaus, P. E., Rymer, W. Z., & Zhou, P. (2014). Sensitivity of fasciculation potential detection is dramatically reduced by spatial filtering of surface electromyography. *Clin Neurophysiol*, 125(7), 1498-1500. doi: 10.1016/j.clinph.2013.11.033

- Jahanmiri-Nezhad, F., Li, X., Barkhaus, P. E., Rymer, W. Z., & Zhou, P. (2014). A clinically applicable approach for detecting spontaneous action potential spikes in amyotrophic lateral sclerosis with a linear electrode array. *J Clin Neurophysiol*, 31(1), 35-40. doi: 10.1097/01.wnp.0000436896.02502.31
- Kallenberg, L. A., & Hermens, H. J. (2006a). Behaviour of motor unit action potential rate, estimated from surface EMG, as a measure of muscle activation level. *J Neuroeng Rehabil*, 3, 15. doi: 10.1186/1743-0003-3-15
- Kallenberg, L. A., & Hermens, H. J. (2006b). Motor unit action potential rate and motor unit action potential shape properties in subjects with work-related chronic pain. *Eur J Appl Physiol*, 96(2), 203-208. doi: 10.1007/s00421-004-1215-1
- Kallio, J., Sogaard, K., Avela, J., Komi, P., Selanne, H., & Linnamo, V. (2012). Age-related decreases in motor unit discharge rate and force control during isometric plantar flexion. *J Electromyogr Kinesiol*, 22(6), 983-989. doi: 10.1016/j.jelekin.2012.05.009
- Kasi, P. K. (2009). *Characterization of Motor Unit Discharge Rate in Patients with Amyotrophic Lateral Sclerosis (ALS)*. (Master of Science in Electrical and Computer Engineering), Worcester Polytechnic Institute.
- Kasi, P. K., Krivickas, L. S., Meister, M., Chew, E., Bonato, P., Schmid, M., . . . Clancy, E. A. (2009, April 29th - May 2nd). *Characterization of Motor Unit Behavior in Patients with Amyotrophic Lateral Sclerosis* Paper presented at the Proceedings of the 4th International IEEE EMBS Conference on Neural Engineering, Antalya, Turkey.
- Kleine, B. U., Boekestein, W. A., Arts, I. M., Zwarts, M. J., Schelhaas, H. J., & Stegeman, D. F. (2012). Fasciculations and their F-response revisited: high-density surface EMG in ALS

- and benign fasciculations. *Clin Neurophysiol*, 123(2), 399-405. doi: 10.1016/j.clinph.2011.06.032
- Kleine, B. U., Stegeman, D. F., Schelhaas, H. J., & Zwarts, M. J. (2008). Firing pattern of fasciculations in ALS: evidence for axonal and neuronal origin. *Neurology*, 70(5), 353-359. doi: 10.1212/01.wnl.0000300559.14806.2a
- Krarup, C. (2011). Lower motor neuron involvement examined by quantitative electromyography in amyotrophic lateral sclerosis. *Clin Neurophysiol*, 122(2), 414-422. doi: 10.1016/j.clinph.2010.06.027
- Kumagai, K., & Yamada, M. (1991). The clinical use of multichannel surface electromyography. *Acta Paediatr Jpn*, 33(2), 228-237.
- Lambert, E. H., & Mulder, D. W. (1957). Electromyographic studies in amyotrophic lateral sclerosis. *Proc Staff Meet Mayo Clin*, 32(17), 441-446.
- Lapatki, B. G., Van Dijk, J. P., Jonas, I. E., Zwarts, M. J., & Stegeman, D. F. (2004). A thin, flexible multielectrode grid for high-density surface EMG. *J Appl Physiol* (1985), 96(1), 327-336. doi: 10.1152/japplphysiol.00521.2003
- Lateva, Z. C., & McGill, K. C. (2001). Estimating motor-unit architectural properties by analyzing motor-unit action potential morphology. *Clin Neurophysiol*, 112(1), 127-135.
- Lateva, Z. C., & McGill, K. C. (2007). Electrophysiological evidence of doubly innervated branched muscle fibers in the human brachioradialis muscle. *Clin Neurophysiol*, 118(12), 2612-2619. doi: 10.1016/j.clinph.2007.09.058
- Lateva, Z. C., McGill, K. C., & Johanson, M. E. (2002). Electrophysiological evidence of adult human skeletal muscle fibres with multiple endplates and polyneuronal innervation. *J Physiol*, 544(Pt 2), 549-565.

- Lateva, Z. C., McGill, K. C., & Johanson, M. E. (2010). The innervation and organization of motor units in a series-fibered human muscle: the brachioradialis. *J Appl Physiol* (1985), 108(6), 1530-1541. doi: 10.1152/japplphysiol.01163.2009
- Lawrence, J. H., & De Luca, C. J. (1983). Myoelectric signal versus force relationship in different human muscles. *J Appl Physiol Respir Environ Exerc Physiol*, 54(6), 1653-1659.
- Li, X., Jahanmiri-Nezhad, F., Rymer, W. Z., & Zhou, P. (2012). An Examination of the Motor Unit Number Index (MUNIX) in muscles paralyzed by spinal cord injury. *IEEE Trans Inf Technol Biomed*, 16(6), 1143-1149. doi: 10.1109/TITB.2012.2193410
- Liu, X. X., Zhang, J., Zheng, J. Y., Zhang, S., Xu, Y. S., Kang, D. X., & Fan, D. S. (2009). Stratifying disease stages with different progression rates determined by electrophysiological tests in patients with amyotrophic lateral sclerosis. *Muscle Nerve*, 39(3), 304-309. doi: 10.1002/mus.21144
- Martin, S., & MacIsaac, D. (2006). Innervation zone shift with changes in joint angle in the brachial biceps. *J Electromyogr Kinesiol*, 16(2), 144-148. doi: 10.1016/j.jelekin.2005.06.010
- Masuda, T., Miyano, H., & Sadoyama, T. (1983). The distribution of myoneural junctions in the biceps brachii investigated by surface electromyography. *Electroencephalogr Clin Neurophysiol*, 56(6), 597-603.
- Masuda, T., & Sadoyama, T. (1986). The propagation of single motor unit action potentials detected by a surface electrode array. *Electroencephalogr Clin Neurophysiol*, 63(6), 590-598.

- Masuda, T., & Sadoyama, T. (1987). Skeletal muscles from which the propagation of motor unit action potentials is detectable with a surface electrode array. *Electroencephalogr Clin Neurophysiol*, 67(5), 421-427.
- McGill, K. C. (2004). Surface electromyogram signal modelling. *Med Biol Eng Comput*, 42(4), 446-454.
- Merletti, R., Botter, A., Troiano, A., Merlo, E., & Minetto, M. A. (2009). Technology and instrumentation for detection and conditioning of the surface electromyographic signal: state of the art. *Clin Biomech (Bristol, Avon)*, 24(2), 122-134. doi: 10.1016/j.clinbiomech.2008.08.006
- Merletti, R., Farina, D., & Gazzoni, M. (2003). The linear electrode array: a useful tool with many applications. *J Electromyogr Kinesiol*, 13(1), 37-47.
- Merletti, R., Holobar, A., & Farina, D. (2008). Analysis of motor units with high-density surface electromyography. *J Electromyogr Kinesiol*, 18(6), 879-890. doi: 10.1016/j.jelekin.2008.09.002
- Mesin, L., Gazzoni, M., & Merletti, R. (2009). Automatic localisation of innervation zones: a simulation study of the external anal sphincter. *J Electromyogr Kinesiol*, 19(6), e413-421. doi: 10.1016/j.jelekin.2009.02.002
- Mesin, L., Merletti, R., & Rainoldi, A. (2009). Surface EMG: the issue of electrode location. *J Electromyogr Kinesiol*, 19(5), 719-726. doi: 10.1016/j.jelekin.2008.07.006
- Mesin, L., Merletti, R., & Vieira, T. M. (2011). Insights gained into the interpretation of surface electromyograms from the gastrocnemius muscles: A simulation study. *J Biomech*, 44(6), 1096-1103. doi: 10.1016/j.jbiomech.2011.01.031

- Mills, K. R. (2011). Detecting fasciculations in amyotrophic lateral sclerosis: duration of observation required. *J Neurol Neurosurg Psychiatry*, 82(5), 549-551. doi: 10.1136/jnnp.2009.186833
- Milner-Brown, H. S., & Stein, R. B. (1975). The relation between the surface electromyogram and muscular force. *J Physiol*, 246(3), 549-569.
- Milner-Brown, H. S., Stein, R. B., & Yemm, R. (1973a). Changes in firing rate of human motor units during linearly changing voluntary contractions. *J Physiol*, 230(2), 371-390.
- Milner-Brown, H. S., Stein, R. B., & Yemm, R. (1973b). The contractile properties of human motor units during voluntary isometric contractions. *J Physiol*, 228(2), 285-306.
- Moritani, T., & deVries, H. A. (1978). Reexamination of the relationship between the surface integrated electromyogram (IEMG) and force of isometric contraction. *Am J Phys Med*, 57(6), 263-277.
- Mottram, C. J., Heckman, C. J., Powers, R. K., Rymer, W. Z., & Suresh, N. L. (2014). Disturbances of motor unit rate modulation are prevalent in muscles of spastic-paretic stroke survivors. *J Neurophysiol*, 111(10), 2017-2028. doi: 10.1152/jn.00389.2013
- Nandedkar, S. D., Barkhaus, P. E., Sanders, D. B., & Stalberg, E. V. (2000). Some observations on fibrillations and positive sharp waves. *Muscle Nerve*, 23(6), 888-894.
- Nandedkar SD, Nandedkar, D, Stalberg EV, Barkhaus PE: Motor Unit Number Index (MUNIX): A new method to study the number of MUs. *IEEE Transactions in Biomedical Engineering*, 2004; 51(12):2009-2011
- Nandedkar, S. D., Barkhaus, P. E., & Stalberg, E. V. (2010). Motor unit number index (MUNIX): principle, method, and findings in healthy subjects and in patients with motor neuron disease. *Muscle Nerve*, 42(5), 798-807. doi: 10.1002/mus.21824

- Navallas, J., & Stalberg, E. (2009). Studying motor end-plate topography by means of scanning-electromyography. *Clin Neurophysiol*, 120(7), 1335-1341. doi: 10.1016/j.clinph.2009.05.014
- Nishihara, K., Chiba, Y., Suzuki, Y., Moriyama, H., Kanemura, N., Ito, T., . . . Gomi, T. (2010). Effect of position of electrodes relative to the innervation zone on surface EMG. *J Med Eng Technol*, 34(2), 141-147. doi: 10.3109/03091900903480754
- Nishihara, K., Kawai, H., Chiba, Y., Kanemura, N., & Gomi, T. (2013). Investigation of innervation zone shift with continuous dynamic muscle contraction. *Comput Math Methods Med*, 2013, 174342. doi: 10.1155/2013/174342
- Noto, Y., Misawa, S., Kanai, K., Shibuya, K., Iose, S., Nasu, S., . . . Kuwabara, S. (2012). Awaji ALS criteria increase the diagnostic sensitivity in patients with bulbar onset. *Clin Neurophysiol*, 123(2), 382-385. doi: 10.1016/j.clinph.2011.05.030
- Patten, C., Kamen, G., & Rowland, D. M. (2001). Adaptations in maximal motor unit discharge rate to strength training in young and older adults. *Muscle Nerve*, 24(4), 542-550.
- Perry, J., & Bekey, G. A. (1981). EMG-force relationships in skeletal muscle. *Crit Rev Biomed Eng*, 7(1), 1-22.
- Piitulainen, H., Rantalainen, T., Linnamo, V., Komi, P., & Avela, J. (2009). Innervation zone shift at different levels of isometric contraction in the biceps brachii muscle. *J Electromyogr Kinesiol*, 19(4), 667-675. doi: 10.1016/j.jelekin.2008.02.007
- Pozzo, M., Bottin, A., Ferrabone, R., & Merletti, R. (2004). Sixty-four channel wearable acquisition system for long-term surface electromyogram recording with electrode arrays. *Med Biol Eng Comput*, 42(4), 455-466.



- Quian Quiroga, R. (2009). What is the real shape of extracellular spikes? *J Neurosci Methods*, 177(1), 194-198. doi: 10.1016/j.jneumeth.2008.09.033
- Rau, G., Schulte, E., & Disselhorst-Klug, C. (2004). From cell to movement: to what answers does EMG really contribute? *J Electromyogr Kinesiol*, 14(5), 611-617. doi: 10.1016/j.jelekin.2004.02.001
- Roeleveld, K., Stegeman, D. F., Vingerhoets, H. M., & Van Oosterom, A. (1997a). Motor unit potential contribution to surface electromyography. *Acta Physiol Scand*, 160(2), 175-183. doi: 10.1046/j.1365-201X.1997.00152.x
- Roeleveld, K., Stegeman, D. F., Vingerhoets, H. M., & Van Oosterom, A. (1997b). The motor unit potential distribution over the skin surface and its use in estimating the motor unit location. *Acta Physiol Scand*, 161(4), 465-472. doi: 10.1046/j.1365-201X.1997.00247.x
- Rosenfeld, J. (2000). Fasciculations without fibrillations: the dilemma of early diagnosis. *Amyotroph Lateral Scler Other Motor Neuron Disord*, 1 Suppl 1, S53-56.
- Seki, K., & Narusawa, M. (1996). Firing rate modulation of human motor units in different muscles during isometric contraction with various forces. *Brain Res*, 719(1-2), 1-7.
- Shefner, J. M., & Gooch, C. L. (2002). Motor unit number estimation in neurologic disease. *Adv Neurol*, 88, 33-52.
- Solomonow, M., Baratta, R., Shoji, H., & D'Ambrosia, R. (1990). The EMG-force relationships of skeletal muscle; dependence on contraction rate, and motor units control strategy. *Electromyogr Clin Neurophysiol*, 30(3), 141-152.
- Sonoo, M., Higashihara, M., & Hokkoku, K. (2011). [Electrodiagnosis of ALS: its practical aspects]. *Rinsho Shinkeigaku*, 51(11), 1111-1113.

- Stalberg, E., & Karlsson, L. (2001a). Simulation of EMG in pathological situations. *Clin Neurophysiol*, 112(5), 869-878.
- Stalberg, E., & Karlsson, L. (2001b). Simulation of the normal concentric needle electromyogram by using a muscle model. *Clin Neurophysiol*, 112(3), 464-471.
- Staudenmann, D., Daffertshofer, A., Kingma, I., Stegeman, D. F., & van Dieen, J. H. (2007). Independent component analysis of high-density electromyography in muscle force estimation. *IEEE Trans Biomed Eng*, 54(4), 751-754. doi: 10.1109/TBME.2006.889202
- Staudenmann, D., Kingma, I., Daffertshofer, A., Stegeman, D. F., & van Dieen, J. H. (2006). Improving EMG-based muscle force estimation by using a high-density EMG grid and principal component analysis. *IEEE Trans Biomed Eng*, 53(4), 712-719. doi: 10.1109/TBME.2006.870246
- Sun, T. Y., Lin, T. S., & Chen, J. J. (1999). Multielectrode surface EMG for noninvasive estimation of motor unit size. *Muscle Nerve*, 22(8), 1063-1070.
- Swash, M. (2000). Shortening the time to diagnosis in ALS: the role of electrodiagnostic studies. *Amyotroph Lateral Scler Other Motor Neuron Disord*, 1 Suppl 1, S67-72.
- Tang, A., & Rymer, W. Z. (1981). Abnormal force--EMG relations in paretic limbs of hemiparetic human subjects. *J Neurol Neurosurg Psychiatry*, 44(8), 690-698.
- Thomas, C. K., & del Valle, A. (2001). The role of motor unit rate modulation versus recruitment in repeated submaximal voluntary contractions performed by control and spinal cord injured subjects. *J Electromyogr Kinesiol*, 11(3), 217-229.
- Vogt, T., & Nix, W. A. (1997). Functional properties of motor units in motor neuron diseases and neuropathies. *Electroencephalogr Clin Neurophysiol*, 105(4), 328-332.

- Vucic, S. (2012). Assessing motor unit firing rates in ALS: A diagnostic and pathophysiological prospect? *Clin Neurophysiol*, 123(11), 2114-2115. doi: 10.1016/j.clinph.2012.04.015
- Watanabe, K., Gazzoni, M., Holobar, A., Miyamoto, T., Fukuda, K., Merletti, R., & Moritani, T. (2013). Motor unit firing pattern of vastus lateralis muscle in type 2 diabetes mellitus patients. *Muscle Nerve*, 48(5), 806-813. doi: 10.1002/mus.23828
- Whaley, N. R., & Rubin, D. I. (2010). Myokymic discharges in amyotrophic lateral sclerosis (ALS): a rare electrophysiologic finding? *Muscle Nerve*, 41(1), 107-109. doi: 10.1002/mus.21540
- Woods, J. J., & Bigland-Ritchie, B. (1983). Linear and non-linear surface EMG/force relationships in human muscles. An anatomical/functional argument for the existence of both. *Am J Phys Med*, 62(6), 287-299.
- Zhang, X., Chen, X., Barkhaus, P. E., & Zhou, P. (2013). Multiscale entropy analysis of different spontaneous motor unit discharge patterns. *IEEE J Biomed Health Inform*, 17(2), 470-476. doi: 10.1109/JBHI.2013.2241071
- Zhang, X., & Zhou, P. (2014). Analysis of surface EMG baseline for detection of hidden muscle activity. *J Neural Eng*, 11(1), 016011. doi: 10.1088/1741-2560/11/1/016011
- Zhou, P., Barkhaus, P. E., Zhang, X., & Rymer, W. Z. (2011). Characterizing the complexity of spontaneous motor unit patterns of amyotrophic lateral sclerosis using approximate entropy. *J Neural Eng*, 8(6), 066010. doi: 10.1088/1741-2560/8/6/066010
- Zhou, P., Li, X., Jahanmiri-Nezhad, F., Rymer, W. Z., & Barkhaus, P. E. (2012). Duration of observation required in detecting fasciculation potentials in amyotrophic lateral sclerosis using high-density surface EMG. *J Neuroeng Rehabil*, 9, 78. doi: 10.1186/1743-0003-9-78

- Zhou, P., Li, X., & Rymer, W. Z. (2013). EMG-force relations during isometric contractions of the first dorsal interosseous muscle after stroke. *Top Stroke Rehabil*, 20(6), 537-544. doi: 10.1310/tsr2006-537
- Zhou, P., Nandedkar, S., & Barkhaus, P. (2014). Voluntary Contraction Direction Dependence of Motor Unit Number Index in Patients with Amyotrophic Lateral Sclerosis. *IEEE Trans Neural Syst Rehabil Eng*. doi: 10.1109/TNSRE.2014.2314391
- Zhou, P., & Rymer, W. Z. (2004a). Can standard surface EMG processing parameters be used to estimate motor unit global firing rate? *J Neural Eng*, 1(2), 99-110. doi: 10.1088/1741-2560/1/2/005
- Zhou, P., & Rymer, W. Z. (2004b). Factors governing the form of the relation between muscle force and the EMG: a simulation study. *J Neurophysiol*, 92(5), 2878-2886. doi: 10.1152/jn.00367.2004
- Zhou, P., Suresh, N. L., & Rymer, W. Z. (2007). Model based sensitivity analysis of EMG-force relation with respect to motor unit properties: applications to muscle paresis in stroke. *Ann Biomed Eng*, 35(9), 1521-1531. doi: 10.1007/s10439-007-9329-3
- Zwarts, M. J., & Stegeman, D. F. (2003). Multichannel surface EMG: basic aspects and clinical utility. *Muscle Nerve*, 28(1), 1-17. doi: 10.1002/mus.10358

# VITA

NAME: Faezeh Jahanmiri-Nezhad

EDUCATION: B.S., Biomedical Engineering, Amirkabir University of Technology, Tehran, Iran, 2003

M.A.Sc., Systems Design Engineering Sep. 2004 - Dec. 2005

PROFESSIONAL EXPERIENCE: **Research Assistant**; Sep 2010 \_ current  
Single Motor Unit Lab, Sensory Motor Performance Program,, Rehabilitation Institute of Chicago, (Chicago, IL)

**Research Engineer**; Apr 2009 – Aug 2010  
Single Motor Unit Lab, Sensory Motor Performance Program, Rehabilitation Institute of Chicago, (Chicago, IL)

**Research Assistant**; summer 2008  
Biomedical Research group, Applied Math Dept, University of Waterloo, (Ontario, Canada)

**Research Assistant**; Fall 2004- Spring 2005  
BioSignal Lab, Department of Systems Design Eng, University of Waterloo, (Ontario, Canada)

**Undergrad intern**; summer 2002  
Research Institute of Biomedical Technology, School of Medicine, Tehran University, (Tehran, Iran)

PUBLICATIONS: **Jahanmiri-Nezhad F**, Barkhaus E.P., Rymer W.Z., Zhou, P, “Spike Sorting Paradigm for Classification of Multi-channel Recorded Fasciculation Potentials”, conditionally accepted, Computers in Biology and Medicine, 2014.

**Jahanmiri-NezhadF**, Li X, Rymer W.Z., Zhou, P. “A Practice of Caution: Action Potential Spikes or Noise?”, submitted to the Journal of NeuroEngineering and Rehabilitation, Under revision.

**Jahanmiri-Nezhad F**, Hu X, Suresh N, Rymer WZ, Zhou P, "EMG-force Relation in the First Dorsal Interosseous Muscle of Patients with Amyotrophic Lateral Sclerosis", *NeuroRehabilitation*, 2014, Jul 2.

**Jahanmiri-Nezhad F**, Li X, Barkhaus PE, Rymer WZ, Zhou P, "Sensitivity of fasciculation potential detection is dramatically reduced by spatial filtering of surface electromyography", *Clinical Neurophysiology* 2013.

**Jahanmiri-Nezhad F**, Li X, Barkhaus PE, Rymer WZ, Zhou P, "A clinical applicable approach for detecting fasciculation potentials in amyotrophic lateral sclerosis with a linear electrode array", *J Clin Neurophysiol.* 2014 Feb;31(1):35-40. doi: 10.1097/01

Zhou P., Li X., **Jahanmiri Nezhad F.**, Rymer W.Z., Barkhaus P., "Duration of Observation Required in Detecting Fasciculation Potentials in Amyotrophic Lateral Sclerosis Using High Density Surface EMG", *Journal of NeuroEngineering and Rehabilitation*, 2012, 9:78

Li X, **Jahanmiri-Nezhad F**, Rymer WZ, Zhou P, "An Examination of the Motor Unit Number Index (MUNIX) in Muscles Paralyzed by Spinal Cord Injury", *IEEE Trans Inf Technol Biomed.* 2012 Apr 4

Parsaei H, **Nezhad FJ**, Stashuk DW, Hamilton-Wright A., "Validation motor unit firing patterns extracted by EMG signal decomposition", *Med Biol Eng Comput.* 2011 Jun;49(6):649-58. Epub 2010 Nov 2

#### ABSTRACTS:

**Faezeh Jahanmiri Nezhad, xiaoyan Li, William Zev Rymer, Ping Zhou**, "Noninvasive detection of spontaneous muscle activity in amyotrophic lateral sclerosis in frequency domain", 56th Annual Meeting - Biophysical Society, San Diego, Feb 2012

**F. Jahanmiri**, Z. Rymer, and P. Zhou, "A Nonlinear Approach for Noise Reduction in Selective Surface EMG". BMES Annual meeting Pittsburg, Oct 2009.

Parsaei H, **Nezhad FJ**, Stashuk DW, Hamilton-Wright A., "Validation of motor unit potential trains using motor unit firing pattern information", *Conf Proc IEEE Eng Med Biol Soc.* 2009;2009:974-7.

H. Parsaei, Hossein, **F. Jahanmiri Nezhad**, D.W. Stashuk, A. Hamilton-Wright, " Validation of Motor Unit Potential Trains Using Motor Unit

Firing Pattern Information", 31st Annual International IEEE EMBS, Conference, September, 2-6, 2009, Hilton Minneapolis, Minnesota, USA.

Hossein Parsaei, Andrew Hamilton-Wright, **Faezeh Jahanmiri Nezhad**, Daniel Stashuk. Development of an SVM classifier for detecting merged motor unit potential trains in ISEK. Niagara Falls, June 2008



THESES:

**Jahanmiri Nezhad F.** Developing knowledge based agents applied on Motor Unit Firing Patterns Electromyographic signal decomposition, for the completion of Master of Applied Science at University of Waterloo, Waterloo, On., 2006


**Jahanmiri Nezhad F.** Designing data acquisition card (DAS card) for a Viscometer system, For the completion of Bachelor of Science at University of AmirKabir, Tehran, Iran, 2003

# APPENDIX

## Statement of Copyright Permission



[Home](#)[Account Info](#)[Help](#)



**Wolters Kluwer**  
Health  
Lippincott Williams & Wilkins  
Requesting permission to  
reuse content from an  
LWW publication.

**Title:** A Clinically Applicable Approach for Detecting Spontaneous Action Potential Spikes in Amyotrophic Lateral Sclerosis With a Linear Electrode Array

**Author:** Faezeh Jahanmiri-Nezhad, Xiaoyan Li, Paul Barkhaus, et al

**Publication:** Journal of Clinical Neurophysiology

**Publisher:** Wolters Kluwer Health

**Date:** Jan 1, 2014

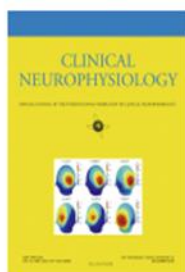
Copyright © 2014, (C) 2014 by the American Clinical Neurophysiology Society

Logged in as:  
Faezeh Jahanmiri

[LOGOUT](#)

This reuse is free of charge. No permission letter is needed from Wolters Kluwer Health, Lippincott Williams & Wilkins. We require that all authors always include a full acknowledgement. Example: AIDS: 13 November 2013 - Volume 27 - Issue 17 - p 2679-2689. Wolters Kluwer Health Lippincott Williams & Wilkins© No modifications will be permitted.





**Title:** Sensitivity of fasciculation potential detection is dramatically reduced by spatial filtering of surface electromyography

**Author:** Faezeh Jahanmiri-Nezhad, Paul E. Barkhaus, William Z. Rymer, Ping Zhou

**Publication:** Clinical Neurophysiology

**Publisher:** Elsevier

**Date:** Jul 1, 2014

Copyright © 2014, Elsevier

Logged in as:  
Faezeh Jahanmiri  
Account #: 3000827208

LOGOUT

## Order Completed

Thank you very much for your order.

This is a License Agreement between Faezeh Jahanmiri-Nezhad ("You") and Elsevier ("Elsevier")  
The license consists of your order details, the terms and conditions provided by Elsevier, and the [payment terms and conditions](#).

License number	Reference confirmation email for license number
License date	Sep 04, 2014
Licensed content publisher	Elsevier
Licensed content publication	Clinical Neurophysiology
Licensed content title	Sensitivity of fasciculation potential detection is dramatically reduced by spatial filtering of surface electromyography
Licensed content author	Faezeh Jahanmiri-Nezhad, Paul E. Barkhaus, William Z. Rymer, Ping Zhou
Licensed content date	July 2014
Licensed content volume number	125
Licensed content issue number	7
Number of pages	3
Type of Use	reuse in a thesis/dissertation
Portion	full article
Format	both print and electronic
Are you the author of this Elsevier article?	Yes
Will you be translating?	No
Title of your thesis/dissertation	Surface EMG Examination of Amyotrophic Lateral Sclerosis
Expected completion date	Sep 2014
Elsevier VAT number	GB 494 6272 12
Billing Type	Invoice
Billing address	1316 rocky Ridge Rd CEDAR FALLS, IA 50613 United States
Permissions price	0.00 USD
VAT/Local Sales Tax	0.00 USD / 0.00 GBP
Total	0.00 USD

CLOSE WINDOW

# **EMG-force relation in the first dorsal interosseous muscle of patients with amyotrophic lateral sclerosis**

Journal [NeuroRehabilitation](#)  
Publisher IOS Press  
ISSN 1053-8135 (Print)  
1878-6448 (Online)  
Subject [Medicine, Clinical Neurology, Exercise & Occupational Therapy](#) and [Rehabilitation & Assistive Technology](#)  
Pages -  
DOI 10.3233/NRE-141125  
Subject [Medicine and Health](#)  
Group  
Online Date Wednesday, July 02, 2014

Dear Faezeh Jahanmiri-Nezhad

We hereby grant you permission to reproduce the below mentioned material in print and electronic format at no charge subject to the following conditions:

1. If any part of the material to be used (for example, figures) has appeared in our publication with credit or acknowledgement to another source, permission must also be sought from that source. If such permission is not obtained then that material may not be included in your publication/copies.

2. Suitable acknowledgement to the source must be made, either as a footnote or in a reference list at the end of your publication, as follows:

“Reprinted from Publication title, Vol number, Author(s), Title of article, Pages No., Copyright (Year), with permission from IOS Press”.

3. This permission is granted for non-exclusive world English rights only. For other languages please reapply separately for each one required.

4. Reproduction of this material is confined to the purpose for which permission is hereby given.

Yours sincerely

Carry Koolbergen (Mrs.)  
Contracts, Rights & Permissions Coordinator  
Not in the office on Wednesday's  
IOS Press BV  
Nieuwe Hemweg 6B